

Geochemistry and petrology of the ferropicrite dikes and associated rocks of Vestfjella, western Dronning Maud Land, Antarctica

JUSSI S. HEINONEN

ACADEMIC DISSERTATION

To be presented, with the permission of the Faculty of Science of the University of Helsinki, for public examination in auditorium E204, Physicum, Kumpula campus, on 27th of May 2011, at 12 o'clock noon.

© Jussi Heinonen (synopsis)

© Reprinted with the kind permission of Elsevier (Paper I, III)

© Reprinted with the kind permission of Springer-Verlag (Paper II)

Cover photo: A view towards West-Muren from East-Muren. Boulders in the foreground have been derived from a weathered mafic dike *in situ*.

Author's address: Jussi Heinonen
Department of Geosciences and Geography
P.O.Box 64
00014 University of Helsinki, Finland
jussi.s.heinonen@helsinki.fi

Supervised by: Doctor Arto Luttinen
Finnish Museum of Natural History
University of Helsinki, Finland

Co-supervised by: Professor Tapani Rämö
Department of Geosciences and Geography
University of Helsinki, Finland

Reviewed by: Professor Eero Hanski
Department of Geology
University of Oulu, Finland

Doctor Teal Riley
British Antarctic Survey
Cambridge, Great Britain

Discussed with: Doctor Sally Gibson
Department of Earth Sciences
University of Cambridge, Great Britain

ISSN 1798-7911

ISBN 978-952-10-6309-1 (paperback)

ISBN 978-952-10-6310-7 (PDF)

<http://ethesis.helsinki.fi>

Unigrafia
Helsinki 2011

Abstract

This study provides insights into the composition and origin of ferropicrite dikes ($\text{FeO}_{\text{tot}} = 13\text{--}17$ wt. %; $\text{MgO} = 13\text{--}19$ wt. %) and associated meimechite, picrite, microbasalt, and basalt dikes found at Vestfjella, western Dronning Maud Land, Antarctica. The dikes crosscut Jurassic Karoo continental flood basalts (CFB) that were emplaced during the early stages of the breakup of the Gondwana supercontinent ~180 Ma ago. Selected samples (31 overall from at least eleven dikes) were analyzed for their mineral chemical, major element, trace element, and Sr, Nd, Pb, and Os isotopic compositions.

The studied samples can be divided into two geochemically distinct types: (1) The depleted type (24 samples from at least nine dikes) is relatively depleted in the most incompatible elements and exhibits isotopic characteristics (e.g., initial ϵ_{Nd} of +4.8 to +8.3 and initial $^{187}\text{Os}/^{188}\text{Os}$ of 0.1256–0.1277 at 180 Ma) similar to those of mid-ocean ridge basalts (MORB); (2) The enriched type (7 samples from at least two dikes) exhibits relatively enriched incompatible element and isotopic characteristics (e.g., initial ϵ_{Nd} of +1.8 to +3.6 and initial $^{187}\text{Os}/^{188}\text{Os}$ of 0.1401–0.1425 at 180 Ma) similar to those of oceanic island basalts. Both magma types have escaped significant contamination by the continental crust.

The depleted type is related to the main phase of Karoo magmatism and originated as highly

magnesian (MgO up to 25 wt. %) partial melts at high temperatures (mantle potential temperature >1600 °C) and pressures (~5–6 GPa) from a sublithospheric, water-bearing, depleted peridotite mantle source. The enriched type sampled pyroxene-bearing heterogeneities that can be traced down to either recycled oceanic crust or melt-metasomatized portions of the sublithospheric or lithospheric mantle.

The source of the depleted type represents a sublithospheric end-member source for many Karoo lavas and has subsequently been sampled by the MORBs of the Indian Ocean. These observations, together with the purported high temperatures, indicate that the Karoo CFBs were formed in an extensive melting episode caused mainly by internal heating of the upper mantle beneath the Gondwana supercontinent.

My research supports the view that ferropicritic melts can be generated in several ways: the relative Fe-enrichment of mantle partial melts is most readily achieved by (1) relatively low degree of partial melting, (2) high pressure of partial melting, and (3) melting of enriched source components (e.g., pyroxenite and metasomatized peridotite). Ferropicritic whole-rock compositions could also result from accumulation, secondary alteration, and fractional crystallization, however, and caution is required when addressing the parental magma composition.

Tiivistelmä (in Finnish)

Mantereiset laakiobasalttiprovinssit ovat suurimpia tunnettuja ilmanalaisia vulkaanisia muodostumia (alkuperäinen tilavuus jopa $2 \times 10^6 \text{ km}^3$). Laakiobasaltteja esiintyy kaikilla mantereilla ja niitä tiedetään muodostuneen miltei läpi maapallon historian. Laakiobasalttien purkautumisella on ollut huomattava vaikutus maapallon ilmastoon ja elämän kehitykseen, mutta niiden synnystä tiedetään edelleen varsin vähän. Tämä johtuu osaltaan siitä, että suurin osa laakiobasalttien kantasulista on reagoinut voimakkaasti mantereisen litosfäärin kanssa ja niiden alkuperäinen, mahdollisesti litosfäärin alaisesta vaipasta peritty geokemiallinen sormenjälki on vaikeasti tunnistettavissa ja tulkittavissa.

Ferropikriitit ovat poikkeuksellisen rautarikkaita ($\text{FeO}_{\text{tot}} > 13\text{--}14 \text{ p. } \%$) ja primitiivisiä ($\text{MgO} \approx 12\text{--}18 \text{ p. } \%$) laavakiviä, joita on kuvattu muutamista laakiobasalttiprovinssista. Toisin kuin tavalliset laakiobasaltit, ferropikriitit eivät yleensä ole merkittävästi reagoineet litosfäärin kanssa ja siksi ne tarjoavat arvokasta tietoa suoraan laakiobasalttimuodostumien alkulähteiltä. Ferropikriitit on usein yhdistetty anomalisen korkeisiin vaipan lämpötiloihin ja vaippapluumeihin, mutta näiden erikoisten kivien syntyyn liittyy useita kysymyksiä: Mistä niiden korkea rautapitoisuus on peräisin? Miten ne kytkeytyvät laakiobasalttien syntyyn?

Tässä väitöskirjatyössä käsitellään Vestfjellan (Kuningatar Maudin maa, Etelämanner) ferropikriittien ($\text{FeO}_{\text{tot}} = 13\text{--}17 \text{ p. } \%$; $\text{MgO} = 13\text{--}19 \text{ p. } \%$) sekä niihin liittyvien muiden primitiivisten magmakivien – pikriittien, meimechiittien, pikrobasalttien ja basalttien – geokemiaa ja petrologiaa. Nämä suureksi osaksi aikaisemmin tuntemattomat kivet leikkaavat juonina Karoon suuren magmaprovinssin laakiobasaltteja, jotka purkautuivat jurakaudella noin 180 mil-

joonaa vuotta sitten Gondwana-supermantereen repeämisprosessin alkuvaiheiden aikana. Valikoiduista näytteistä (yhteensä 31 vähintään yhdestätoista juonesta) analysoitiin mineraalien koostumuksia sekä pääalkuaine-, hivenalkuaine-, ja Sr-, Nd-, Pb- ja Os-isotooppikoostumuksia.

Analysoidut näytteet voidaan jakaa hivenalkuaine- ja isotooppikoostumuksensa perusteella kahteen magmatyyppiin: (1) Köyhtynyt magmatyyppi (24 näytettä vähintään yhdestä juonesta) on köyhtynyt sopeutumattomimmista alkuaineista ja muistuttaa isotooppikoostumukseltaan valtamerten keskiselänteiden basaltteja; (2) Rikastunut magmatyyppi (7 näytettä vähintään kahdesta juonesta) on suhteellisen rikastunut sopeutumattomimmista alkuaineista ja muistuttaa hivenalkuaine- ja isotooppikoostumukseltaan merellisten saarten basaltteja. Kumpikaan magmatyyppi ei ole merkittävästi saastunut kuorellisella aineksella.

Köyhtynyt magmatyyppi on peräisin hyvin MgO -rikkaista (jopa 25 p. %) kantasulista, jotka muodostuivat Karoon päävaiheen aikana korkeissa vaipan lämpötiloissa ($>1600 \text{ }^\circ\text{C}$) ja paineissa (n. 5–6 GPa) pääosin vesipitoisesta, köyhtyneestä ylävaipan peridotiitista. Rikastuneen magmatyyppin lähteenä ovat vaipan heterogeeniset pyrokseenipitoiset komponentit, jotka muodostuivat joko subduktoituneen merellisen kuoren reagoidessa vaipan peridotiitin kanssa tai sulametasomatoosin seurauksena.

Geokemiallisen mallinnuksen perusteella monet litosfäärin aineksilla saastuneista Karoon laakiobasalteista ovat saaneet alkunsa samasta vaippalähteestä kuin köyhtynyt magmatyyppi. Tästä lähteestä ovat todennäköisesti peräisin myös isotooppikoostumukseltaan hyvin samankaltaiset Intian Valtameren keskiselänteen basaltit. Nämä havainnot ja köyhtyneelle magmatyy-

pille arvioidut korkeat lähdelämpötilat viittaavat siihen, että Karoon laakiobasaltit saivat suurimaksi osaksi alkunsa Gondwana-supermantereen alaisen vaipan sisäisen lämpenemisen, ei niinkään ylävaippaan tunkeutuneen syvän vaippapluumin, seurauksena.

Tutkimukseni tukee näkemystä siitä, että ferropikriittiset sulat voivat syntyä monin eri tavoin: poikkeuksellisen korkea rautapitoisuus saavutetaan todennäköisimmin, jos lähdemateriaali vaipassa sulaa (1) alhaisella

asteella (2) ja/tai korkeassa paineessa ja/ tai (3) lähdemateriaali sisältää rikastuneita komponentteja (esim. pyroksemiittia tai metasomatoitunutta peridotiittia). On kuitenkin huomionarvoista, että ferropikriittinen kokokivikoostumus voi olla myös seurausta akkumulaatiosta, sekundaarisesta muuttumisesta tai fraktioivasta kiteytymisestä, ja erityistä huomiota on siksi kiinnitettävä kantamagman koostumuksen määrittämiseen.

Acknowledgements

This work could not have been completed without the assistance and support of numerous individuals and organizations. For an individual like me, the odds for remembering to mention them all are short. I try my best.

First of all, my chief supervisor Arto Luttinen deserves my lifelong gratitude for his dedication to this project. He contributed significantly to my understanding of the complexity of petrological processes as well as to the quality of my scientific writing skills. He was the driving force in the front line with me and his devotion and enthusiasm as my mentor are things I will never forget. My second supervisor and AMANDA project director Tapani Rämö also has had a significant impact on my work. Despite being busy also with several other projects, he always had time to answer my questions and assist on planning my next moves. He is also held responsible for initially lighting up my interest in igneous petrology during my first semester as an undergraduate student. Yrjö Kähkönen deserves my gratitude for introducing me into handling and interpreting geochemical data during the time I worked on my Master's thesis.

I am very grateful to the Academy of

Finland, Finnish Graduate School in Geology, and University of Helsinki from which I received the funding for my research. Academy of Finland was the primary financial supporter from March 2006 to the end of 2009 (grant no. 210640) and with the financial help of Finnish Graduate School in Geology and University of Helsinki I was able to complete this project. I was fortunate to get my thesis reviewed by experts on the subject: Eero Hanski and Teal Riley are thanked for their constructive and encouraging comments on the original manuscript.

During the course of this project, I made an unforgettable field trip to Antarctica. The Finnish Antarctic Expedition Program, Finnish Marine Research Institute (now defunct), and Antarctic Logistics Centre International are recognized with a gratitude for organizing and providing logistics for the 2007 expedition. FINNARP 2007 crew comprising Mika Kalakoski, Ilona Romu, Teppo Mäkelä, Jari Pitkänen, Kaius Kaartinen, Aki Virkkula, Milla Johansson and Juha Taskinen as well as Sheila Kirkwood and Ingemar Wolf of SWEDARP 2007/08 party provided the basis for a highly successful field season. Ilona was especially important companion when mapping and

interpreting the geological features of Vestfjella. I was lucky to have her and Mika accompany me during a three-day snow storm that demolished our mess tent in the middle of nowhere. Petri Heinonen, Eivor Lahtinen, Janne Tikkinen, and Juhani Ollila provided domestic support and important advices prior to and during the expedition. Mika Räisänen and Henrik Grind, who were part of the earlier FINNARP expeditions, are also thanked for providing some of the samples for my studies.

Diane Cornelius, Charles Knaack, and Richard Conrey of the GeoAnalytical Lab of the Washington State University provided high quality XRF and ICP-MS analyses and Bo Johanson, Lassi Pakkanen, and Marjaleena Lehtonen of the Geological Survey of Finland (GTK) provided invaluable help with the mineral chemical analyses. Hannu Huhma, Tuula Hokkanen, and Arto Pulkkinen are hugely thanked for being mostly responsible for the isotopic analyses made at the GTK. I also had an opportunity to work at the Department of Terrestrial Magnetism (Carnegie Institution of Washington), one of the finest and most advanced geochemical laboratories on the globe. Richard Carlson guided me into the world of isotopic analyses and was an influential character along with Carnegie fellows Steven Shirey, Matt Jackson, Mary Horan, and Timothy Mock, who provided assistance and support during my stay there. I also warmly thank Ann Hawkins for accommodating me during my visit. Juhani Virkanen and Arto Peltola provided important assistance in Finland when I was preparing my samples for the analyses.

I thank the personnel of the Department of Geosciences and Geography (Department of Geology prior to 2010), University of Helsinki for their overall support and assistance. Mia Kotilainen, Kirsi-Marja Äyräs, and Farida Raitso

deserve special thanks for helping me with my bureaucracy disabilities and Mikko Haaramo is thanked for helping with IT-related issues. Matti Poutiainen and Tuija Vaahtojärvi provided technical and laboratory assistance, respectively, and Helena Korkka is thanked for providing me with some very fine quality thin sections.

I would like to warmly thank all my friends (many of whom were already listed above) – the amount of fun I've shared with you outside and inside work is overwhelming. Hilarious (and sometimes even serious) discussions with my workroom mate Aku Heinonen pretty much prevented me from slipping into a coma during long working hours. Special thanks go also to Tommi Karesvuori, who initially introduced me to the exciting world of climbing, and (among many others) shared the experience of embracing every inch of some of the great rock walls sculpted by nature. Finding the way to complete your next move without falling while hanging tens of meters above the ground is certainly one of the best ways to clear your mind out of trivial work-related issues. Besides friends, I would also like to acknowledge some of the greatest punk rock bands, notably NOFX, Lagwagon, Propagandhi, Choke, Raised Fist, A Wilhelm Scream, Wastepaper Basket, and The Offspring, whose music and honesty have greatly influenced my life and way of thinking since my teenage years.

Last but certainly not the least; I am more than thankful for the support I have gotten from my family (Antti, Ulla, and Eero) through the years. They have never questioned my choices and always encouraged me to find my own way in this sometimes uneasy world. And Elina, my dearest, provided invaluable support and understanding. Her smile reminds me of the most important thing in life – I would not have survived without love.

*“Morals are not a substance you can shove in someone’s ear.
They are basically a bi-product of a mind thinking clear.”*

- Mike Burkett (in “The Plan” by NOFX)

Contents

Abstract	3
Tiivistelmä (in Finnish).....	4
Acknowledgements	5
List of original publications	9
Author's contribution	9
Abbreviations	10
List of tables and figures	11
 1 Introduction	 12
1.1 Continental flood basalts – an unsolved mystery	12
1.1.1 The Karoo large igneous province	14
1.2 Ferropicrites – continental messengers from the sublithospheric mantle....	16
1.3 Objectives of this study	21
1.4 Sampling and analytical methods	21
 2 Review of the original publications.....	 21
2.1 Paper I.....	21
2.2 Paper II.....	22
2.2 Paper III	23
 3 Discussion.....	 24
3.1 Petrogenesis of the Vestfjella ferropicrites	24
3.1.1 Depleted type	24
3.1.2 Enriched type	27
3.2 Implications on the origin of the Karoo continental flood basalt province .	28
3.2.1 Geochemical comparisons and petrogenetic relationships	28
3.2.2 The origin of the Karoo flood basalts	31
3.3 Implications on the origin of ferropicrites	32
3.3.1 Ferropicrite whole-rocks vs. ferropicrite melts.....	32
3.3.2 Pyroxenite vs. peridotite source.....	33
3.3.3 Hydrous or anhydrous magmas?.....	38
3.3.4 Mantle thermometry and relation to mantle plumes	39
3.3.5 The origin of the relative Fe enrichment.....	41
 4 Conclusions	 42
 References.....	 43
Appendix I	

List of original publications

This thesis is based on the following peer-reviewed publications:

- I **Heinonen, J.S.** & Luttinen, A.V. (2008) Jurassic dikes of Vestfjella, western Dronning Maud Land, Antarctica: geochemical tracing of ferropicrite sources. *Lithos*, **105**, 347–364.
- II **Heinonen, J.S.** & Luttinen, A.V. (2010) Mineral chemical evidence for extremely magnesian subalkaline melts from the Antarctic extension of the Karoo large igneous province. *Mineralogy and Petrology*, **99**, 201–217.
- III **Heinonen, J.S.**, Carlson, R.W., & Luttinen, A.V. (2010) Isotopic (Sr, Nd, Pb, and Os) composition of highly magnesian dikes of Vestfjella, western Dronning Maud Land, Antarctica: a key to the origins of the Jurassic Karoo large igneous province? *Chemical Geology*, **277**, 227–244.

The publications are referred to in the text by their roman numerals.

Author's contribution

- I: Fully responsible for sample selection, petrographical observations, and geochemical modeling. Mostly responsible for writing, illustrations, and data interpretation.
- II: Fully responsible for sample selection, petrographical observations, geochemical modeling, and controlling the mineral chemical analyses. Mostly responsible for writing, illustrations, and data interpretation.
- III: Fully responsible for sample preparation and geochemical modeling. Mostly responsible for sample selection, writing, illustrations, isotopic analyses, and data interpretation. Minor contribution to field observations and sampling.

Abbreviations

AFC	assimilation-fractional crystallization
cf.	<i>confer</i>
CFB	continental flood basalt
CT1, CT2, CT3, CT4	continental tholeiite magma types of Vestfjella
EC-AFC	energy-constrained assimilation-fractional crystallization
e.g.	<i>exempli gratia</i>
EM	enriched mantle
EPMA	electron probe micro-analyzer
F	degree of melting
HFSE	high field strength element
ICP-MS	inductively coupled plasma mass spectrometry/spectrometer
i.e.	<i>id est</i>
K_d	mineral/melt partition coefficient
K_D	mineral/melt bulk partition coefficient
LILE	large-ion lithophile element
LIP	large igneous province
LOI	loss on ignition (~volatile content)
Ma	million years / million years ago
MORB	mid-ocean ridge basalt
N-MORB	normal mid-ocean ridge basalt
OIB	oceanic island basalt
P	pressure
SCLM	subcontinental lithospheric mantle
T	temperature
T_{ex}	excess potential temperature relative to ambient upper mantle
T_p	mantle potential temperature
TIMS	thermal ionization mass spectrometry
TTG	tonalite-trondhjemite-granodiorite
XRF	X-ray fluorescence

List of tables and figures

Table 1 *Ferropicrites of the world and their characteristics*, page 19

Table 2 *Input parameters for the EC-AFC and AFC models*, page 30

Fig. 1 *Locations of Phanerozoic ferropicrites and LIPs that show CFB characteristics*, page 13

Fig. 2 *Schematic model of flood basalt generation*, page 14

Fig. 3 *Distribution of Mesozoic CFBs in reconstructed Gondwana supercontinent*, page 15

Fig. 4 *Classification and nomenclature for the highly magnesian volcanic rocks*, page 17

Fig. 5 *Variations of FeO_{tot} , Al_2O_3 , TiO_2 , and $(\text{Sm}/\text{Yb})_N$ vs. MgO for ferropicrites*, page 17

Fig. 6 *Ferropicrites shown in $\epsilon_{\text{Nd}(t)}$ vs. t diagram*, page 18

Fig. 7 *Distribution of Jurassic CFBs in western Dronning Maud Land and ferropicrites and associated rocks in Vestfjella*, page 22

Fig. 8 *Geochemical characteristics of Vestfjella ferropicrites and associated rocks shown in FeO_{tot} vs. MgO diagram and La/Sm vs. Sm/Yb diagram*, page 25

Fig. 9 *Clinopyroxene phenocryst chemistry of a Vestfjella depleted ferropicrite, enriched ferropicrite, and meimechite shown in TiO_2 vs. MgO diagram*, page 26

Fig. 10 *Results of lithospheric contamination modeling illustrated in primitive mantle –normalized incompatible element patterns along with representative CT lava compositions*, page 31

Fig. 11 *Geochemical characteristics of ferropicrites compared with peridotite and pyroxenite experimental partial melts and continental picrites and komatiites in FeO_{tot} vs. MgO , CaO vs. Al_2O_3 , and TiO_2 vs. Na_2O diagrams*, page 35

Fig. 12 *Ferropicrites shown in Zn/Fe ($\cdot 10^4$) diagram*, page 37

Fig. 13 *Phanerozoic ferropicrites shown in initial ϵ_{Nd} vs. $^{87}\text{Sr}/^{86}\text{Sr}$, $^{87}\text{Sr}/^{86}\text{Sr}$ vs. $^{206}\text{Pb}/^{204}\text{Pb}$, $^{207}\text{Pb}/^{204}\text{Pb}$ vs. $^{206}\text{Pb}/^{204}\text{Pb}$, and $^{208}\text{Pb}/^{204}\text{Pb}$ vs. $^{206}\text{Pb}/^{204}\text{Pb}$ diagrams*, page 40

Fig. 14 *Ferropicrites shown in logarithmic Nb/Y vs. Zr/Y diagram*, page 41

1 Introduction

1.1 Continental flood basalts – an unsolved mystery

Several times in the history of planet Earth, enormous volumes ($>0.1 \text{ Mkm}^3$) of magma have been emplaced into the crust and on the surface of the Earth far away from major plate boundaries in relatively short periods of time ($\leq 50 \text{ Ma}$; $>75\%$ of total volume within $\sim 5 \text{ Ma}$; Bryan & Ernst 2008). The remains of these catastrophic events have been coined Large Igneous Provinces (LIP). These include oceanic plateaus, ocean basin flood basalts, giant continental dike swarms, silicic LIPs, Archean tholeiite-komatiite associations, volcanic rifted margins, and continental flood basalt (CFB) provinces (Bryan & Ernst 2008). Continental flood basalt provinces (Fig. 1) are of particular importance as their formation commonly preceded or was coeval with continental break-up and their emplacement likely had a significant effect on the contemporary climate and biosphere.

Continental flood basalts have been extensively studied, but their origin is still a matter of considerable debate: a great variety of models have been proposed in order to explain their petrogenesis and geological characteristics (see, e.g., Macdougall 1988; Saunders 2005; Bryan & Ernst 2008). The formation of CFBs was traditionally considered to be controlled by crustal tectonics and/or ambient mantle convection (e.g., Gibson 1966; Clifford 1968; Cox 1978) until Richards *et al.* (1989) suggested that the arrival of the “head” of a lower-mantle-sourced thermal upwelling, i.e., mantle plume (Morgan 1971) onto the base of the continental lithosphere could be responsible for the extensive magma production. The plume hypothesis (to explain CFB origins) was further developed during the 1990’s (e.g., Campbell & Griffiths

1990; Kent *et al.* 1992; Farnetani & Richards 1994; Bercovici & Mahoney 1994), but has been increasingly challenged by recently developed lithosphere-focused models that include decompression melting triggered by delamination (Elkins-Tanton & Hager 2000; Elkins-Tanton 2005), melting of fertile mantle components (Anderson 1994, 2005, 2007) associated with extension (Foulger 2007), and edge-driven convection (King & Anderson 1995, 1998). Furthermore, the Siberian Traps CFB province has been considered by Jones *et al.* (2002) as the result of melting related to an impact of an extraterrestrial projectile. In some models plate tectonic processes are accompanied by mantle plumes (White & McKenzie 1989) and temperature increases in the subcontinental mantle are explained by “passive” processes, such as internal heating of supercontinent-insulated mantle (e.g., Gurnis 1988; Coltice *et al.* 2007). Nevertheless, a central question in the discussion on the CFB origins is whether these huge manifestations of basic magmatism were associated with notable positive thermal anomalies in the subcontinental upper mantle ($T_{\text{ex}} \geq 100 \text{ }^\circ\text{C}$; e.g., Richards *et al.* 1989; White & McKenzie 1989; Johnston & Thorkelson 2000; Thompson & Gibson 2000; Coltice *et al.* 2007) or not ($T_{\text{ex}} \approx 0 \text{ }^\circ\text{C}$; e.g., King & Anderson 1995; Anderson 2000, 2005; Elkins-Tanton 2005; Foulger 2007).

The debate on the origin of CFBs is largely fueled by the lack of knowledge on the parental magmas and mantle sources involved. This stems from the fact that CFBs generally are fairly evolved ($\text{MgO} < 10 \text{ wt. } \%$) and show strong lithospheric geochemical signatures, which hinder the identification of their parental melt compositions and ultimate mantle sources (Fig. 2; e.g., Hawkesworth *et al.* 1992; Hooper & Hawkesworth 1993; Lightfoot *et al.* 1990, 1993; Wooden *et al.* 1993; Pik *et al.* 1999; Luttinen & Furnes 2000; Sano *et al.* 2001; Tommasini *et al.*

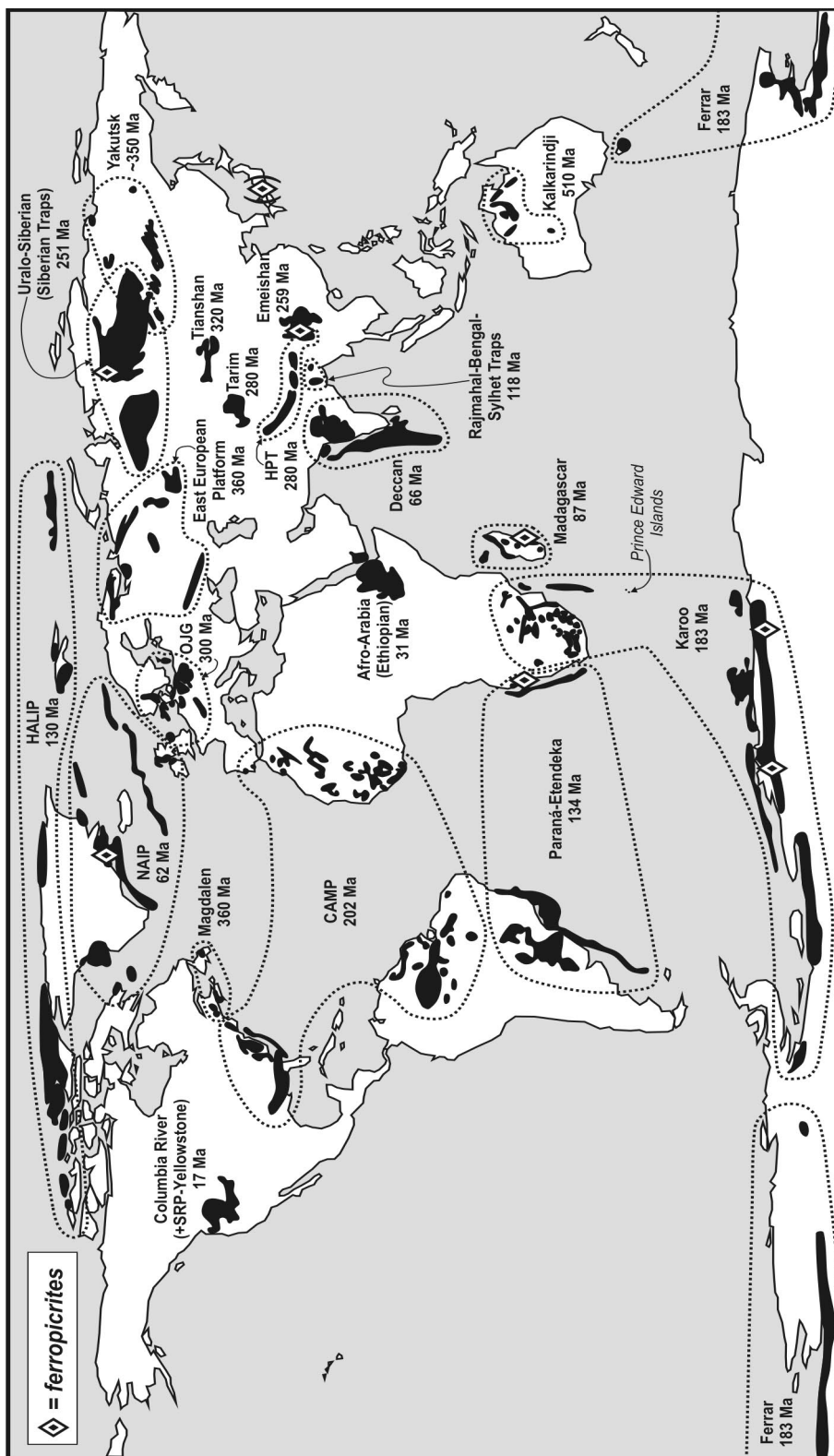


Figure 1. Locations of Phanerozoic ferropicrites and LIPs that show CFB characteristics (after Bryan & Ernst 2008). Prince Edward oceanic island group also shown. Ages denote the onset of the first major magmatic pulse (cf. Bryan & Ernst 2008). HALIP = High Arctic Large Igneous Province; NAIP = North Atlantic Igneous Province; CAMP = Central Atlantic Magmatic Province; OJG = Oslo-Jutland-NE Germany; HPT = Himalaya-Panjal Traps; SRP = Snake River Plain.

2005; Jourdan *et al.* 2007a). Some investigators have even questioned whether sublithospheric sources are needed at all and have suggested that some CFBs may have formed solely by partial melting of lithospheric mantle (e.g., Turner *et al.* 1996). There is also a considerable debate on whether the possible sublithospheric end-member components represent mantle sources

similar to those of mid-ocean ridge basalts (MORBs; derived from ambient depleted upper mantle) and/or ocean island basalts (OIB; derived from anomalous upper mantle or mantle plume) (e.g., Macdougall 1988; Ellam & Cox 1989, 1991; Ellam *et al.* 1992; Menzies 1992; Horan *et al.* 1995; Ellam & Stuart 2000; Peate *et al.* 2003; Carlson *et al.* 2006; Ellam 2006).

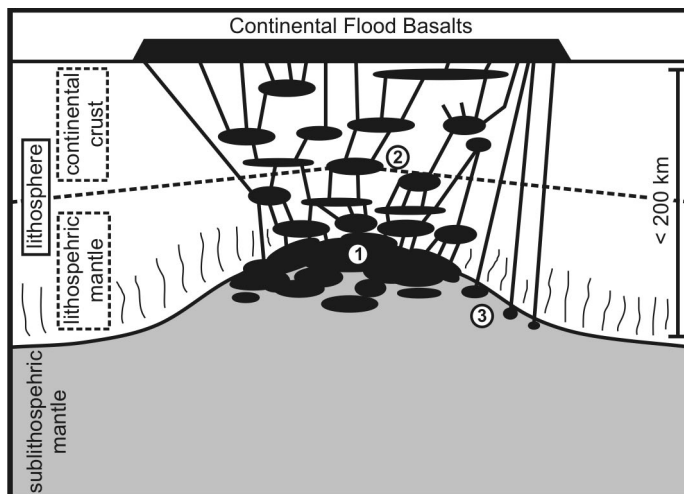


Figure 2. Schematic model of flood basalt generation (cf. Paper III). The parental melts originate in the subcontinental mantle (1) and subsequently evolve, assimilate, and mix in magma chambers within the lithosphere (2). In rare occasions (such as in the case of many ferropicrites), sublithospheric mantle-derived melts avoid lithospheric contamination (3).

1.1.1 The Karoo large igneous province

The Karoo LIP is a Jurassic CFB province that manifests huge outpourings of basaltic magma (up to $2 \times 10^6 \text{ km}^3$; Richards *et al.* 1989) in a developing rift between Africa and Antarctica during the early stages of the breakup of the Gondwana supercontinent (Figs. 1, 3). Other CFB provinces related to the early stages of Gondwana dispersal are the coeval Ferrar CFB province and the Cretaceous Paraná-Etendeka CFB province (Fig. 3). The bulk of the exposed Karoo CFBs are located in southern Africa, but their remnants can also be found in several nuna-

taks of western Dronning Maud Land, Antarctica (Figs. 1, 3). Karoo-related dike swarms and sills are more widespread than the lavas (Fig. 3) and, in places, also areally overlap with contemporaneous Ferrar-type intrusive rocks (Leat *et al.* 2006; Riley *et al.* 2006). The $^{40}\text{Ar}/^{39}\text{Ar}$ datings of Karoo-related rocks indicate that magmatism was active over ~16 Ma (190–174 Ma) with the main volume of mafic magmas being emplaced within ~184–178 Ma (Duncan *et al.* 1997; Zhang *et al.* 2003; Jourdan *et al.* 2005, 2007b; Riley *et al.* 2005).

Most of the Karoo CFBs and related rocks show geochemical evidence of strong litho-

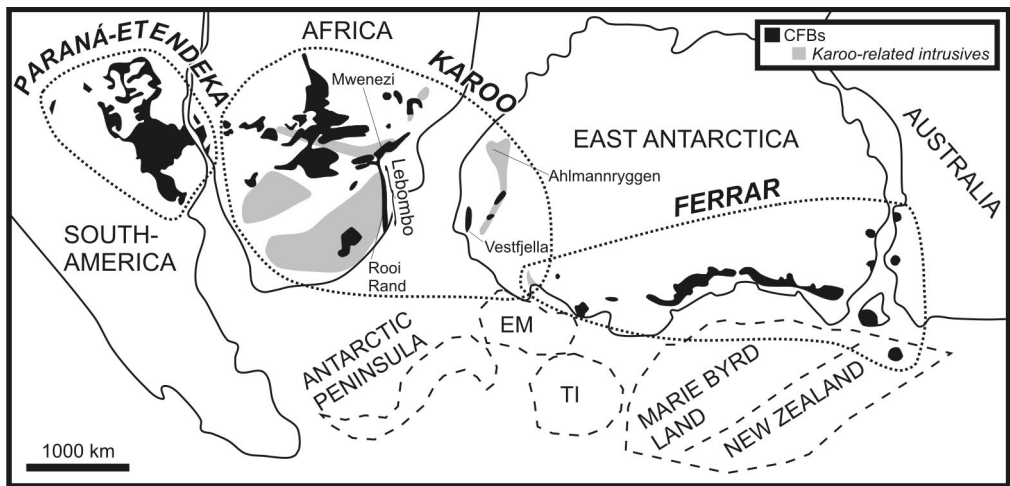


Figure 3. Distribution of Mesozoic CFBs in reconstructed Gondwana supercontinent. In the case of the Karoo province, the known extent of intrusive equivalents (found outside CFBs) is also shown. Reconstruction modified after Hergt *et al.* (1991), Storey *et al.* (1992), Segev (2002), Leat *et al.* (2006), and Jourdan *et al.* (2004). EM = Ellsworth-Whitmore Mountains, TI = Thurston Island.

spheric influence (e.g., Hawkesworth *et al.* 1984; Sweeney *et al.* 1994; Luttinen *et al.* 1998; Luttinen & Furnes 2000; Riley *et al.* 2005; Ellam 2006; Jourdan *et al.* 2007a) and undisturbed sublithospheric magma compositions are rare. Even the most primitive Karoo volcanic rocks found in southern Africa, the Mwenezi picrites (Fig. 3), are characterized by enriched lithospheric geochemical signatures (Ellam & Cox 1989, 1991; Sweeney *et al.* 1991; Ellam *et al.* 1992; Ellam 2006). In southern Africa, some of the MORB-like basaltic dikes of Rooi Rand (Fig. 3) are the only known examples of Karoo rocks that have been thought to preserve sublithospheric mantle-derived compositions (Duncan *et al.* 1990). They have been ascribed to the final stages of Karoo magmatism at ~174 Ma and mark the initiation of ocean floor spreading between Africa and Antarctica (Duncan *et al.* 1990; Watkeys 2002; Jourdan *et al.* 2007b).

Most of the Karoo-related rocks with sublithospheric geochemical affinities have been found within the Antarctic extension of the Karoo LIP. They include MORB-like dikes (CT2 subtype) at Vestfjella (Luttinen & Furnes

2000) and ferropicrite dikes and related rocks at Ahlmannryggen (Group 3; Riley *et al.* 2005) and Vestfjella (OIB-like CT4 magma type; Luttinen *et al.* 1998) (Fig. 3). The ferropicrites of Ahlmannryggen have been dated at ~190 Ma, although with considerable uncertainty, and could thus be related to the initial stages of the Karoo magmatism (Riley *et al.*, 2005). The absolute ages of the uncontaminated mantle-derived magma types of Vestfjella have not been reliably constrained (cf. Zhang *et al.* 2003).

The Karoo province has been at the focus of CFB research throughout the history of modern petrology. Notable studies including those of Cox *et al.* (1965, 1967) and Cox (1970, 1972) and the South African National Geodynamics Programme “Petrogenesis of the Volcanic Rocks of the Karoo Province” (Erlank 1984) laid down the foundations for research of Karoo volcanic rocks and resulted in significant amounts of geochemical data on them. The plume model for Karoo volcanism was first invoked by Burke & Dewey (1972). Richards *et al.* (1989) further considered Karoo CFBs to represent magmas produced by the plume “head” and the Prince

Edward islands in the Indian Ocean (Fig. 1) to manifest the current location of the hotspot and volcanism caused by the subsequent thermal upwelling related to the plume “tail”. The plume model has recently been supported by paleostress and liquidus temperature estimates for some Karoo dikes in Antarctica (Riley *et al.* 2005; Curtis *et al.* 2008). Structural analyses, geochemical affinities, and temporal relationships of the great majority of Karoo-related rocks, however, point to a strong control of lithosphere on the magmatism (Cox *et al.* 1967; Cox 1988; Duncan *et al.* 1984; Ellam & Cox 1989; Sweeney *et al.* 1991, 1994; Luttinen *et al.* 1998; Luttinen & Furnes 2000; Jourdan *et al.* 2005, 2006, 2007a, 2007b), and in many cases, question a plume origin. Recently, rifting associated with prolonged period of internal mantle heating beneath an insulating supercontinent has been also suggested as the dominant cause for the Karoo magmatism (Coltice *et al.* 2009; cf. Silver *et al.* 2006).

1.2 Ferropicrites – continental messengers from the sub-lithospheric mantle

Ferropicrites (Fig. 4) are subalkaline or mildly alkaline primitive rocks that were first described from the Paleoproterozoic Pechenga volcanic belt in Fennoscandia (Hanski & Smolkin 1989, 1995; Hanski 1992). Since then, they have been found to represent a volumetrically minor, yet petrologically fundamental magma type in several other Precambrian volcanic belts that show within-plate affinities (e.g., within Dharwar Craton in India, Onverwacht Group volcanic succession in South Africa, and Slave and Superior Provinces in North America; Table 1; Stone *et al.* 1995; Francis *et al.* 1999; Gibson 2002; Goldstein & Francis 2008) and in Phanerozoic CFB provinces (Karoo, Paraná-Etendeka, North Atlantic Volcanic Province,

Siberian Traps, and Madagascar; Table 1; Fig. 1; Gibson *et al.* 2000; Gibson 2002; Riley *et al.* 2005). Ferropicritic whole-rock compositions have also been published from the Phanerozoic Emeishan CFB province (Zhang *et al.* 2006) and highly magnesian olivine cumulates from a Permian accreted oceanic plateau in Japan have been considered “ferropicritic” in character (Ichiyama *et al.* 2006, 2007) (Fig. 1). Phanerozoic ferropicrites are found as lava flows that represent the lowermost stratigraphic portions of CFB provinces and/or as dikes that crosscut the CFBs and/or the surrounding basement rocks (Table 1; Gibson *et al.* 2000; Gibson 2002; Riley *et al.*, 2005).

The mineral composition of unaltered ferropicrites is dominated by olivine phenocrysts and groundmass consisting of clinopyroxene, plagioclase, and Fe-Ti oxides (e.g., Gibson *et al.* 2000). Igneous amphibole and spinifex textures have also been described from some Precambrian ferropicrites (e.g., Hanski 1992; Hanski & Smolkin 1995; Stone *et al.* 1995, 1997; Fiorentini *et al.*, 2008). In addition to high FeO_{tot} contents, the geochemical characteristics of ferropicrites include relatively low Al_2O_3 , high TiO_2 , high Sm/Yb, and generally positive (depleted) initial ϵ_{Nd} values (Figs. 5, 6).

Ferropicrites, some picrites, and meimechites (Fig. 4) are among the few Phanerozoic continental intraplate volcanic rock types that have been thought to crystallize largely from uncontaminated, sublithospheric mantle-derived near-primary melts (Fig. 2; e.g., Gibson *et al.* 2000; Peate *et al.* 2003; Carlson *et al.* 2006). The geochemical characteristics of ferropicrites and meimechites indicate derivation by lower degree of mantle melting (and/or from more enriched sources) at higher pressures relative to common CFB picrites that originate as more homogenized and voluminous melt patches at lower pressures (Fig. 2; e.g., Arndt *et al.* 1998; Gibson 2002).

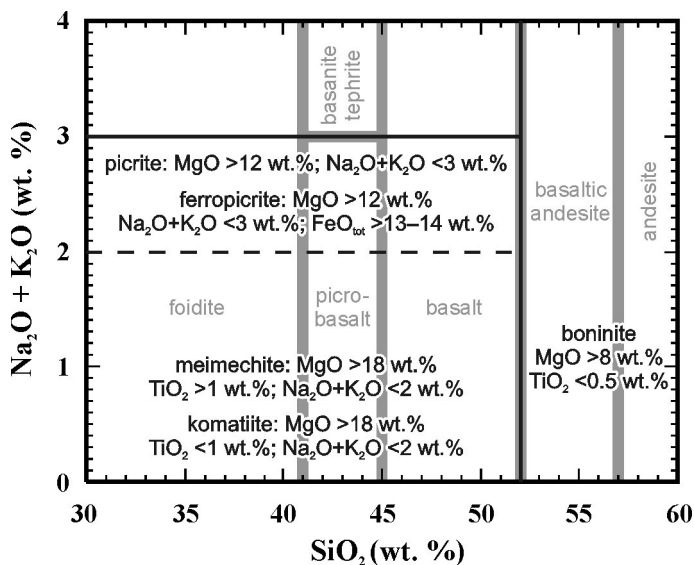


Figure 4. Classification and nomenclature for the highly magnesian volcanic rocks (defined by black lines) after Le Bas (2000), except ferropicrite classification after Hanski & Smolkin (1989), Gibson *et al.* (2000), and Paper I. Total alkali-silica classification scheme for common volcanic rocks (Le Bas *et al.* 1986) shown in gray in the background.

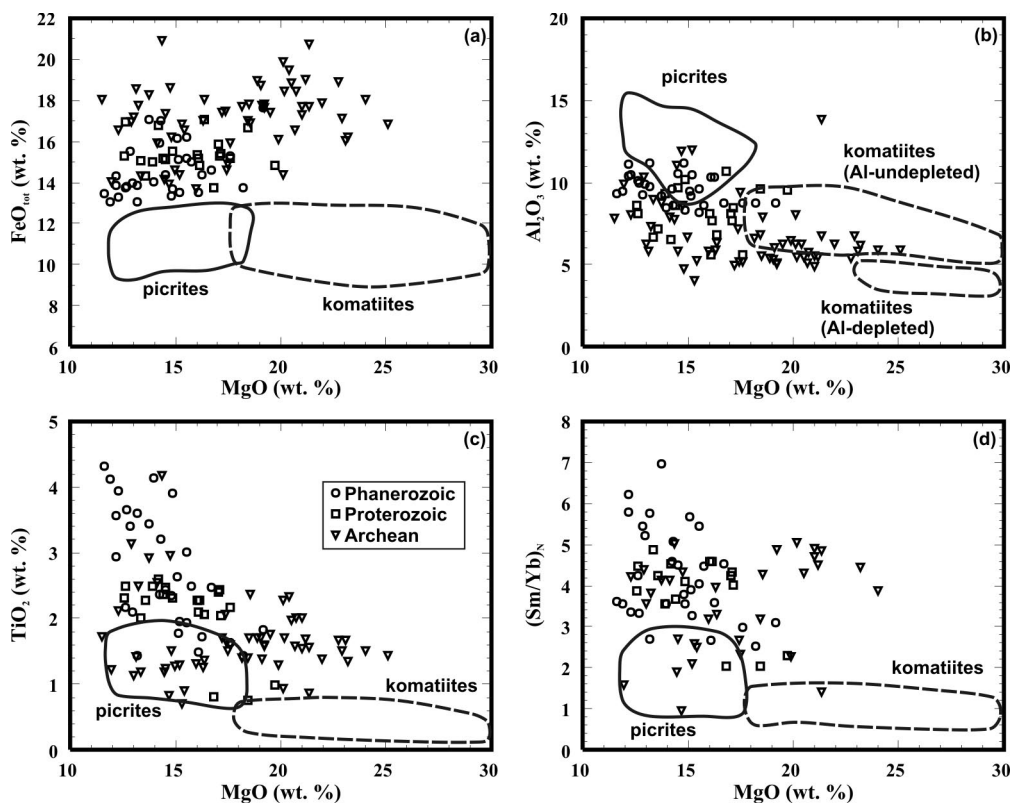


Figure 5. Variations of FeO_{tot} (a), Al_2O_3 (b), TiO_2 (c), and $(\text{Sm}/\text{Yb})_N$ (d) vs. MgO for ferropicrites. Fields for continental picrites and komatiites are shown for comparison (compiled from GEOROC: <http://georoc.mpchmainz.gwdg.de/georoc/>). Legend is shown in c.

Therefore, ferropicrites and meimechites are more likely to sample relatively small-scale heterogeneities and are particularly important in constraining the composition of the subcontinental upper mantle and understanding the origin of CFBs.

Several workers have discussed the mantle sources of ferropicrites. Hanski (1992) and Hanski & Smolkin (1995) were the first to recognize that ferropicrites, such as those found in the Pechenga complex, cannot represent primary melts derived from ambient mantle peridotite at any reasonable pressure. They suggested that the ferropicrite mantle sources were metasomatized by Fe- and incompatible element-enriched low-degree melts shortly prior to the main melting event. Their conclusions were also supported by subsequent studies on Archean ferropicrites (e.g., Stone *et al.* 1995). The expanding dataset of Archean ferropicrites led Francis *et al.* (1999) to suggest that Archean mantle reservoirs were enriched in iron relative to modern mantle. This suggestion was subsequently questioned on the basis of findings of several Phanerozoic ferropicrites, however (Gibson *et al.* 2000; Gibson 2002). Gibson (2002) provided a general petrogenetic model that emphasizes the significance of recycled oceanic crust as a “re-fertilizer” of peridotite in the starting-heads of mantle plumes since the Archean times. Such re-fertilized peridotites would melt at higher pressures relative to ambient mantle and, at CFB settings, thick continental lithosphere would restrict subsequent mixing with larger-fraction picritic melts at lower pressures (Gibson 2002). Analogous models, with recycled eclogite-bearing (Ichiyama *et al.* 2006) or pyroxenitic (Tuff *et al.* 2005) mantle source, have recently been developed for Phanerozoic Fe-rich suites, whereas peridotitic mantle sources have been favored for Precambrian ferropicrites (Goldstein & Francis 2008). In the recycled source models, the relative Fe-enrichment has

been ascribed to partial melting of pyroxenite at high pressures (≥ 5 GPa; Tuff *et al.* 2005) and/or entrainment of relatively Fe-rich subducted oceanic crustal component (Ichiyama *et al.* 2006), whereas in the most recent peridotite source models it has been attributed to melting of primordial, Fe-rich olivine cumulates in the mantle (Goldstein & Francis 2008). In their study on silicate liquid immiscibility, Jakobsen *et al.* (2005) suggested that ferropicrites could also form by mixing of evolved, immiscible Fe-rich liquids with picritic mantle melts.

In addition to discussion on the major element composition and lithological nature of the ferropicrite mantle sources, opinions differ whether these sources were water-bearing (Hanski 1992; Stone *et al.* 1997) or anhydrous (Gibson 2002). Nevertheless, although high water contents have profound implications for the estimated liquidus temperatures of ferropicrite melts (by lowering them), ferropicrites have generally been attributed to anomalously hot mantle sources and mantle plumes (e.g., Hanski & Smolkin 1995; Stone *et al.* 1995; Walker *et al.* 1997; Gibson *et al.* 2000; Gibson 2002; Riley *et al.* 2005; Goldstein & Francis 2008).

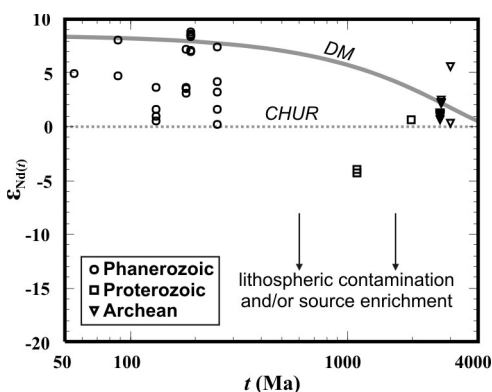


Figure 6. Known ferropicrites shown in $\epsilon_{\text{Nd}(t)}$ vs. t diagram. CHUR (the chondritic uniform reservoir) denotes the evolution of undifferentiated Earth (Wasserburg *et al.* 1981). The evolution path of the depleted mantle (DM) is after DePaolo (1981a). $\epsilon_{\text{Nd}(t)}$ is calculated using chondritic values of $^{143}\text{Nd}/^{144}\text{Nd} = 0.512636$ and $^{147}\text{Sm}/^{144}\text{Nd} = 0.1966$. Data sources are given in Table 1.

Table 1. Known ferropicrites and their characteristics (average CFB picrite and Precambrian komatiite shown for comparison).

Suite and age	Samples	Occurrence	MgO*	FeO _{tot} *	LOI*	Nb/Y	(Sm/Yb) _N [®]	Olivine Fo [§]	Nature [§]	References
NAVP/East										
Greenland	MF91-57b, MF91-57c	basal lava flows	12.2–13.2	13.9	3.5–3.6	?	5.8	?	uncertain	Fram & Leshner 1997
Phan. (65 Ma)										
Madagascar	MAN90-45, MAN90-47	basal lava flows	13.7–15.1	16.1–17.1	3.5–3.6	0.9–1.0	5.7–7.0	?	uncertain	Storey <i>et al.</i> 1997
Phan. (88 Ma)										
Paraná-Etendeka/	97SB63, 97SB73	dike & basal lava	12.2-14.3	14.3-15.9	0.9-1.6	0.9-1.1	4.6-6.2	76-85 (82)	primary	Gibson <i>et al.</i> 2000
Namibia	96SB48, 97SB67,	basal lava flows	12.6-15.5	13.8-15.1	0.2-0.5	0.5-0.7	3.9-4.2	64-81 (67)	cumulate	Gibson <i>et al.</i> 2000
Phan. (132 Ma)	97SB68									
	SMG105, SMG016	basal lava flows	15.2-16.2	13.5-14.4	?	0.6-0.9	3.3-3.6	?	uncertain	Ewart <i>et al.</i> 1998
Karoo/Vestfjella	AL/B14e-98,									
depleted type	AL/B16-98,	two dikes	14.5-16.7	14.4-15.0	1.1-3.8	0.4-0.5	4.5	79-89 (83)	differentiated	Paper I, II
Phan. (180 Ma)	AL/MM1b-98									
Karoo/Vestfjella	AL/B20a-98,									
enriched type	14-KHG-90,	a dike	12.8-15.5	15.5-17.0	2.4-5.5	0.7-0.8	5.1-5.5	78-83 (81)	primary	Paper I, III
Phan. (180 Ma?)	JSH/B006									
Karoo/	Z.1812.1, Z.1812.2,									
Ahlmamnyggen	Z.1812.3, Z.1813.1,	dikes	11.6-14.8	13.1-14.0	0.9-2.6	0.2-0.3	3.3-3.6	70-86 (?)	uncertain	Riley <i>et al.</i> 2005
Phan. (190 Ma?)	Z.1816.2, Z.1817.2									
Siberian Traps/	SG-32 2245.5,	basal lava flows	13.2-18.2	13.1-15.3	7.4-8.4	0.4-1.0	2.7-3.0	72-81? (78?)	cumulate?	Wooden <i>et al.</i> 1993
Gudchichinsky	SG-32 2301,									Lightfoot <i>et al.</i> 1993
Phan. (250 Ma)	SG-32 2332.7, 1F(18)									Olivine: Sect. 3.1.1.
Emeishan/Lijiang	DJ-2, DJ-35	basal lava flows	13.0-14.8	13.4-14.0	4.1-5.2	1.3-1.4	3.8-5.2	?	alkaline?	Zhang <i>et al.</i> 2006
Phan. (250 Ma)	DJ-26	basal lava flow	19.1	17.7	5.2	1.1	3.1	85-88 (86)	primary	Zhang <i>et al.</i> 2006
Average CFB	compilation (n=375)	lavas and dikes	14.7	11.0	2.9	0.6	2.1	commonly	-	GEOROC database ^a
picrite								<90		
Keweenaw Rift	PC-7, PC-8, TK-13	basal lava flows	16.8-19.7	13.7-16.7	?	0.1-0.2	2.0-2.3	?	uncertain	Shirey <i>et al.</i> 1994
Prot. (1100 Ma)										
Pechenga	1-4, Locations: 1Or,									Hanski 1992
complex	2Ki-4Ki, 6Sh-13Sh	basal lava flows	12.5-17.6	14.3-17.0	3.8-11.5	0.8-0.9	3.6-4.9	83-84 (84)**	primary?	Hanski &
Prot. (1980 Ma)	(cf. References)									Smolkin 1995

continued on next page...

Table 1. (continued)

Suite and age	Samples	Occurrence	MgO*	FeO _{tot} *	LOI*	Nb/Y	(Sm/Yb) _N [§]	Olivine Fo [§]	Nature [#]	References
Slave Province/ Lake of the Enemy Arch. (2660 Ma)	EN-3, EN-5, EN-9, EN-12, EN-14, EN-16, EN-18, EN-22	amphibolite lenses within metasediments	12.3-17.4	14.6-20.9	0.7-2.0	0.7-1.2	2.7-5.0	olivine not preserved	primary?	Francis <i>et al.</i> 1999
Western Superior Province/Grassy Portage Bay Arch. (2700 Ma)	GP-1, GP-3 GP-5-GP-9, GP-10-GP-20	amphibolite facies metatuffs within metasediments	14.5-24.0	13.7-19.9	0.8-5.6	0.8-1.1	2.7-4.9	olivine not preserved	primary?	Goldstein & Francis 2008
Western Superior Province/ Lumby Lake Arch. (2700 Ma)	LM-27-LM29, LM-33-LM35, LM-37, LM-42, LM-43	greenschist facies metatuffs relatively high in the stratigraphy	11.5-25.1	16.2-20.8	1.0-14.3	0.4-1.8	1.4-4.8	olivine not preserved	primary?	Goldstein & Francis 2008
Western Superior Province/ Boston Creek Flow Arch. (2720 Ma)	1-J29, 1-36, 1-43	metatuffs (basal?)	13.0-15.4	16.6-17.2	3.3-4.8	0.6-0.8	2.5-3.5	olivine not preserved	primary?	Stone <i>et al.</i> 1995
Kolar Schist Belt (India) Arch. (2900 Ma)	13-4, 17-10, 18-10, 19-7, 23-9	amphibolite facies metatuffs	14.5-19.9	13.9-16.1	?	0.2-0.4	1.0-2.3	olivine not preserved	primary?	Rajamani <i>et al.</i> 1985
Western Superior Province/ Steep Rock belt Arch. (3000 Ma)	SR-1, SR-3-SR-7, SR-17, SR-26-SR-28, SR-30, SR-48	greenschist facies basal metatuffs	14.8-22.8	15.9-19.0	5.7-13.5	1.1-1.6	4.5-5.0	olivine not preserved	primary?	Goldstein & Francis 2008
Onverwacht Group (S Africa) Arch. (3500 Ma)	5048-5050	basal metatuffs	12.0-20.1	14.0-14.4	0.5-3.5	0.2-0.3	1.6	olivine not preserved	primary?	Jahn <i>et al.</i> 1982
Average Prec. komatiite	compilation (n=897)	metavolcanic rocks	24.7	10.9	5.9	0.2	1.2	<95 (rare)	-	GEOROC database ^a

* MgO, FeO_{tot}, and LOI (loss on ignition) given in wt. %. [§] Normalized to chondrite of McDonough & Sun (1995). [§] Range of core compositions and average (in parentheses);** olivines found in associated sills. [#] Primary nature of the suites assessed (cf. Section 3.3.1; Paper I). ^a <http://georoc.mpch-mainz.gwdg.de/georoc/>.

1.3 Objectives of this study

The Karoo-related ferropicrites of Vestfjella were first described by Luttinen *et al.* (1998) and Luttinen & Furnes (2000) as the CT4 magma type, one of the four Karoo “continental tholeiite” magma types of the Vestfjella area. The main emphasis in these studies was on the abundant lithosphere-signatured lava flows (CT1–CT3) and CT4 was only superficially treated as a rare occurrence of OIB-like volcanic rocks, possibly derived from a mantle plume. The subsequent realization of their anomalously high Fe contents and findings of previously unknown ferropicrites with relatively depleted, more MORB-like incompatible trace element composition (Luttinen & Huhma 2005) were the initial sparks for my Ph.D. study, which I started after finishing my M.Sc. studies in March 2006.

Given the overall rarity of primitive, sublithospheric mantle-derived volcanic rocks related to CFB provinces, my main goals were to provide high precision geochemical, mineral chemical, and isotopic data on these rare rocks and their differentiates, define the nature of their mantle sources, and find answers to the greatly discussed origins of Karoo CFBs and ferropicrites in general.

1.4 Sampling and analytical methods

This study is based on field observations and petrographical and geochemical analysis of 31 whole-rock samples from at least eleven dikes (some samples have been collected from dike-derived boulders). The field observations were made and the samples were collected during several Antarctic expeditions between 1990 and 2007; a detailed map of the study area with sampling locations is given in Fig. 7.

Major and trace element data presented in Papers I and III have been obtained with X-ray

fluorescence spectrometer (XRF) and inductively coupled plasma mass spectrometer (ICP-MS) at the GeoAnalytical Laboratory of the Washington State University. In addition to Paper I, detailed descriptions of the GeoAnalytical Laboratory procedures are given in Johnson *et al.* (1999) and Knaack *et al.* (1994), respectively. Mineral chemical major element data presented in Papers I–III have been obtained with electron probe micro-analyzer (EPMA) by using five wavelength-dispersive spectrometers (at the Geological Survey of Finland; Paper II, III) or one energy-dispersive spectrometer (at the Department of Earth Sciences, University of Cambridge; Paper I). Operation conditions and statistical data for the microprobes are given in Papers I and II. Isotopic data have been obtained by using thermal ionization mass spectroscopy (TIMS) at the Unit for Isotope Geology, Geological Survey of Finland (for Sr and Nd; Papers I and III) and by using TIMS and ICP-MS at the Department of Terrestrial Magnetism, Carnegie Institution of Washington (for Sr, Nd, Pb, and Os; Paper III). Detailed descriptions of the analytical methods are given in Papers I and III, respectively.

2 Review of the original publications

2.1 Paper I

Paper I provides field, petrographic, and whole-rock geochemical descriptions of the ferropicrite dikes and associated rocks of Vestfjella and discusses the nature of their mantle sources. In addition, olivine mineral chemical data are presented for two ferropicrite samples. On the basis of trace element and isotopic composition, the ferropicrites are divided into two distinct groups: (1) The relatively depleted type exhibits

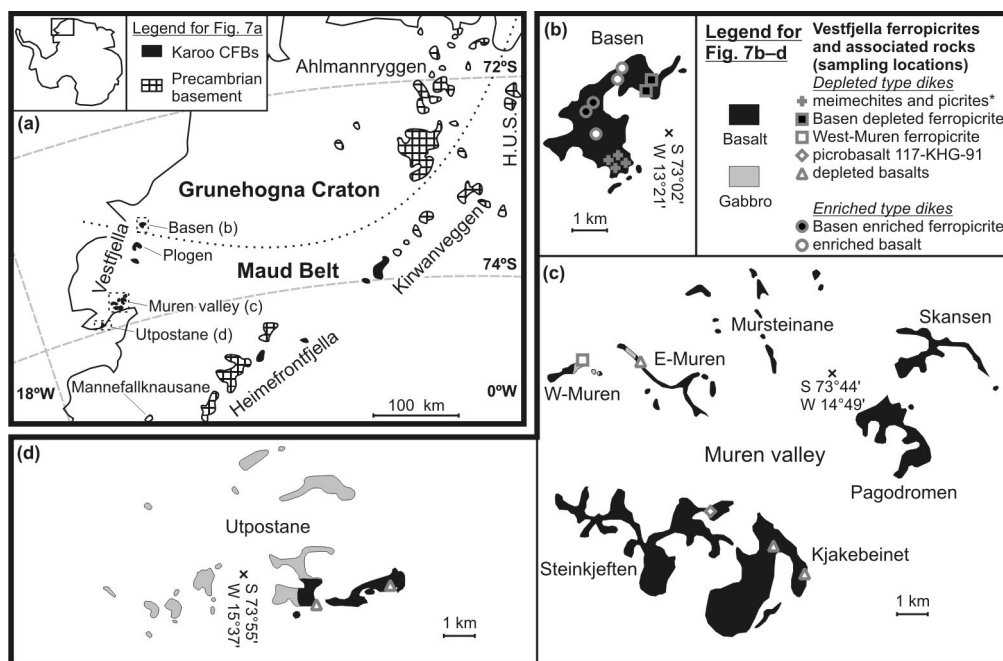


Figure 7. Distribution of Jurassic CFBs in western Dronning Maud Land (a) and ferropicrites and associated rocks (sampling locations shown) in Vestfjella (b-d). Lithospheric boundary between Archean Grunehogna craton and Proterozoic Maud Belt in (a) is after Corner (1994). H.U.S. = H. U. Sverdrupfjella. * Meimechites and picrites are only found as dike-derived boulders.

chondrite-normalized $(\text{La}/\text{Sm})_{\text{N}}$ of 1.2–1.3 and $(\text{Sm}/\text{Yb})_{\text{N}}$ of 4.5, and initial ϵ_{Sr} from -18 to -19 and ϵ_{Nd} from +7 to +8 (at 180 Ma); (2) The relatively enriched type (CT4 magma type of Luttinen *et al.* 1998) exhibits chondrite-normalized $(\text{La}/\text{Sm})_{\text{N}}$ of 1.7 and $(\text{Sm}/\text{Yb})_{\text{N}}$ of 5.1–5.4, and initial ϵ_{Sr} from 0 to +1 and ϵ_{Nd} from +3 to +4. Geochemical modeling and the presence of relatively Mg-rich olivine phenocrysts (Fo_{79-88}) indicate that at least the depleted ferropicrites are likely to represent near-primary mantle melts that have largely avoided lithospheric contamination and derive from anomalous hot mantle sources. The meimechite ($\text{MgO} > 18$ wt. %) and basalt ($\text{MgO} \leq 10$ wt. %) samples are considered as cumulates and differentiates from ferropicritic magmas, respectively. The relatively high Fe and Ti contents and oceanic island picrite- and OIB-like trace element signatures of the ferropicrites are considered to indicate derivation

from recycled, pyroxenitic mantle sources. On the basis of the unusually high primitive-mantle-normalized $(\text{V}/\text{Lu})_{\text{N}}$ of the depleted ferropicrites (1.9–2.2), the recycled component in their case is thought to comprise oceanic Fe-Ti gabbros. Global comparison reveals that many samples described as ferropicrites in the literature may in fact represent olivine cumulates or altered alkaline rocks and not crystallized equivalents of exceptionally Fe-rich subalkaline melts. High $(\text{V}/\text{Lu})_{\text{N}}$ appears to be a characteristic feature of several ferropicrites and is thought to indicate that Fe-Ti gabbro component was prevalent in the mantle sources of such suites.

2.2 Paper II

Paper II concentrates on the mineral chemistry (~400 EPMA analyses) of four depleted meimechite samples of Vestfjella, and their

petrological implications. For comparison, mineral chemical data are also provided for two samples from a depleted ferropicrite dike. Two of the meimechites are characterized by “picritic” olivines (Fo_{84-85}) and they obviously represent cumulates from picritic magmas (cf. Paper I). The other two meimechites, however, are characterized by olivines that show extremely high Fo contents (Fo_{90-91} ; up to Fo_{92}). These olivines are euhedral to subhedral, exhibit high CaO (≥ 0.19 wt. %), and contain Ti-rich (volcanic) spinel inclusions, and are thus considered likely to represent true phenocrysts and not xenocrysts from mantle peridotite. Moreover, the presence of igneous amphibole as inclusions in these olivines is thought to indicate that the olivines crystallized from magmas that had H_2O contents of $\sim 1\text{--}2$ wt. %. Calculations based on olivine-liquid equilibria indicate that the meimechite parental magmas were very MgO-rich (up to 25 wt. %) and derived from extremely hot mantle sources ($T_p > 1600^\circ\text{C}$)¹ compatible with the plume theory. The highly magnesian nature of the meimechites and their geochemical and mineral chemical similarity to the depleted ferropicrites casts doubt on the previously purported pyroxenite origins for the depleted magma type (cf. Paper I) and, instead, suggest dominantly peridotitic sources for them. Major and trace element comparisons with other highly magnesian Phanerozoic magma types reveal similarities between the Vestfjella meimechites, meimechites from the Siberian Traps LIP, and the purported komatiite parental melts associated with the Paraná-Etendeka LIP, and indicate their derivation from broadly similar sources and/or by similar melting processes in anomalously hot sublithospheric mantle.

¹ T_p is the temperature a parcel of mantle would have if it were adiabatically expanded to pressure of 1 kbar (McKenzie & Bickle 1988).

2.3 Paper III

Paper III presents high-precision whole-rock isotope (Sr, Nd, Pb, and Os) geochemical data on the meimechites, ferropicrites, and associated rocks of Vestfjella ($n = 8$), and progresses on to place tighter constraints on their mantle sources and interpret implications on the origins of the Karoo LIP and the breakup of the Gondwana supercontinent. Additional reference datasets are presented for samples of CT1, CT3, and MORB-like Low-Nb magma types of Vestfjella ($n = 5$). Major and trace element whole-rock geochemical data and olivine mineral chemical data are also provided for a relatively fresh sample of the enriched ferropicrite dike. The isotopic data confirm that, unlike most of the Karoo magmas, the depleted ferropicrites and associated rocks have not been significantly contaminated by lithospheric materials. Their isotopic signature is indistinguishable from that of SW Indian Ridge MORB and the MORB-like Low-Nb type dikes of Vestfjella. This implies derivation from long-term depleted upper mantle sources and cast doubt on their previously purported plume origin (cf. Paper I, II). The enriched ferropicrites and associated rocks are likely to sample pyroxenitic heterogeneities (cf. Paper I). Whether this source was present in the lithospheric mantle (e.g., as metasomatic veins) or sublithospheric mantle (e.g., as veins or recycled lithospheric materials) remains an open question. The overall isotopic similarity to EM-signatured OIBs could indicate a recycled component with up to $\sim 15\%$ of sedimentary material. Given the probability that the enriched type and especially the depleted type were derived from anomalously hot upper mantle sources, the recently introduced internal heating model of the upper mantle beneath a supercontinent (Coltice *et al.* 2007, 2009) is considered to be the most likely cause for the generation of the Karoo LIP.

3 Discussion

3.1 Petrogenesis of the Vestfjella ferropicrites

In this section, I analyze and summarize the interpretations on the origin of the Vestfjella ferropicrites (Paper I–III) and present some further views that were not considered in the original papers. All the available data support the division of the Vestfjella ferropicrites and related rocks into relatively depleted and enriched types that sampled distinct mantle sources (Paper I–III). Accordingly, I treat them separately in two subsections.

3.1.1 Depleted type

One of the most important findings on the depleted type ferropicrites was that they do not represent undifferentiated mantle melts, as ferropicrites often are presumed to do (cf. Paper I), but likely were derived by olivine fractionation from even more magnesian meimechitic parental melts (Paper II). The geochemical and isotopic modeling indicates that these parental melts originated from hydrated Indian Ridge MORB-source upper mantle peridotite at high pressures (~5–6 GPa) and temperatures ($T_p > 1600$ °C) (Paper II, III). Preliminary ^{40}Ar – ^{39}Ar age data for three ferropicrite-related basaltic dikes (Kurhila *et al.* 2008; A. V. Luttinen *et al.* in prep.) are compatible with interpretations that imply crystallization of depleted type magmas during the main phase of Karoo magmatism at ~180 Ma (cf. Paper III).

The depleted type has been treated as a largely coherent magma type (Paper I–III), but there are indications that some of the dikes may have crystallized from separately evolved melt batches. For example, the relatively large within-group

variations in FeO_{tot} , La/Sm, and Sm/Yb ratios are difficult to explain solely by differentiation (e.g., olivine-fractionation and contamination), but rather require differences in mantle melting conditions (Fig. 8). At least three subtypes that likely derive from distinct highly magnesian parental magmas can be distinguished: (1) meimechites and picrites (and possibly also depleted basalts), (2) the Basen ferropicrite, and (3) the West-Muren ferropicrite (Fig. 8). These observations along with the overall undifferentiated nature of the rocks imply that the most primitive magmas did not become significantly mixed or homogenized in large crustal magma chambers, but rather intruded as relatively fast-moving separate magma pulses in a way somewhat similar to kimberlitic magmas (cf. Paper II). On the other hand, relatively wide within-sample variations in olivine phenocryst compositions (Paper II), reversely zoned olivines in the West-Muren ferropicrite (Paper I; cf. Appendix I) and rare, resorbed, and oscillatory zoned clinopyroxenes in cumulate meimechite sample AL/B5-03 (Fig. 9) indicate that minor mixing took place in some of the individual magma feeding channels. In addition, the relatively large within-sample variations in spinel inclusion compositions (Paper II) could be ascribed to magma mixing, but they may also well record post-entrapment modification and re-equilibration with associated melt droplets (cf. Kamenetsky *et al.* 2001). Nevertheless, the aforementioned evidence on magma mixing indicates that although magma ascent velocities likely were high (cf. Section 3.3.3), the nature of the ascent may have been pulsating, thus allowing some mixing of cogenetic magmas in early stages of differentiation (cf. Larsen & Pedersen 2000). Importantly, sample AL/B5-03 with evidence of mixing of clinopyroxene-saturated (although still relatively MgO-rich; cf. Fig. 9) magmas has not been used in the parental melt calculations (cf. Paper II).

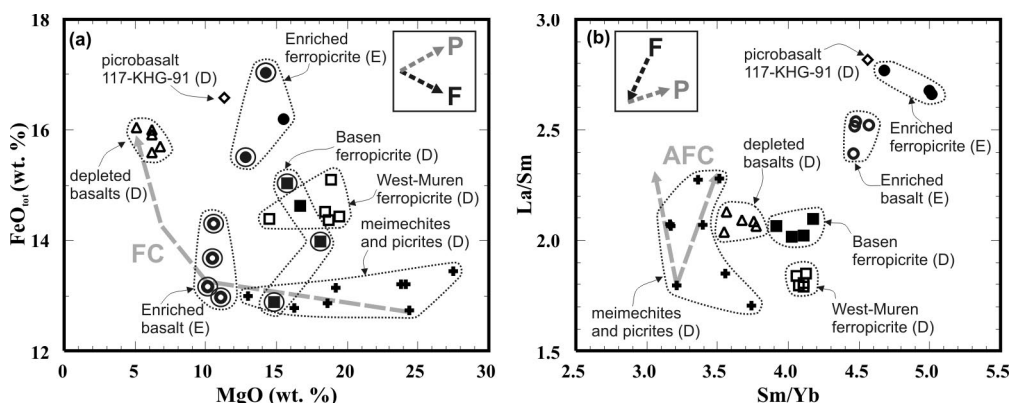


Figure 8. Geochemical characteristics of Vestfjella ferropicrites and associated rocks shown in (a) FeO_{tot} vs. MgO diagram and (b) La/Sm vs. Sm/Yb diagram. Highly altered samples ($\text{LOI} > 3$ wt. %) are encircled in (a); D = depleted types; E = enriched types. Fractional crystallization model (FC) as in Paper I, but with sample AL/B9-03 as a starting composition. Assimilation-fractional crystallization modeling (AFC; $r = 0.5$) performed by using lamproite (AL/KB8-98; Luttinen *et al.* 2002) and average upper continental crust (Rudnick & Gao 2003) as contaminants. Effects of pressure (P) and degree of melting (F) estimated on the basis of the experiments of Walter (1998) and Adam & Green (2006).

Although the major element and isotopic compositions of the depleted type indicate derivation from depleted upper mantle peridotite, comparison of the Vestfjella data with experimental results on peridotite partial melting reveal some minor discrepancies related to minor and trace elements. Firstly, the TiO_2 contents of the depleted type (> 1 wt. % in the parental melts; Paper II) are higher than in partial melts of KLB-1 peridotite (estimated to correspond to depleted MORB-source) even at very low degrees of melting (< 1 wt. % in general; cf. Herzberg & Zhang 1996). However, Ti is not enriched in our samples relative to other similarly incompatible elements (e.g., Eu and Gd; cf. Paper I), indicating a general enrichment in all incompatible elements relative to KLB-1 partial melts. I provide five alternative explanations for this discrepancy: (1) The peridotitic source is not as depleted in incompatible elements as KLB-1; for example, partial melting experiments on fertile (“pyrolitic”) garnet peridotite have resulted in partial melt TiO_2 contents up to 1.7 wt. % at ~ 10 % of melting (Walter 1998); (2) The peridotitic source contains subordinate pyroxenite components; (3) The peridotitic source has

been enriched by metasomatic fluids. This had to happen relatively shortly before melt generation or otherwise it would likely have affected the isotope systematics; (4) The incompatible trace element characteristics have been inherited from very low-degree, high-pressure initial peridotite partial melts, whereas the major element compositions reflect subsequent more extensive melting processes at lower pressures (McKenzie 1985; Saunders *et al.* 1988); (5) The presence of water affected the partial melting process by decreasing K_D values (e.g., Gaetani *et al.* 2003) thus resulting in high incompatible element concentrations in the partial melts. It should be noted that the Indian Ridge MORB do not represent N-MORB, but show relatively enriched compositions indicative of possible subordinate enriched source components in the upper mantle beneath Indian Ocean (e.g., Janney *et al.* 2005; Nishio *et al.* 2007); importantly, Indian Ocean MORB and the Vestfjella depleted type are both characterized by similar mild enrichments in large-ion lithophile elements (LILE) (Paper III). Bearing this in mind, none of the aforementioned alternatives is in discordance with the purported ambient upper mantle source for the depleted type.

One problem highlighted in Paper III is that the mantle potential temperatures calculated for the depleted type parental magmas ($T_p \approx 1640$ – 1700 °C; Paper II) exceed those predicted by the internal mantle heating model (~ 1600 °C at maximum; Coltice *et al.* 2007). Temperature calculations in Paper II were based on olivine-liquid equilibration following the method of Putirka *et al.* (2007), but here I also performed additional thermobarometric modeling by using the method of Lee *et al.* (2009). The advantage of this method is that it can be utilized on any subalkaline whole-rock that represents olivine-controlled melt composition derived from a peridotitic mantle source. By using the samples AL/WM1b-98, AL/B16-98, and AL/B9-03 as the melt compositions (cf. Paper I, II), altering the H_2O^{liq} between 1 and 2 wt. % (cf. Paper II), and assuming depleted (KLB-1; Davis *et al.* 2009) or fertile (KR4003; Xue *et al.* 1990) peridotite as the source material, the method results in T_p values ranging from 1630 to 1740 °C and pressures from 4 to 7 GPa. The minimum temperatures are marginally lower compared to those calculated in Paper II and were attained with $H_2O^{liq} = 2$ wt. % and fertile peridotite source. The fertile peridotite source alternative is particularly important as it may correspond to the possible entrainment of subordinate enrichments (cf. above) that are likely to decrease the solidus temperatures. It should also be noted that the estimated errors of the methods of Lee *et al.* (2009) and Putirka *et al.* (2007) are ~ 3 % and ~ 5 % that correspond to T_p variations of ~ 48 and ~ 80 °C at 1600 °C, respectively. One additional factor that could lower the calculated temperatures and has not been considered is the CO_2 content of the parental magma. There is growing evidence that carbonated peridotites may comprise a significant source component for the alkaline OIBs (e.g., Dasgupta *et al.* 2006, 2007). In addition, CO_2 has been suggested to be involved in the

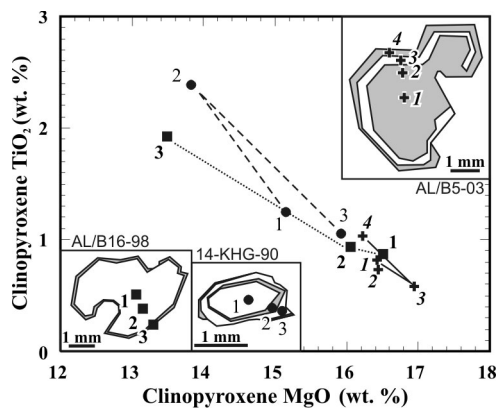


Figure 9. Clinopyroxene phenocryst chemistry of a Vestfjella depleted ferropicrite (AL/B16-98), enriched ferropicrite (14-KHG-90), and meimechite (AL/B5-03) shown in TiO_2 vs. MgO diagram. The phenocryst in 14-KHG-90 represents a part of a glomerocryst ($\varnothing \approx 6$ mm). Data from Paper II and Appendix I.

petrogenesis of the meimechites of the Siberian Traps and lower the melt origination temperatures on the order of 100–150 °C (Elkins-Tanton *et al.* 2007). The overall subalkaline character of the depleted type and the absence of associated carbonatites do not indicate marked mantle CO_2 influence in the case of Vestfjella, however (cf. Gibson *et al.* 2000; Elkins-Tanton *et al.* 2007). In summary, it seems that the Vestfjella depleted type is difficult to explain without an involvement of a significant thermal anomaly ($T_p > 1600$ °C) in the sub-Gondwanan upper mantle (cf. Paper II).

Overall, the depleted type was a challenging magma type to study. As more and more data came available during the course of this project, some of the original fundamental hypotheses on their origin were subjected to significant revisions. In Paper I, the depleted type was thought to originate by plume-induced partial melting of pyroxenite sources that entrained significant amounts of recycled oceanic Fe-Ti gabbros. In Paper II, the mineral chemical data indicated that the depleted type actually had fractionated from highly magnesian parental magmas that were derived from dominantly peridotitic, instead of

pyroxenitic, mantle sources. Paper III presented isotopic evidence on the upper mantle origin of the depleted type and thus questioned its plume origin (cf. Paper I, II). The depleted type may be considered a prime example of how scientific knowledge is revised and refined on the basis of new – and sometimes unexpected – findings.

3.1.2 Enriched type

In contrast to the depleted type ferropicrites, there are no indications of highly magnesian parental magmas for the enriched type ferropicrites. Their relatively low MgO contents, high FeO_{tot} and TiO_2 contents, and enriched OIB-like trace element and isotopic signatures are all compatible with their derivation from pyroxene-rich (recycled?) mantle source (Paper I, III).

Similar to the depleted type, the enriched type dikes also show relatively large differences in FeO_{tot} contents and La/Sm and Sm/Yb ratios suggesting that they evolved as two separate magmatic systems. Generalizing, the higher FeO_{tot} , La/Sm, and Sm/Yb of the enriched ferropicrite suggest derivation by lower degree of melting and from more garnet-rich mantle relative to the enriched basalt (Fig. 8). Although one enriched ferropicrite sample contains a glomerocryst of oscillatory zoned clinopyroxene (and minor altered olivine) that could indicate magma mixing (Fig. 9), the absence of such glomerocrysts and other mixing-related textures in all the other samples and the overall compositional homogeneity of the olivine population (Paper III) indicate that the geochemical effect of possible mixing processes has been negligible.

The implication of pyroxene-rich source notably hinders assessment of the physical conditions of mantle melting (e.g., P , T_p), because the available models are only compatible with peridotite sources (e.g., Putirka *et al.* 2007; Lee *et al.* 2009). Nevertheless, the melting conditions

of the enriched type parental magmas can be tentatively estimated on the basis of melting experiments performed by Tuff *et al.* (2005) on geochemically similar Paraná-Etendeka ferropicrites (Gibson *et al.* 2000; cf. Paper III). The experiments indicated that the Paraná-Etendeka parental melts originated at pressures of ≥ 5 GPa and T_p of ~ 1550 °C from a garnet-pyroxenitic source. Although it is tempting to suggest similar conditions also for the enriched type, it should be noted that whereas the Paraná-Etendeka ferropicrites were thought to originate from an anhydrous source (Gibson *et al.* 2000; Gibson 2002), the enriched type shows evidence of hydrous parental melts by containing igneous amphibole in olivine-hosted inclusions and as a groundmass phase (Paper III; Appendix I). Petrography-based correction for 50% crystallization of an anhydrous mineral assemblage (olivine + clinopyroxene) indicates that the enriched type parental magma contained ~ 1.5 wt. % of H_2O (cf. Paper II). If this difference in primary H_2O contents between the enriched type and Paraná-Etendeka ferropicrites is real and not a result of false interpretations (cf. Section 3.3.3), it could indicate lower temperatures of initial melting for the former relative to the latter.

Although all the evidence point to a pyroxene-rich source for the enriched type, the nature and origin of this source have not been tightly constrained: recycled ferrobasalts (Paper I), sediment-bearing oceanic crust (Paper III), and metasomatic veins (Paper III) have been suggested, but, linking specific recycled crustal materials to EM-like mantle reservoir signatures has been proven to be a complicated task at best (Paper III; cf. Stracke *et al.* 2003). Moreover, some have recently questioned the idea of recycled crust as a major OIB source contributor and more emphasis has been given to the role of recycled lithospheric mantle sections (e.g., Niu & O'Hara 2003; Niu 2009). Bearing this in mind

and given the significant pitfalls in modeling the alteration, subduction, dehydration, metamorphism, blending, and recycling of oceanic crust (e.g., Stracke *et al.* 2003), the ultimate origin of the enriched type source remains ambiguous until more sophisticated methods for such evaluations are available (cf. Paper III).

The temporal position of the enriched type relative to Karoo magmatism is unclear. The fact that they sample relatively small-scale heterogeneities in the sub-Gondwanan mantle, however, may imply that they originated either shortly before or after the main magmatic phase (~184–178 Ma) that was associated with relatively large-scale mantle melting (cf. Paper I; Gibson 2002). The fact that the enriched type is found as dikes that further show reverse paleomagnetic polarity (Peters 1989) – as opposed to the normally polarized CFBs that they crosscut (Hargraves *et al.* 1997) – is more compatible with the latter option.

In summary, there are many open questions in the petrogenesis of the enriched type: the ultimate nature of the source components, the melting conditions in this source, as well as the temporal relationship to the Karoo magmatism remain uncertain. Although their rarity (only two dikes known) indicates that they represent a rather anomalous type of magmatism which probably did not contribute significantly to the Karoo magmatism in general (cf. Paper III, Section 3.2.1), they are important in providing evidence that the sub-Gondwanan upper mantle contained enriched sources similar to those of OIB.

3.2 Implications on the origin of the Karoo large igneous province

3.2.1 Geochemical comparisons and petrogenetic relationships

Geochemical comparisons between Vestfjella

ferropicrites and other Karoo magma types have been minutely performed in Papers I and III. In general, the lack of detailed trace element and isotopic (namely Pb and Os) data on the Karoo CFBs restricts comparisons and, in the case of many Karoo lavas and related intrusive rocks, any kind of compositional information has not been published (e.g., parts of Zambia, Zimbabwe, and South Africa; cf. Jourdan *et al.* 2007a). Moreover, the fact that ferropicrites initiate under anomalous melting conditions (e.g., relatively low-degree and high pressure of melting; Section 3.3; Paper I) makes the comparison with common CFBs difficult even in the case of a possible common mantle source. As a starting point, the Vestfjella ferropicrites have potential to sample Karoo source end-members, because they were derived directly from the subcontinental mantle (Paper III).

Volcanic rocks that exhibit identical compositional characteristics (e.g., high Fe and Sm/Yb) with the Vestfjella ferropicrites are not known from the Karoo province. Some Fe-rich lavas of Lebombo (Sweeney *et al.* 1994) have been speculated to represent contaminated differentiates of enriched ferropicrite-like parental magmas (Paper I), but further comparison is hampered by inadequate geochemical data also in their case (cf. Paper III). On the other hand, their relatively low Ti contents (cf. Fig. 12 of Paper I) may imply that they sampled a more Ti-poor source relative to the enriched type. The relatively high Nb content of the enriched type is also a very peculiar feature within the Karoo framework (Paper III). Such a characteristic is difficult to explain by lithospheric contamination and indicates derivation from an anomalous source component (Paper III). On the other hand, effective contamination of such Nb-rich magmas with crustal materials may result in Nb-depleted volcanic rocks, possibly represented by some Karoo CFBs (cf. Fig. 7 in Paper III). Nevertheless, given the

peculiar OIB-like compositional characteristics of the enriched type, and the fact that it is only known from two dikes on Basen nunatak (Fig. 7b), I suggest that they were derived from an anomalous pyroxene-rich upper mantle source that was not involved in the generation of the majority of Karoo CFBs (cf. Paper III).

The Vestfjella depleted type, on the other hand, originated from the same ambient upper mantle source that produced the MORB-like low-Nb dikes of Vestfjella (Paper III). These magma types are isotopically indistinguishable and the differences in their major and trace element composition can be readily attributed to differences in initial melting conditions (Paper III). In order to investigate the importance of this upper mantle source in the petrogenesis of Antarctic Karoo CFBs in general, I modeled lithospheric contamination of low-Nb type magmas that, rather than depleted ferropicrites that originated as low-degree melts at extremely high pressures, are likely to provide more feasible parental magma compositions for the modeling. Accordingly, I used a fractionation-corrected ($\sim 30\%$ of olivine) low-Nb sample P27-AVL with the highest initial ϵ_{Nd} (+7.7) and lowest initial ϵ_{Sr} (-15.7) as the parental melt composition (cf. Luttinen & Furnes 2000) and modeled contamination with crustal and subcontinental lithospheric mantle (SCLM) material separately (cf. Paper III). Energy-constrained assimilation and fractional crystallization (EC-AFC; Bohrson & Spera 2001; Spera & Bohrson 2001) modeling of crustal contamination takes into account the latent heat of crystallization and partial melting of wall rock. Crustal contaminants used in the model are an Archean TTG (representing Grunehogna craton; Fig. 7) and average upper and lower continental crust (representing Maud Belt; Fig. 7). Conventional AFC modeling (DePaolo 1981b) was preferred in the case of SCLM, because of significant uncertain-

ties regarding its physicochemical nature (cf. Paper III). Lamproitic contaminant is thought to represent a fair approximation of a SCLM-derived low-degree partial melt composition (Luttinen *et al.* 2002). The input parameters for the contamination models are presented in Table 2 and the results that are most reminiscent of the various CT lava signatures are presented in Fig. 10. Modeling was utilized only on high field strength elements (HFSE) that, unlike LILE, are not mobile during secondary alteration.

The CT1 lavas exhibit strong indications of lithospheric contamination by showing high Th/Ta, La/Sm, Ce/Nb, and Ce/P and low Ti/Zr ratios and highly unradiogenic initial ϵ_{Nd} (Fig. 10a). The model replicates the CT1 signature fairly well by 4% contamination of a low-Nb parental melt with Archean crustal material (Fig. 10a). It is important to note, however, that the Ti contents of the most depleted CT1 samples are lower than in the hypothetical parental melt (Fig. 10a). This feature, along with the differences in the heavy rare earth element contents between the model and CT1 lavas (Fig. 10a), can be readily explained by derivation of CT1 and low-Nb parental melts by distinct melting conditions (e.g., higher degree of melting at higher pressure in the case of CT1). The CT2 signature is replicated even more satisfactorily by 2% contamination of average (Proterozoic) upper crust (Fig. 10b). The CT3 signature, on the other hand, is possible to explain by negligible (1%) contamination with SCLM and/or lower crust (Fig. 10c). In fact, the most depleted CT3 samples show incompatible element compositions that approach those of the hypothetical low-Nb parental magma.

In summary, my contamination modeling indicates that the major geochemical characteristics of the CT lavas could be explained by lithospheric contamination of low-Nb type parental magmas. Importantly, the application

Table 2. Input parameters for the EC-AFC and AFC models.

Variable	PM [†]		AC*	UC**	LC***	SCLM [#]
Model	EC-AFC & AFC		EC-AFC	EC-AFC	EC-AFC	AFC
Magma liquidus T (initial T) [°C]	1600		-	-	-	-
Assimilant liquidus T [°C]	-		1000	1000	1100	-
Assimilant initial T [°C]	-		300	300	600	-
Solidus T [°C]	-		900	900	950	-
Equilibration T [°C]	-		1100	1100	1100	-
Isobaric specific heat [J/kg K]	1668		1370	1370	1388	-
Crystallization enthalpy [J/Kg]	600000		-	-	-	-
Fusion enthalpy [J/Kg]	-		270000	270000	350000	-
	K_D^{\oplus}					
Th [ppm]	0.16	(0.001)	3.6	10.5	1.2	26.1
Nb [ppm]	2.19	(0.02)	5	12	5	170
Ta [ppm]	0.12	(0.01)	0.4	0.9	0.6	14.6
Ce [ppm]	8.55	(0.001)	64	63	20	502
P [ppm]	458	(0.05)	698	655	436	15099
Nd [ppm]	7.37	(0.003)	22	27	11	229
Zr [ppm]	60	(0.05)	132	193	68	1076
Hf [ppm]	1.72	(0.05)	3.4	5.3	1.9	26.6
Sm [ppm]	2.7	(0.003)	3.52	4.7	2.8	36.4
Eu [ppm]	1.00	(0.01)	1.01	1.0	1.1	10
Ti [ppm]	7428	(0.08)	1739	3837	4916	23860
Gd [ppm]	3.04	(0.02)	3.8	4.0	3.1	23
Tb [ppm]	0.55	(0.02)	0.4	0.7	0.48	2.91
Y [ppm]	15.40	(0.06)	10	21	16	37
Yb [ppm]	1.21	(0.06)	0.5	1.96	1.5	1.48
Lu [ppm]	0.18	(0.06)	0.1	0.31	0.25	0.23
$^{143}\text{Nd}/^{144}\text{Nd}^{\S}$	0.512829		0.510551	0.511800	0.511806	0.512275
$\epsilon_{\text{Nd}}^{\S}$	+8.3		-36.2	-11.8	-11.7	-2.5

All thermal parameters after Paper III. [†] Parental melt: trace element composition after fractionation-corrected Low-Nb sample P27-AVL (Section 3.2.1; cf. Luttinen & Furnes 2000); Nd isotopic composition after the model in Paper III.

* Archean crust: trace element and Nd isotopic composition after TTG sample 96/203 (Kreissig *et al.* 2000; Ta and Hf estimated after Kleinhanns *et al.* 2003). ** Upper (Proterozoic) crust: trace element composition after the average upper crust of Rudnick & Gao (2003); Nd isotopic composition after the model of Jourdan *et al.* (2007a). *** Lower (Proterozoic) crust: trace element composition after the average lower crust of Rudnick & Gao (2003); Nd isotopic composition after granulite 21BD6 (Talarico *et al.* 1995). [#] Subcontinental lithospheric mantle: trace element and Nd isotopic composition after lamproite AL/KB8-98 (Luttinen *et al.* 2002). AFC process ($r = 0.5$) has been modeled to take place after the same level of fractionation of PM than in the case of EC-AFC model with lower crustal contaminant.

[⊕] K_D values for the parental melt estimated from GERM database (<http://earthref.org/>); All K_D values for the crustal contaminants are 0.1. [§] Calculated at 180 Ma except for SCLM-derived lamproite at 159 Ma.

of EC-AFC modeling overcomes the previous shortcomings related to AFC modeling of crustal contamination that suggest superfluous (e.g., >20 % in the case of CT1) degrees of contamination to produce CT geochemical signatures (cf. Luttinen & Furnes 2000). Therefore, given

that the low-Nb dikes are likely to represent the uncontaminated correlatives of many Vestfjella CFBs and, accordingly, similar CFBs of Sabie River Basalt Formation in the African part of Karoo (Duncan *et al.* 1984; Hawkesworth *et al.* 1984; Sweeney *et al.* 1994; cf. Luttinen &

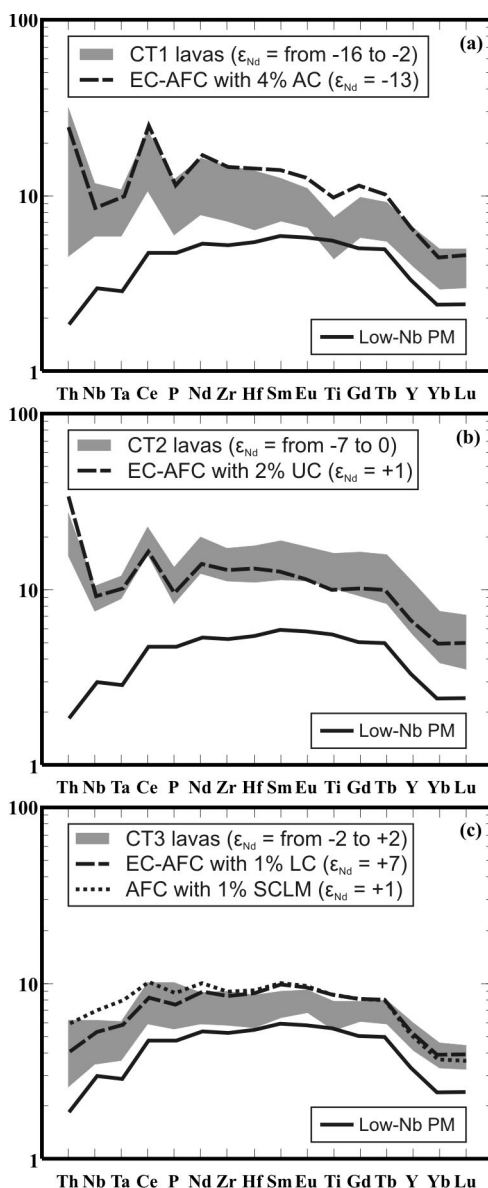


Figure 10. Representative results of lithospheric contamination modeling of a low-Nb type parental melt illustrated in primitive mantle (Sun & McDonough 1989)-normalized incompatible element patterns along with representative CT1 ($n=29$) (a), CT2 ($n=14$) (b), and CT3 ($n=20$) (c) lava compositions. See Table 2 for model parameters.

Furnes 2000), depleted ferropicrites seem to have sampled a sublithospheric upper mantle end-member source of Karoo magmatism (cf. Paper III). It is possible that this sublithospheric mantle source was variably LILE-enriched (cf.

Luttinen & Furnes, 2000) and had much less important role in the petrogenesis of most of the strongly lithosphere-signatured Karoo lavas of southern Africa (cf. Jourdan *et al.* 2007a). It is important to note that if the low-Nb dikes had not been discovered, finding the apparent petrogenetic relationships between the depleted ferropicrites and CT lavas would have been difficult to impossible (cf. Paper III).

3.2.2 The origin of the Karoo flood basalts

The ferropicrites of Vestfjella (especially the depleted type) provide an important addition into the debate on the origins of the Karoo flood basalts. The association of the depleted type with the main phase of Karoo magmatism at ~ 180 Ma, and its petrogenetic relationship with Karoo lavas (Paper III; cf. previous Section) indicate that it sampled an important sublithospheric end-member for Karoo magmatism. These findings are in strong discordance with studies that suggest that the parental melts of the Karoo CFBs formed solely in the lithospheric mantle (e.g., Hawkesworth *et al.* 1984; Elburg & Goldberg 2000; Scenario 1 of Jourdan *et al.* 2007a).

The derivation of the depleted type from anomalously hot mantle sources ($T_p > 1600$ °C; Paper II) indicate that sub-Gondwanan mantle was heated to temperatures of at least ~ 200 °C above that of ambient mantle. The fact that the depleted type represents melts largely derived from ambient MORB-source mantle, however, is more compatible with the internal mantle heating model (Coltice *et al.* 2007, 2009) than the plume model (Morgan 1971; Richards *et al.* 1989) (Paper III). Although there is a possibility that some other processes suggested for CFB generation (cf. Section 1.1; Bryan & Ernst 2008) were also active, I propose that the internal heating effect significantly enhanced the melt production

in the sub-Gondwanan mantle and was largely responsible for the generation of vast amounts of basaltic magma represented by Karoo (and Ferrar) CFBs at ~180 Ma (cf. Paper III).

3.3 Implications on the origin of ferropicrites

3.3.1 Ferropicrite whole-rocks vs. ferropicrite melts

Paper I highlights some important issues that should be considered when interpreting the petrogenesis of ferropicrites: ferropicritic whole-rock compositions do not necessarily represent crystallized equivalents of ferropicrite melts (i.e., primary ferropicrites), but may also record accumulation of relatively Fe-rich olivine ($<Fo_{80}$) in basaltic melts or by hydrothermal alteration of alkaline volcanic rocks (i.e., secondary ferropicrites). Careful examinations on petrography, geochemistry, and mineral chemistry of ferropicrites are required in order to evaluate whether their compositions are of primary or secondary origin. Obviously, the trace element or isotope compositions of secondary ferropicrites should not be utilized in order to study the petrogenesis of ferropicrite melts.

Normative mineral calculations (CIPW) performed on highly magnesian ferropicrite whole-rock compositions (e.g., $FeO_{tot} \approx 14$ wt. %; $MgO \approx 18$ wt. %) result in normative olivine contents of <40 vol. %. Broadly, this could mean that if the modal olivine content in a ferropicrite sample is higher, the rock may contain accumulated olivine. More elaborate means to address the cumulate issue is to perform detailed mineral chemical analyses on olivine phenocrysts and evaluate whether they are in or out of equilibrium with the host whole-rock composition (Paper I). Unfortunately, this evaluation is impossible for highly altered or metamorphosed

ferropicrites that do not contain primary igneous olivine: in the case of Precambrian ferropicrites, the samples that have been collected close to presumed chilled margins of the lava flows or from pyroclastic successions have been thought to be devoid of accumulation effects and closely represent primitive Fe-rich liquid compositions (e.g., Hanski & Smolkin 1995; Stone *et al.* 1995; Goldstein & Francis 2008; cf. Table 1). Surprisingly limited olivine mineral chemical data exist for ferropicrites that contain fresh olivine (Table 1; cf. Paper I): specific analyses have only been provided for the ferropicrites of Vestfjella (Paper I–III; Appendix I), Paraná-Etendeka (Gibson *et al.* 2000), and Emeishan (Zhang *et al.* 2006). The Vestfjella ferropicrites, the most Fe-rich Emeishan ferropicrite, and two Paraná-Etendeka samples have likely crystallized from primitive Fe-rich melts as they are characterized by relatively Mg-rich olivines ($\geq Fo_{81}$; Table 1; Paper I–III). Three of the Paraná-Etendeka samples, however, show evidence of olivine accumulation (Table 1; Paper I) and likely did not crystallize from ferropicritic melts. Importantly, these samples can also be distinguished from the primary Paraná-Etendeka ferropicrites on the basis of trace element characteristics (Table 1) and thus they possibly represent separately evolved magma type (or types). These cumulate Paraná-Etendeka samples have thus been excluded from the following discussion on ferropicrite petrogenesis. Less detailed olivine data (e.g., not sample-specific) have been provided for Ahlmannryggen (Riley *et al.* 2005) and Siberia (Ryabov *et al.* 1977; Zolotukhin & Al'mukhamedov, 1991; Zolotukhin *et al.* 1991). Without further olivine analyses, the primitive nature of these and all the other ferropicrite suites that lack olivine mineral chemical data and do not sample chilled margins remains uncertain (Table 1; cf. Paper I).

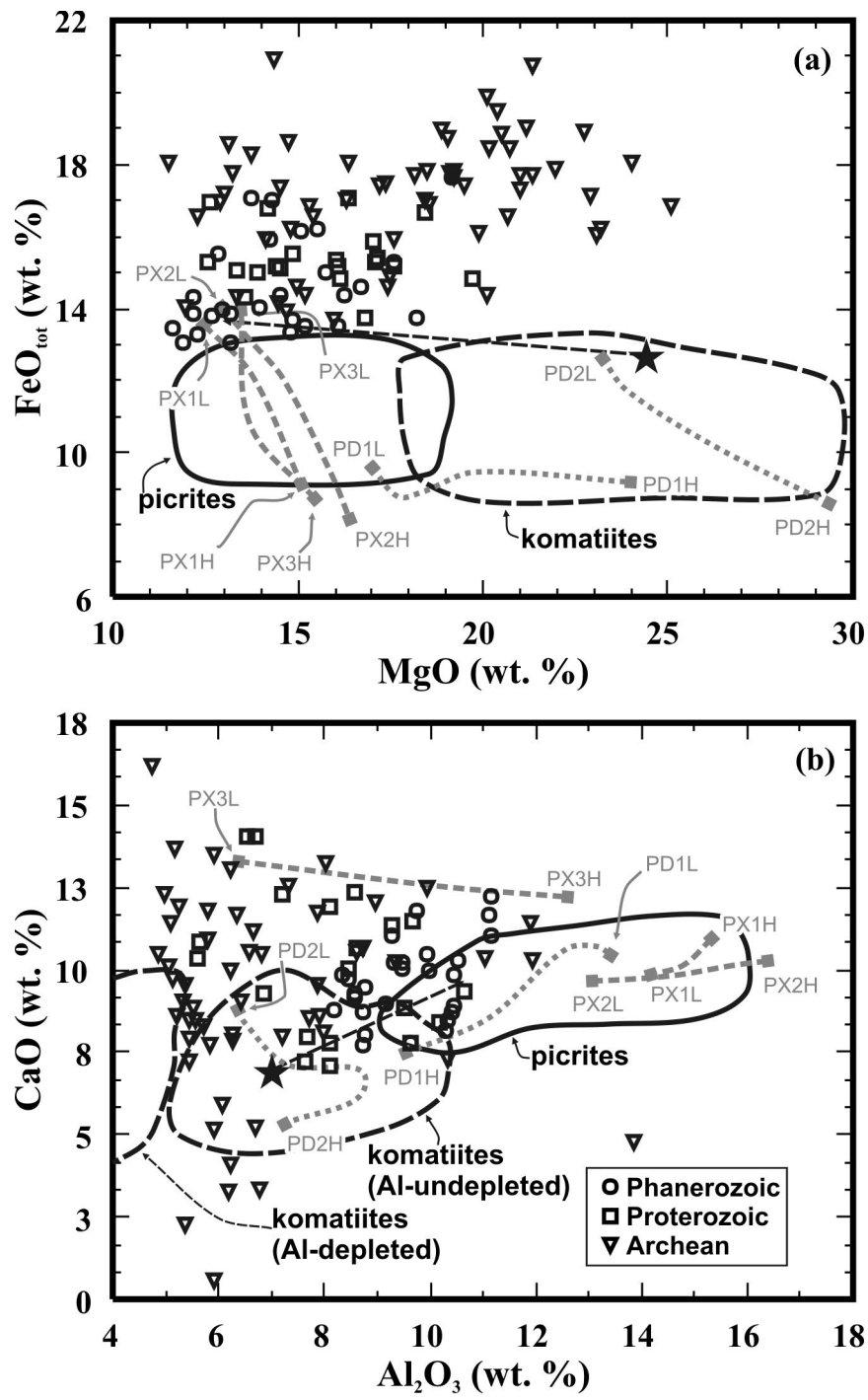
Many ferropicrites show petrographical

and geochemical (e.g., LOI >3 wt. %; Table 1) evidence of post-crystallization hydrothermal alteration. In addition, Archean ferropicrites have invariably been subjected to greenschist-to-amphibolite facies metamorphism (Table 1). During alteration or metamorphism, volcanic rocks are prone to gain or lose fluid mobile elements (such as Si, Na, and K) which may complicate the identification of primary subalkaline and alkaline magma types (cf. Paper I). Pearce (1996) tackled this problem by introducing a trace element classification diagram that utilizes immobile trace element ratios Zr/Ti and Nb/Y , where Nb/Y is considered to be an indicator of alkalinity (cf. Fig. 10 in Paper I). Volcanic rocks that show Nb/Y ratios of higher than about 1 are likely to be of alkaline origin. For example, some of the lavas from Prinsen af Wales Bjerre formation, East Greenland (Peate *et al.* 2003) exhibit ferropicritic whole-rock compositions (e.g., $MgO = 13.2\text{--}19.9$ wt. %; $FeO_{tot} = 13.5\text{--}16.1$ wt. %; $Na_2O + K_2O = 2.5\text{--}3.1$), but are slightly altered (e.g., LOI = 1–3 wt. %) and show high Nb/Y ratios (1.7–3.1) and thus likely derive from alkaline parental magmas (Peate *et al.* 2003). Ferropicritic whole-rock compositions have also been described from oceanic settings (e.g., Hawaii; Reiners & Nelson 1998) where they are also characterized by high degrees of hydrothermal alteration and are thus unlikely related to ferropicrite parental melts (cf. Paper I). It is also important to note that the distinction between ferropicrites and highly alkaline Mg-rich volcanic rocks may simply relate to differences in mantle melting conditions (e.g., degree of melting; cf. Section 3.3.2) and, theoretically, a whole spectrum of subalkaline to alkaline Fe- and Mg-rich melt compositions may be generated from the same mantle source under favorable conditions (cf. Gudfinnsson & Presnall 2005). Although most of the CFB-related alkaline volcanic rocks have been thought to derive

from the lithospheric mantle (e.g., Harmer *et al.* 1998; Gibson *et al.* 2006; Song *et al.* 2008; Srivastava *et al.* 2009), the Prinsen af Wales Bjerre lavas have been interpreted to sample sublithospheric mantle heterogeneities (Peate *et al.* 2003) and should thus be considered equally important in studying deep origins of CFBs as ferropicrites.

3.3.2 Pyroxenite vs. peridotite source

It is evident that ferropicrite liquids cannot originate by direct partial melting of ambient, depleted mantle peridotite (Hanski 1992; Stone *et al.* 1995; Gibson *et al.* 2000; Gibson 2002; Goldstein & Francis 2008; Paper I). In Vestfjella, however, the depleted ferropicrites likely represent differentiates from even more primitive (meimechitic) parental magmas that were generated by relatively low-degree, high-pressure melting of a mantle source dominated by depleted upper mantle peridotite (Paper II, III). The question of whether ferropicrites represent near-primary or already significantly differentiated melts should thus be carefully addressed (cf. Fig. 11). It should also be noted that mixing of peridotite-derived picritic melts with evolved Fe-rich basalts or immiscible liquids could theoretically result in ferropicritic whole-rock compositions (Jakobsen *et al.* 2005). However, such mixing processes would be expected to result in significant igneous disequilibrium textures and textural and geochemical heterogeneities within individual magma bodies, and these are not characteristic of ferropicrites. In addition, this model provides no explanation for the fact that ferropicrites are only found in CFB provinces and not, for example, in mid-ocean ridges. These observations strongly suggest that liquid immiscibility (and subsequent mixing) is very unlikely cause for the generation of most ferropicrite melts (cf.



continued on next page...

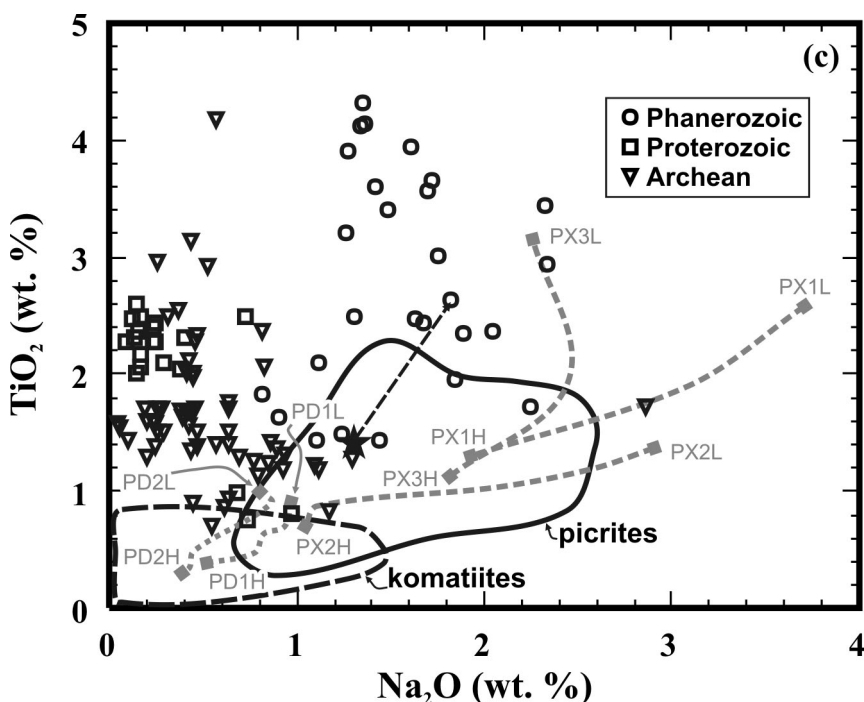


Figure 11. Geochemical characteristics of ferropicrites compared with peridotite and pyroxenite experimental partial melts and continental picrites and komatiites in FeO_{tot} vs. MgO (a), CaO vs. Al_2O_3 (b), and TiO_2 vs. Na_2O (c) diagrams. Star indicates Vestfjella meimechite sample AL/B9-03 that closely corresponds to a parental melt composition of the Vestfjella depleted type (Paper II); stippled line corresponds to ~30% fractionation of olivine. Gray stippled lines approximate the compositional progression of partial melt composition between low- and high-degree melt end-members: PD1L–PD1H = peridotite at 3 GPa and 14–53% of melting (Walter 1998); PD2L–PD2H = peridotite at 6 GPa and 11–65% of melting (Walter 1998); PX1L–PX1H = pyroxenite at 2.5 GPa and 21–67% of melting (Hirschmann *et al.* 2003); PX2L–PX2H = pyroxenite at 2.5 GPa and 18–99% of melting (Keshav *et al.* 2004); PX3L–PX3H = pyroxenite at 5 GPa and 19–75% of melting (Kogiso *et al.* 2003). Legend is given in b and c.

Goldstein & Francis, 2008). The most likely mantle sources for unfractionated ferropicrite melts are enriched peridotite and pyroxenite – the only mantle rock types that exhibit Mg and Fe contents high enough to produce these exceptional liquid compositions (cf. Paper I).

Whether pyroxenite represents a major melt-producing rock type in the sources of several oceanic islands and CFB provinces has been debated (e.g., Putirka 1999; Stolper *et al.* 2004; Sobolev *et al.* 2005, 2007; Herzberg 2006; Elkins *et al.* 2008). The situation is similar in the case of ferropicrites: based on melting experiments, Tuff *et al.* (2005) concluded that Paraná-Etendeka ferropicrites are most likely

to represent partial melts of garnet pyroxenite at high pressures (≥ 5 GPa), whereas Goldstein & Francis (2008) noted that peridotite-basalt mixtures and most garnet pyroxenite xenoliths have insufficient Fe, Mg, or both to produce melts that correspond to the exceptionally Fe-rich Archean ferropicrites (cf. Fig. 5; Table 1). The geochemical similarities of the Vestfjella ferropicrites with pyroxenite partial melts and purported pyroxenite-sourced Hawaiian picrites initially led to the suggestion that the former also represent partial melts of recycled pyroxenites (Paper I). Nevertheless, the question arises if there are any means to distinguish between Fe-enriched peridotite and pyroxenite as ulti-

mate sources for ferropicrite melts.

Pyroxenite partial melting experiments that have resulted in picritic glass compositions are relatively few (Hirschmann *et al.* 2003; Kogiso *et al.* 2003; Keshav *et al.* 2004; cf. Fig. 11). Moreover, experiments on incompatible-element-enriched peridotites are lacking, the closest correlatives being experiments performed on a fertile (pyrolitic) peridotite starting material (e.g., Walter 1998). The published major element data on pyroxenite and fertile peridotite partial melts in the pressure range of 2.5–6 GPa are compared with the Phanerozoic, Proterozoic, and Archean ferropicrites in Fig. 11. Firstly, it is important to note that only one of the experimental partial melts exceed 14 wt. % of FeO_{tot} (14.03 wt. %; pyroxenite partial melt at 2.5 GPa, $F = 18\%$; Fig. 11a), which may reflect the absence of both anomalous (e.g., Fe-rich) starting materials and data on low-degree melt compositions ($F < 10\%$) in the melting experiments, or that the experimental melts represent isobaric batch melts and not polybaric aggregate melts that are likely to have higher Fe content (cf. Gibson 2002). Although relatively high FeO_{tot} and TiO_2 of ferropicrites are more compatible with pyroxenitic rather than peridotitic sources on the basis of available experimental data (cf. Paper I), the high MgO of some Archean ferropicrites have not been attained in pyroxenite melting experiments (Figs. 11a and c; Goldstein & Francis 2008). It is also evident from Fig. 11 that the effects of pressure, degree of melting, and source compositions on the partial melt compositions are difficult to distinguish from each other (cf. Hirschmann *et al.* 1999). For example, the relatively higher Al_2O_3 of the Phanerozoic ferropicrites relative to the Archean ferropicrites may indicate that the Phanerozoic samples were derived by (1) higher degree of pyroxenite melting, (2) lower pressure of pyroxenite melting, (3) lower degree of peridotite melting, (4) lower pressure of peri-

dotite melting, or (5) from more pyroxene-rich sources relative to the Archean samples (Fig. 11b). Although the first alternative is not very likely on the basis that mantle melting was more extensive in the early Earth in general, the rest of the alternatives seem equally viable. The considerably higher Na_2O of the Phanerozoic ferropicrites at a given TiO_2 , however, is difficult to explain solely by melting conditions and may suggest that Phanerozoic ferropicrites contained more pyroxene-rich mantle sources in general (Fig. 11c). Nevertheless, it should also be kept in mind that Na_2O contents of some Precambrian ferropicrites have likely been modified during metamorphism (cf. Section 3.3.1).

In Paper I, the high V/Lu ratio of many ferropicrites was thought to indicate a major role for recycled Fe-Ti gabbro component in their mantle sources. However, many incompatible trace element ratios, including V/Lu, are prone to vary according to melting conditions (e.g., P and T), and the distinction between these effects and the nature of the source is thus difficult to make (cf. Paper III). On the other hand, Le Roux *et al.* (2010) recently argued that elevated Zn/Fe ratio of several OIBs is hard to explain by melting of peridotitic mantle at varying temperature or pressure, but rather indicates pyroxene- and garnet-rich sources for the parental magmas. The purported peridotite-origin of the Vestfjella depleted ferropicrites is compatible with this claim: they show Zn/Fe ratios similar to peridotites and MORBs (Fig. 12). East Greenland and Steep Rock ferropicrites also show peridotitic Zn/Fe ratios, whereas the Vestfjella enriched type and the Ahlmannryggen ferropicrites exhibit consistently high Zn/Fe ratios suggestive of more pyroxene-rich sources for these magma types. Other ferropicrites show less coherent and/or less definitive Zn/Fe ratios: this may reflect heterogeneous sources and/or, especially in the case of Precambrian ferropicrites, secondary altera-

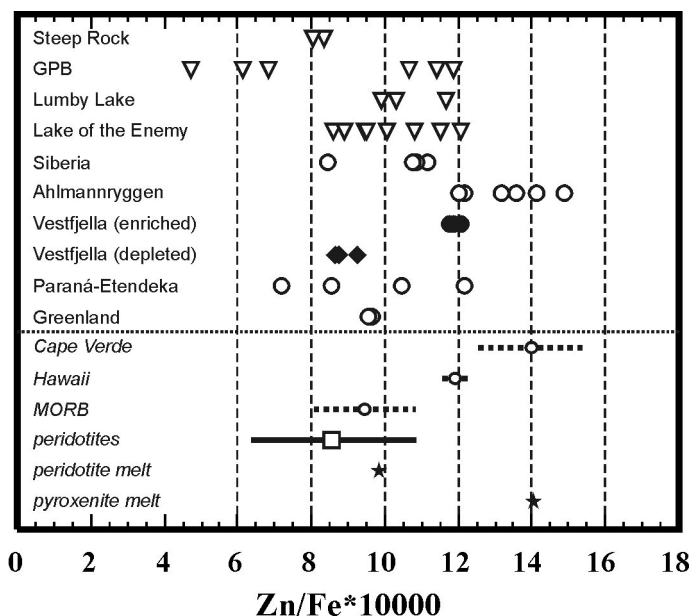


Figure 12. Ferropicrites shown in Zn/Fe ($\times 10^4$) diagram. Selected oceanic suites (Cape Verde, Hawaii, and MORB), peridotites, and representative experimental peridotite and pyroxenite partial melts shown for comparison. Cape Verde has the highest Zn/Fe ratios of oceanic rocks reported in Le Roux *et al.* (2010). In the case of oceanic suites, the circle represents the value calculated for the entire suite at MgO = 12 wt. % with standard error bars (stippled lines) shown (cf. Le Roux *et al.* 2010). In the case of peridotites, the square represents the average value and the line represents the range of compositions. Data sources for ferropicrites are reported in Table 1, for other data sources see Le Roux *et al.* (2010). Zn/Fe ratios are not prone to vary by fractional crystallization in basaltic/picritic magmas that have MgO >8.5 wt. % (Le Roux *et al.* 2010). GPB = Grassy Portage Bay.

tion and metamorphism.

Compositions of olivine phenocrysts have also been used to estimate the nature of the mantle sources of intraplate basalts. Sobolev *et al.* (2007, 2008) suggested that the proportion of pyroxenitic source component could be quantitatively assessed on the basis of Ni, Mn, Fe, and Mg contents of primitive olivine phenocrysts: relatively high Ni and low Mn/Fe were thought to be unaffected by melting conditions and indicate predominantly pyroxenitic mantle sources for several intraplate suites (e.g., Hawaii, Karoo, Siberian Traps; Sobolev *et al.* 2007). The lack of olivine mineral chemical data on Precambrian ferropicrites restricts the assessment of these methods in their case and the olivine analyzes on Phanerozoic ferropi-

crites (Karoo, Paraná-Etendeka, and Emeishan) do not meet the high analytical standards [e.g., high probe currents (~ 300 nA) and long counting times (>100 s)] required by the formulas of Sobolev *et al.* (2007, 2008). It should also be noted that recent studies indicate negative depth effect on $K_d^{ol-liq}(Ni)$ thus undermining the basis of the equations of Sobolev *et al.* (2007) (Li & Ripley 2010). Nevertheless, the evaluation of ferropicrite sources on the basis of very high-precision olivine mineral chemical data may be considered a potential subject for future studies.

Sobolev *et al.* (2008) also found a quantitative link between purported pyroxenite sources (on the basis of olivine chemistry) and Os isotopic composition in Icelandic lavas: samples that indicated more pyroxene-rich sources showed

more radiogenic $^{187}\text{Os}/^{188}\text{Os}$. Radiogenic Os in volcanic rocks has been considered evidence of pyroxene-rich sources also in several other studies (e.g., Hauri & Hart 1993; Reisberg *et al.* 1993; Hauri *et al.* 1996; Carlson & Nowell 2001; Carlson *et al.* 2006; Day *et al.* 2009), mainly because mantle peridotites are characterized by relatively unradiogenic $^{187}\text{Os}/^{188}\text{Os}$ in general (initial $\gamma_{\text{Os}}^1 \leq 0$; Shirey & Walker 1998; Chesley *et al.* 2004). Osmium isotopic data are available for the ferropicrites of Vestfjella and Pechenga only. The Vestfjella depleted ferropicrites have inherited their relatively unradiogenic Os (initial γ_{Os} from -0.5 to -2.1 at 180 Ma) from their highly magnesian parental magmas that originated from depleted peridotite sources (Paper III). The Vestfjella enriched ferropicrites (initial γ_{Os} from +9.2 to +11.1 at 180 Ma) and Pechenga ferropicrites (initial γ_{Os} from +4.1 to +5.5 at 180 Ma), however, show relatively radiogenic Os composition that has been linked to entrainment of (recycled) lithospheric materials (Paper III; Walker *et al.* 1997) and thus imply pyroxene-rich sources for them (cf. Sobolev *et al.* 2005, 2007, 2008).

In summary, the issue of pyroxenite vs. peridotite sources is hard to assess in the case of many ferropicrites due to difficulties in interpreting major element data and inadequate mineral chemical and Os isotopic data. In addition, most incompatible trace element ratios are dependent on melting conditions and are generally difficult to utilize in order to distinguish mantle sources. Nevertheless, the importance of recycled-origin pyroxenites as potential mantle source components has probably increased through time and this progress may reflect also on ferropicrites (cf. Figs. 11 and 12). Moreover, the fact that at least the Phanerozoic ferropicrites represent

melts generated at very high pressures beneath continental lithosphere indicate that they were generated by melting of the most fusible (e.g., pyroxene-rich) mantle materials (cf. Gibson 2002; Sobolev *et al.* 2005; Tuff *et al.* 2005). On the other hand, the most important findings of the present work is that ferropicritic magmas may also evolve by fractionation from even more magnesian (meimechitic/komatiitic) parental melts. In such a case, peridotite is the primary source (Paper II).

3.3.3 Hydrous or anhydrous magmas?

The significance of water in the petrogenesis of ferropicrites is poorly understood. Despite the presence of primary igneous amphibole in some Precambrian ferropicrites (e.g., Hanski 1992; Stone *et al.* 1997; Fiorentini *et al.*, 2008), Gibson (2002) concluded that ferropicrites derive from anhydrous mantle sources. The Vestfjella samples are the first Phanerozoic ferropicrites that have been found to contain igneous amphibole (Paper I–III). The presence of these amphiboles (as well as the Precambrian ones) as inclusions in olivine that likely crystallized at significant depths (cf. Paper II) is difficult to explain by reaction with meteoric waters (cf. Stone *et al.*, 1995). The amphibole-bearing inclusions likely represent melt droplets that got trapped within olivine phenocrysts during the early stages of magma evolution. In addition, the overall uncontaminated nature of the ferropicrites does not suggest contamination with water-rich lithosphere either. These constraints strongly suggest high mantle-derived H_2O content for the parental melts (Paper II; Stone *et al.* 1997; Fiorentini *et al.*, 2008). In the Vestfjella depleted type, amphibole is confined to olivine-hosted inclusions and is not found in the groundmass at all. Moreover, the absence of any other hydrous groundmass phases indicates

¹ Calculated using bulk-earth parameters of $^{187}\text{Os}/^{188}\text{Os} = 0.1296$ and $^{187}\text{Re}/^{188}\text{Os} = 0.4353$ (Meisel *et al.* 2001; cf. Carlson 2005)

that the original high water contents were lost (e.g., by degassing) prior to groundmass crystallization (Paper II). This possibility should also be considered in the case of other Phanerozoic ferropicrites and future studies should concentrate on evaluating the role of volatiles by, for example, focusing on mapping and analyzing possible olivine-hosted melt inclusions. In standard petrographical inspection using optical microscopes, the presence of small amphibole crystals in olivine-hosted inclusions can easily go unnoticed.

Irrespective of whether water was involved in the petrogenesis of ferropicrites or not, the characteristic high Fe contents of ferropicrites are not likely the result of wet mantle melting (e.g., Hanski 1992; Paper II; cf. Gibson 2002), because experimental water-bearing and dry systems tend to produce melts with comparable Fe contents at similar degrees of melting (cf. Hirose & Kawamoto 1995). The most important consequences of elevated water contents in the source are to promote partial melting and decrease both the density and viscosity of ultramafic magmas thus allowing their rapid ascent through thick lithosphere without significant interaction with country rocks (Paper II, III; cf. Arndt *et al.* 1998).

3.3.4 Mantle thermometry and relation to mantle plumes

Despite the debate on the water contents of the ferropicrite primary melts and their mantle sources, ferropicrites have generally been associated with anomalously hot mantle (e.g., Hanski & Smolkin 1995; Stone *et al.* 1995; Gibson *et al.* 2000; Gibson 2002; Riley *et al.* 2005; Goldstein & Francis 2008). Findings on the Vestfjella ferropicrites provide support for this view (Paper I, II). The purported high temperatures, however, are not necessarily indicative of plumes reaching the upper mantle;

ferropicrites are commonly related to supercontinent break-up processes and thus may record high temperatures induced by internal mantle heating (cf. Coltice *et al.* 2007, 2009). The Vestfjella depleted type, for example, exhibits Indian Ridge MORB-like isotopic (Sr, Nd, Pb, and Os) compositions and low Nb/Y at a given Zr/Y that provide strong evidence for an upper mantle (i.e., non-plume) source (Paper III).

Isotopic and trace element data of ferropicrites and volcanic rocks derived from distinct mantle reservoirs are presented in Figs. 13 and 14. In order to minimize time-integrated correction (and uncertainties involved) and maximize readability, only Phanerozoic ferropicrites are shown in the isotope diagrams (Fig. 13). It is evident from Fig. 13 that, except for the Vestfjella depleted type, none of the Phanerozoic ferropicrites exhibit depleted-mantle- or MORB-like isotopic signatures. In particular, Phanerozoic ferropicrites are rather characterized by relatively elevated initial $^{87}\text{Sr}/^{86}\text{Sr}$ ratios. Although this is compatible with relatively enriched mantle sources, it could also indicate minor lithospheric contamination (Fig. 13). Nevertheless, the fact that the great majority of ferropicrites plot within the fields of OIBs and “Iceland Plume Array” in Nb/Y vs. Zr/Y diagram is difficult to explain solely by minor lithospheric contamination of depleted mantle-derived magmas, and strongly suggest a major role of relatively Nb-enriched and anomalous mantle sources in their petrogenesis (Fig. 14; cf. Fitton *et al.* 1997; Paper III). Relating these anomalous signatures strictly to mantle plumes is quite an extrapolation, however, because enriched components are believed to form an intrinsic part of the upper mantle as well (Cooper *et al.* 2009; cf. Paper III). In addition to the Vestfjella depleted type, ferropicrites that had relatively Nb-poor mantle sources are found in Ahlmannryggen, the Keweenawan Rift, and the Kolar Schist Belt (Fig. 14). However,

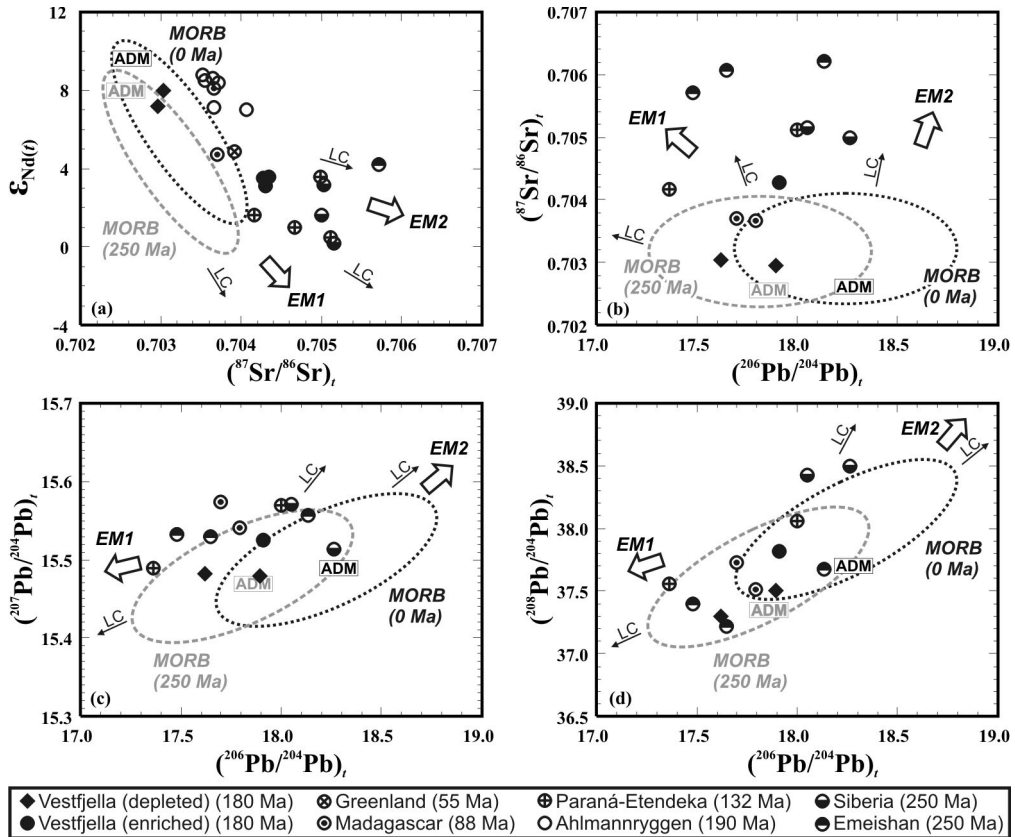


Figure 13. Phanerozoic ferropicrites shown in initial ϵ_{Nd} vs. $^{87}Sr/^{86}Sr$ (a), $^{87}Sr/^{86}Sr$ vs. $^{206}Pb/^{204}Pb$ (b), $^{207}Pb/^{204}Pb$ vs. $^{206}Pb/^{204}Pb$ (c), and $^{208}Pb/^{204}Pb$ vs. $^{206}Pb/^{204}Pb$ (d) diagrams. Average depleted MORB mantle (ADM; Workman & Hart, 2005) and field of worldwide MORBs (estimated after Klein 2003) shown at 0 and 250 Ma. The compositions at 250 Ma were back-calculated by using ADM mantle reservoir composition recommended by Workman & Hart (2005). Approximate compositions of EM1 and EM2 mantle reservoirs estimated after Eisele *et al.* (2002) and Workman *et al.* (2004), respectively (cf. Paper III). LC arrows denote the effect of lithospheric contamination with variable contaminant compositions (cf. Paper III).

this does not necessarily indicate their derivation from low-degree high-pressure partial melts of MORB-source upper mantle. For example, the very high HFSE contents (e.g., $TiO_2 \approx 4$ wt. %), high Zn/Fe (Fig. 12), and the combination of relatively radiogenic initial $^{87}Sr/^{86}Sr$ and very high initial ϵ_{Nd} of the Ahlmannryggen ferropicrites provide strong evidence for an anomalous depleted, possibly pyroxenitic, source component (cf. Section 3.3.2; Riley *et al.* 2005).

In summary, given the deficiencies of the plume theory in explaining the origin of many CFB provinces (e.g., Foulger *et al.* 2005) and the growing evidence of other processes capable

of creating significant sublithospheric temperature anomalies (e.g. Coltice *et al.* 2007), the association of ferropicrite sources and their high potential temperatures with deep-seated mantle plumes is not straightforward. The generally enriched isotopic signatures and high Nb/Y, however, indicate that the great majority of ferropicrites sampled anomalous relatively enriched (recycled?) mantle sources. The evaluation of whether all these sources are related to mantle plumes is beyond the scope of this thesis and must be considered separately in every case (cf. Paper III).

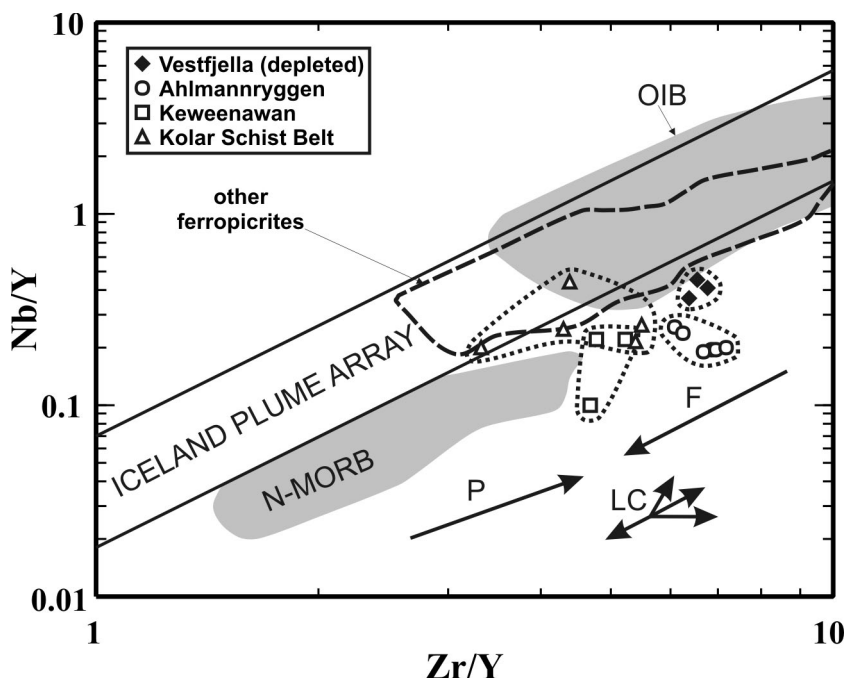


Figure 14. Ferropicrites shown in logarithmic Nb/Y vs. Zr/Y diagram (data sources listed in Table 1). The Iceland Plume Array and fields for N-MORB and OIB after Fitton *et al.* (2003). P and F arrows denote the effect of increasing pressure and degree of melting, respectively (cf. Fitton *et al.* 1997). LC arrows denote the effect of lithospheric contamination with variable contaminant compositions (cf. Paper III).

3.3.5 The origin of the relative Fe enrichment

On the basis of this thesis and earlier studies on ferropicrite petrogenesis (Hanski & Smolkin, 1995; Gibson *et al.*, 2000; Gibson, 2002; Goldstein & Francis, 2008), I present three fundamental ferropicrite factors that promote generation of these exceptional subalkaline melt compositions:

1. Relatively low degree of melting

Low-degree melting of mantle rock types results in relatively Fe-rich partial melts (cf. Fig. 11a). At very low-degrees of melting (e.g., $F \leq 1\%$) the partial melts tend to be alkaline in character, however.

2. Melting at relatively high pressures

High-pressure melting of mantle rock types

results in relatively Fe-rich partial melts (cf. Fig. 11a).

3. Enriched source components

Enriched source components may be needed in order to result in $\text{FeO}_{\text{tot}}^{\text{liq}} > 14\text{ wt. \%}$ (cf. Fig. 11a; Section 3.3.2.). Fertile source composition also promotes melting at higher pressures.

Given these factors, ferropicritic magmas can be generated in several ways. The most well-established models are the following: (1) fractional crystallization of olivine from highly magnesian parental magmas derived from predominantly ambient peridotitic sources at high pressures (the Vestfjella depleted type; Paper II), (2) high-pressure partial melting of relatively Fe-rich (metasomatized?) peridotite (e.g., some Precambrian ferropicrites; Hanski & Smolkin 1995; Stone *et*

al. 1995), and (3) high-pressure partial melting of pyroxenite that possibly contains recycled components (e.g., the Vestfjella enriched type and Paraná-Etendeka; cf. Paper I, III; Tuff *et al.* 2005). Combining geochemical, mineral chemical, and isotopic data and tracking down the primary melt compositions is important in addressing the various possibilities. It should also be noted that thick continental lithosphere appears to be prerequisite for the preservation of ferropicrite parental melts until their eruption: thick lithospheric lid effectively prevents subsequent mixing with mantle melts generated at higher degree of melting, at lower pressures, and from less fertile mantle components (cf. Fig. 2; Gibson 2002).

4 Conclusions

The ferropicrites (and related meimechites, picrites, picrobasalts, and basalts) of Vestfjella, western Dronning Maud Land, are found as dikes that crosscut the continental flood basalts of the Antarctic extension of the Jurassic Karoo LIP. The dikes show division into two distinct geochemical types, one showing relatively flat primitive-mantle-normalized incompatible element patterns and depleted isotope signatures (depleted type) and the other showing more enrichment in the highly incompatible elements and relatively enriched isotope signatures (enriched type). The depleted type is related to the main phase of Karoo magmatism at ~180 Ma and originated as highly magnesian (MgO up to 25 wt. %) partial melts from peridotitic upper mantle source (presently sampled by SW Indian Ridge MORB) at considerable temperatures ($T_p > 1600^\circ\text{C}$) and pressures (5–6 GPa) beneath the Gondwana supercontinent. The enriched type was derived from pyroxenitic components that were formed either by melt metasomatism or by

recycling of oceanic crust in the subcontinental mantle. The source of the depleted type represents an important sublithospheric end-member for Karoo CFBs and its purported origin is compatible with the theory that the Karoo LIP was formed in an extensive melting episode caused mainly by internal heating of the upper mantle beneath the Gondwana supercontinent. The relative Fe-enrichment of primary ferropicrites seems to require one or more of the following: (1) relatively low degree of partial melting, (2) high pressure of partial melting, and (3) melting of enriched source components. Nevertheless, I address the importance in identifying the parental magma composition, because ferropicritic whole-rock compositions could also result from accumulation, secondary alteration, and fractional crystallization.

References

- Adam, J. & Green, T.H. (2006) Trace element partitioning between mica- and amphibole-bearing garnet lherzolite and hydrous basanitic melt: 1. Experimental results and the investigation of controls on partitioning behaviour. *Contributions to Mineralogy and Petrology*, **152**, 1–17.
- Anderson, D.L. (1994) The sublithospheric mantle as the source of continental flood basalts: the case against the continental lithosphere and plume head reservoirs. *Earth and Planetary Science Letters*, **123**, 269–280.
- Anderson, D.L. (2000) The thermal state of the upper mantle: no role for mantle plumes. *Geophysical Research Letters*, **27**, 3623–3626.
- Anderson, D.L. (2005) Large igneous provinces, delamination, and fertile mantle. *Elements*, **1**, 271–275.
- Anderson, D.L. (2007) The eclogite engine: chemical geodynamics as a Galileo thermometer. In *Plates, Plumes, and Planetary Processes* (eds G.R. Foulger & D.M. Jurdy), pp. 47–64. Geological Society of America, Special Paper, **430**.
- Arndt, N.T., Chauvel, C., Czamanske, G.K., & Fedorenko, V.A. (1998) Two mantle sources, two plumbing systems: tholeiitic and alkaline magmatism of the Maymecha River basin, Siberian flood volcanic province. *Contributions to Mineralogy and Petrology*, **133**, 297–313.
- Bercovici, D. & Mahoney, J.J. (1994) Double flood basalts and plume head separation at the 660-kilometer discontinuity. *Science*, **266**, 1367–1369.
- Bohrson, W.A. & Spera, F.J. (2001) Energy-constrained open-system magmatic processes II: Application of energy-constrained assimilation-fractional crystallization (EC-AFC) model to magmatic systems. *Journal of Petrology*, **42**, 1019–1041.
- Bryan, S.E. & Ernst, R.E. (2008) Revised definition of large igneous provinces (LIPs). *Earth-Science Reviews*, **86**, 175–202.
- Burke, K. & Dewey, J.F. (1973) Plume-generated triple junctions: key indicators in applying plate tectonics to old rocks. *Journal of Geology*, **81**, 406–433.
- Campbell, I.H. & Griffiths, R.W. (1990) Implications of mantle plume structure for the evolution of flood basalts. *Earth and Planetary Science Letters*, **99**, 79–93.
- Carlson, R.W. (2005) Application of the Pt-Re-Os isotopic systems to mantle geochemistry and geochronology. *Lithos*, **82**, 249–272.
- Carlson, R.W. & Nowell, G.M. (2001) Olivine-poor sources for mantle-derived magmas: Os and Hf isotopic evidence from potassic magmas of the Colorado Plateau. *Geochemistry, Geophysics, Geosystems*, **2**, doi:10.1029/2000GC000128.
- Carlson, R.W., Czamanske, G.K., Fedorenko, V.A., & Ilupin, I. (2006) A comparison of Siberian meimechites and kimberlites: implications for the source of high-Mg alkalic magmas and flood basalts. *Geochemistry, Geophysics, Geosystems*, **7**, doi:10.1029/2006GC001342.
- Chesley, J.T., Richter, K., & Ruiz, J. (2004) Large-scale mantle metasomatism: a Re/Os perspective. *Earth and Planetary Science Letters*, **219**, 49–60.
- Clifford, P.M. (1968) Flood basalts, dike swarms and sub-crustal flow. *Canadian Journal of Earth Sciences*, **5**, 93–96.
- Coltice, N., Phillips, B.R., Bertrand, H., Ricard, Y., & Rey, P. (2007) Global warming of the mantle at the origin of flood basalts over supercontinents. *Geology (Boulder)*, **35**, 391–394.
- Coltice, N., Bertrand, H., Rey, P., Jourdan, F., Phillips, B.R., & Ricard, Y. (2009) Global warming of the mantle beneath continents back to the Archaean. *Gondwana Research*, **15**, 254–266.
- Cooper, K.M., Eiler, J.M., Sims, K.W.W., & Langmuir, C.H. (2009) Distribution of recycled crust within the upper mantle: Insights from the oxygen isotope composition of MORB from the Australian-Antarctic Discordance. *Geochemistry, Geophysics, Geosystems*, **10**, doi:10.1029/2009GC002728.
- Comer, B. (1994) Geological evolution of western Dronning Maud Land within a Gondwana framework: Geophysics subprogramme. Final project report to SACAR, Department of Geophysics, Witwaterstrand University, South Africa.
- Cox, K.G. (1970) Tectonics and volcanism of the Karoo period and their bearing on the postulated fragmentation of Gondwanaland. In *African Magmatism and Tectonics* (eds T.N. Clifford & I.G. Gass), pp. 211–235. Oliver & Boyd, Edinburgh.
- Cox, K.G. (1972) The Karoo volcanic cycle. *Journal of the Geological Society of London*, **128**, 311–336.
- Cox, K.G. (1978) Flood basalts, subduction and the break-up of Gondwanaland. *Nature*, **274**, 47–49.
- Cox, K.G. (1988) The Karoo province. In *Continental Flood Basalts* (ed J.D. MacDougall), pp. 239–271. Kluwer Academic Publishers, Dordrecht.
- Cox, K.G., Johnson, R.L., Monkman, L.J., Stillman, C.J., Vail, J.R., & Wood, D.S. (1965) The geology of the Nuanetsi igneous province. *Philosophical Transactions of the Royal Society of London, Series A: Mathematical and Physical Sciences*, **257**, 71–218.
- Cox, K.G., Macdonald, R., & Hornung, G. (1967) Geochemical and petrographic provinces in the Karoo basalts of southern Africa. *American*

- Mineralogist*, **52**, 1451–1474.
- Curtis, M.L., Riley, T.R., Owens, W.H., Leat, P.T., & Duncan, R.A. (2008) The form, distribution and anisotropy of magnetic susceptibility of Jurassic dykes in H.U. Sverdrupfjella, Dronning Maud Land, Antarctica. Implications for dyke swarm emplacement. *Journal of Structural Geology*, **30**, 1429–1447.
- Dasgupta, R., Hirschmann, M.M., & Stalker, K. (2006) Immiscible transition from carbonate-rich to silicate-rich melts in the 3 GPa melting interval of eclogite + CO₂ and genesis of silica-undersaturated ocean island lavas. *Journal of Petrology*, **47**, 647–671.
- Dasgupta, R., Hirschmann, M.M., & Smith, N.D. (2007) Partial Melting Experiments of Peridotite + CO₂ at 3 GPa and Genesis of Alkaline Ocean Island Basalts. *Journal of Petrology*, **48**, 2093–2124.
- Davis, F.A., Tangeman, J.A., Tenner, T.J., & Hirschmann, M.M. (2009) The composition of KLB-1 peridotite. *American Mineralogist*, **94**, 176–180.
- Day, J.M.D., Pearson, D.G., Macpherson, C.G., Lowry, D., & Carracedo, J. (2009) Pyroxenite-rich mantle formed by recycled oceanic lithosphere: oxygen-osmium isotope evidence from Canary Island lavas. *Geology (Boulder)*, **37**, 555–558.
- DePaolo, D.J. (1981a) Neodymium isotopes in the Colorado Front Range and crust-mantle evolution in the Proterozoic. *Nature*, **291**, 193–196.
- DePaolo, D.J. (1981b) Trace element and isotopic effects of combined wallrock assimilation and fractional crystallization. *Earth and Planetary Science Letters*, **53**, 189–202.
- Duncan, A.R., Erlank, A.J., & Marsh, J.S. (1984) Regional geochemistry of the Karoo igneous province. In *Petrogenesis of the Volcanic Rocks of the Karoo Province* (ed A.J. Erlank), pp. 355–388. Geological Society of South Africa, Special Publication, **13**.
- Duncan, A.R., Armstrong, R.A., Erlank, A.J., Marsh, J.S., & Watkins, R.T. (1990) MORB-related dolerites associated with the final phases of Karoo flood basalt volcanism in Southern Africa. In *Mafic Dykes and Emplacement Mechanisms; Proceedings of the Second International Dyke Conference* (eds A.J. Parker, P.C. Rickwood & D.H. Tucker), pp. 119–129. Balkema, Rotterdam.
- Duncan, R.A., Hooper, P.R., Rehacek, J., Marsh, J.S., & Duncan, A.R. (1997) The timing and duration of the Karoo igneous event, southern Gondwana. *Journal of Geophysical Research*, **102**, B8, 18,127–18,138.
- Eisele, J., Sharma, M., Galer, S.J.G., Blichert-Toft, J., Devey, C.W., & Hofmann, A.W. (2002) The role of sediment recycling in EM-1 inferred from Os, Pb, Hf, Nd, Sr isotope and trace element systematics of the Pitcairn Hotspot. *Earth and Planetary Science Letters*, **196**, 197–212.
- Elburg, M. & Goldberg, A. (2000) Age and geochemistry of Karoo dolerite dykes from Northeast Botswana. *Journal of African Earth Sciences*, **31**, 539–554.
- Elkins, L.J., Gaetani, G.A., & Sims, K. (2008) Partitioning of U and Th during garnet pyroxenite partial melting: Constraints on the source of alkaline ocean island basalts. *Earth and Planetary Science Letters*, **265**, 270–286.
- Elkins-Tanton, L.T. (2005) Continental magmatism caused by lithospheric delamination. In *Plates, Plumes, and Paradigms* (eds G.R. Foulger, J.H. Natland, D.C. Presnall & D.L. Anderson), pp. 449–461. Geological Society of America, Special Publication, **388**.
- Elkins-Tanton, L.T. & Hager, B.H. (2000) Melt intrusion as a trigger for lithospheric foundering and the eruption of the Siberian flood basalts. *Geophysical Research Letters*, **27**, 3937–3940.
- Elkins-Tanton, L.T., Draper, D.S., Agee, C.B., Jewell, J., Thorpe, A., & Hess, P.C. (2007) The last lavas erupted during the main phase of the Siberian flood volcanic province: results from experimental petrology. *Contributions to Mineralogy and Petrology*, **153**, 191–209.
- Ellam, R.M. (2006) New constraints on the petrogenesis of the Nuanetsi picrite basalts from Pb and Hf isotope data. *Earth and Planetary Science Letters*, **245**, 153–161.
- Ellam, R.M. & Cox, K.G. (1989) A Proterozoic lithospheric source for Karoo magmatism: evidence from the Nuanetsi picrites. *Earth and Planetary Science Letters*, **92**, 207–218.
- Ellam, R.M. & Cox, K.G. (1991) An interpretation of Karoo picrite basalts in terms of interaction between asthenospheric magmas and the mantle lithosphere. *Earth and Planetary Science Letters*, **105**, 330–342.
- Ellam, R.M. & Stuart, F.M. (2000) The sub-lithospheric source of North Atlantic basalts: evidence for, and significance of, a common end-member. *Journal of Petrology*, **41**, 919–932.
- Ellam, R.M., Carlson, R.W., & Shirey, S.B. (1992) Evidence from Re-Os isotopes for plume-lithosphere mixing in Karoo flood basalt genesis. *Nature*, **359**, 718–721.
- Erlank, A.J. (ed) (1984) *Petrogenesis of the Volcanic Rocks of the Karoo Province*. Geological Society of South Africa, Special Publication, **13**.
- Ewart, A., Milner, S.C., Armstrong, R.A., & Duncan, A.R. (1998) Etendeka volcanism of the Goboboseb Mountains and Messum igneous complex, Namibia. Part I: Geochemical evidence of Early Cretaceous Tristan plume melts and the role of crustal contamination in the Paraná-Etendeka CFB. *Journal of Petrology*, **39**, 191–225.
- Farnetani, C.G. & Richards, M.A. (1994) Numerical investigations of the mantle plume initiation model for flood basalt events. *Journal of Geophysical*

- Research*, **99**, B7, 13,813–13,833.
- Fitton, J.G., Saunders, A.D., Norry, M.J., Hardarson, B.S., & Taylor, R.N. (1997) Thermal and chemical structure of the Iceland Plume. *Earth and Planetary Science Letters*, **153**, 197–208.
- Fitton, J.G., Saunders, A.D., Kempton, P.D., & Hardarson, B.S. (2003) Does depleted mantle form an intrinsic part of the Iceland Plume? *Geochemistry, Geophysics, Geosystems*, **4**, doi:10.1029/2002GC000424.
- Fiorentini, M.L., Beresford, S.W., Deloule, E., Hanski, E.J., Stone, W.E., Pearson, N.J. (2008). The role of mantle-derived volatiles in the petrogenesis of Palaeoproterozoic ferropicrites in the Pechenga greenstone belt, northwestern Russia: insights from in-situ microbeam and nanobeam analysis of hydromagmatic amphibole. *Earth and Planetary Science Letters*, **268**, 2–14.
- Foulger, G.R. (2007) The “plate” model for the genesis of melting anomalies. In *Plates, Plumes, and Planetary Processes* (eds G.R. Foulger & D.M. Jurdy), pp. 1–28. Geological Society of America, Special Paper, **430**.
- Foulger, G.R., Natland, J.H., Presnall, D.C., & Anderson, D.L. (eds) (2005) *Plates, Plumes, and Paradigms*. Geological Society of America, Special Publication, **388**.
- Fram, M.S. & Leshner, C.E. (1997) Generation and polybaric differentiation of East Greenland early Tertiary flood basalts. *Journal of Petrology*, **38**, 231–275.
- Francis, D., Ludden, J., Johnstone, R., & Davis, W. (1999) Picrite evidence for more Fe in Archean mantle reservoirs. *Earth and Planetary Science Letters*, **167**, 197–213.
- Gaetani, G.A., Kent, A.J.R., Grove, T.L., Hutcheon, I.D., & Stolper, E.M. (2003) Mineral/melt partitioning of trace elements during hydrous peridotite partial melting. *Contributions to Mineralogy and Petrology*, **145**, 391–405.
- Gibson, I.L. (1966) Crustal flexures and flood basalts. *Tectonophysics*, **3**, 447–456.
- Gibson, S.A. (2002) Major element heterogeneity in Archean to Recent mantle plume starting-heads. *Earth and Planetary Science Letters*, **195**, 59–74.
- Gibson, S.A., Thompson, R.N., & Dickin, A.P. (2000) Ferropicrites: geochemical evidence for Fe-rich streaks in upwelling mantle plumes. *Earth and Planetary Science Letters*, **174**, 355–374.
- Gibson, S.A., Thompson, R.N., & Day, J.A. (2006) Timescales and mechanisms of plume-lithosphere interactions: $^{40}\text{Ar}/^{39}\text{Ar}$ geochronology and geochemistry of alkaline igneous rocks from the Parana-Etendeka large igneous province. *Earth and Planetary Science Letters*, **251**, 1–17.
- Goldstein, S.B. & Francis, D. (2008) The petrogenesis and mantle source of Archean ferropicrites from the Western Superior Province, Ontario, Canada. *Journal of Petrology*, **49**, 1729–1753.
- Gudfinnsson, G.H. & Presnall, D.C. (2005) Continuous gradations among primary carbonatitic, kimberlitic, melilititic, basaltic, picritic, and komatiitic melts in equilibrium with garnet lherzolite at 3–8 GPa. *Journal of Petrology*, **46**, 1645–1659.
- Gurnis, M. (1988) Large-scale mantle convection and the aggregation and dispersal of supercontinents. *Nature*, **332**, 695–699.
- Hanski, E.J. (1992) Petrology of the Pechenga ferropicrites and cogenetic Ni-bearing gabbro-wehrlite intrusions, Kola Peninsula, Russia. *Geological Survey of Finland – Bulletin*, **367**.
- Hanski, E.J. & Smolkin, V.F. (1989) Pechenga ferropicrites and other early Proterozoic picrites in the eastern part of the Baltic Shield. *Precambrian Research*, **45**, 63–82.
- Hanski, E.J. & Smolkin, V.F. (1995) Iron- and LREE-enriched mantle source for early Proterozoic intraplate magmatism as exemplified by the Pechenga ferropicrites, Kola Peninsula, Russia. *Lithos*, **34**, 107–125.
- Hargraves, R.B., Rehacek, J., & Hooper, P.R. (1997) Palaeomagnetism of the Karoo igneous rocks in Southern Africa. *South African Journal of Geology*, **100**, 195–212.
- Harmer, R.E., Lee, C.A., & Eglington, B.M. (1998) A deep mantle source for carbonatite magmatism: evidence from the nephelinites and carbonatites of the Buhara District, SE Zimbabwe. *Earth and Planetary Science Letters*, **158**, 131–142.
- Hauri, E.H. & Hart, S.R. (1993) Re-Os isotope systematics of HIMU and EMII oceanic island basalts from the South Pacific Ocean. *Earth and Planetary Science Letters*, **114**, 353–371.
- Hauri, E.H., Lassiter, J.C., & DePaolo, D.J. (1996) Osmium isotope systematics of drilled lavas from Mauna Loa, Hawaii. *Journal of Geophysical Research*, **101**, B5, 11,793–11,806.
- Hawkesworth, C.J., Marsh, J.S., Duncan, A.R., Erlank, A.J., & Norry, M.J. (1984) The role of continental lithosphere in the generation of the Karoo volcanic rocks: evidence from combined Nd- and Sr-isotope studies. In *Petrogenesis of the Volcanic Rocks of the Karoo Province* (ed A.J. Erlank), pp. 341–354. Geological Society of South Africa, Special Publication, **13**.
- Hawkesworth, C.J., Gallagher, K., Kelley, S., Mantovani, M., Peate, D.W., Regelous, M., & Rogers, N.W. (1992) Parana magmatism and the opening of the South Atlantic. In *Magmatism and the Causes of Continental Break-Up* (eds B.C. Storey, T. Alabaster & R.J. Pankhurst), pp. 221–240. Geological Society of London, Special Publication, **68**.
- Hergt, J.M., Peate, D.W., & Hawkesworth, C.J. (1991) The petrogenesis of Mesozoic Gondwana low-Ti flood basalts. *Earth and Planetary Science Letters*, **105**, 134–148.

- Herzberg, C. (2006) Petrology and thermal structure of the Hawaiian plume from Mauna Kea volcano. *Nature*, **444**, 605–609.
- Herzberg, C. & Zhang, J. (1996) Melting experiments on anhydrous peridotite KLB-1: composition of magmas in the upper mantle and transition zone. *Journal of Geophysical Research*, **101**, B4, 8271–8295.
- Hirose, K. & Kawamoto, T. (1995) Hydrous partial melting of lherzolite at 1 GPa: the effect of H₂O on the genesis of basaltic magmas. *Earth and Planetary Science Letters*, **133**, 463–473.
- Hirschmann, M.M., Ghiorso, M.S., & Stolper, E.M. (1999) Calculation of peridotite partial melting from thermodynamic models of minerals and melts. II. Isobaric variations in melts near the solidus and owing to variable source composition. *Journal of Petrology*, **40**, 297–313.
- Hirschmann, M.M., Kogiso, T., Baker, M.B., & Stolper, E.M. (2003) Alkaline magmas generated by partial melting of garnet pyroxenite. *Geology (Boulder)*, **31**, 481–484.
- Hooper, P.R. & Hawkesworth, C.J. (1993) Isotopic and geochemical constraints on the origin and evolution of the Columbia River Basalt. *Journal of Petrology*, **34**, 1203–1246.
- Horan, M.F., Walker, R.J., Fedorenko, V.A., & Czamanske, G.K. (1995) Osmium and neodymium isotopic constraints on the temporal and spatial evolution of Siberian flood basalt sources. *Geochimica et Cosmochimica Acta*, **59**, 5159–5168.
- Ichiyama, Y., Ishiwatari, A., Hirahara, Y., & Shuto, K. (2006) Geochemical and isotopic constraints on the genesis of the Permian ferropicritic rocks from the Mino-Tamba belt, SW Japan. *Lithos*, **89**, 47–65.
- Ichiyama, Y., Ishiwatari, A., Koizumi, K., Ishida, Y., & Machi, S. (2007) Olivine-spinifex basalt from the Tamba Belt, Southwest Japan: evidence for Fe- and high field strength element-rich ultramafic volcanism in Permian Ocean. *Island Arc*, **16**, 493–503.
- Jahn, B., Gruau, G., & Glikson, A.Y. (1982) Komatiites of the Onverwacht Group, S. Africa: REE geochemistry, Sm/Nd age and mantle evolution. *Contributions to Mineralogy and Petrology*, **80**, 25–40.
- Jakobsen, J.K., Veksler, I.V., Tegner, C., & Brooks, C.K. (2005) Immiscible iron- and silica-rich melts in basalt petrogenesis documented in the Skaergaard Intrusion. *Geology (Boulder)*, **33**, 885–888.
- Janney, P.E., le Roex, A.P., & Carlson, R.W. (2005) Hafnium isotope and trace element constraints on the nature of mantle heterogeneity beneath the central Southwest Indian Ridge (13°E to 47°E). *Journal of Petrology*, **46**, 2427–2464.
- Johnson, D.M., Hooper, P.R., & Conrey, R.M. (1999) XRF Analysis of Rocks and Minerals for Major and Trace Elements on a Single Low Dilution Li-tetraborate Fused Bead. *Advances in X-ray Analysis*, **41**, 843–867.
- Johnston, S.T. & Thorkelson, D.J. (2000) Continental flood basalts: episodic magmatism above long-lived hotspots. *Earth and Planetary Science Letters*, **175**, 247–256.
- Jones, A.P., Price, G.D., Price, N.J., DeCarli, P.S., & Clegg, R.A. (2002) Impact induced melting and the development of large igneous provinces. *Earth and Planetary Science Letters*, **202**, 551–561.
- Jourdan, F., Féraud, G., Bertrand, H., Kampunzu, A.B., Tshoso, G., Watkeys, M.K., & Le Gall, B. (2005) Karoo large igneous province: Brevity, origin, and relation to mass extinction questioned by new ⁴⁰Ar/³⁹Ar age data. *Geology (Boulder)*, **33**, 745–748.
- Jourdan, F., Féraud, G., Bertrand, H., Watkeys, M.K., Kampunzu, A.B., & Le Gall, B. (2006) Basement control on dyke distribution in large igneous provinces: case study of the Karoo triple junction. *Earth and Planetary Science Letters*, **241**, 307–322.
- Jourdan, F., Bertrand, H., Schaerer, U., Blichert-Toft, J., Féraud, G., & Kampunzu, A.B. (2007a) Major and trace element and Sr, Nd, Hf, and Pb isotope compositions of the Karoo large igneous province, Botswana-Zimbabwe: lithosphere vs mantle plume contribution. *Journal of Petrology*, **48**, 1043–1077.
- Jourdan, F., Féraud, G., Bertrand, H., & Watkeys, M.K. (2007b) From flood basalts to the inception of oceanization: example from the ⁴⁰Ar/³⁹Ar high-resolution picture of the Karoo large igneous province. *Geochemistry, Geophysics, Geosystems*, **8**, doi:10.1029/2006GC001392.
- Kamenetsky, V.S., Crawford, A.J., & Meffre, S. (2001) Factors controlling chemistry of magmatic spinel: an empirical study of associated olivine, Cr-spinel and melt inclusions from primitive rocks. *Journal of Petrology*, **42**, 655–671.
- Kent, R.W., Storey, M., & Saunders, A.D. (1992) Large igneous provinces: sites of plume impact or plume incubation? *Geology (Boulder)*, **20**, 891–894.
- Keshav, S., Gudfinnsson, G.H., Sen, G., & Fei, Y. (2004) High-pressure melting experiments on garnet clinopyroxenite and the alkalic to tholeiitic transition in ocean-island basalts. *Earth and Planetary Science Letters*, **223**, 365–379.
- King, S.D. & Anderson, D.L. (1995) An alternative mechanism of flood basalt formation. *Earth and Planetary Science Letters*, **136**, 269–279.
- King, S.D. & Anderson, D.L. (1998) Edge-driven convection. *Earth and Planetary Science Letters*, **160**, 289–296.
- Klein, E.M. (2003) Geochemistry of the Igneous Ocean Crust. In *The Crust* (ed R.L. Rudnick),

- Treatise on Geochemistry, **3**, pp. 433–463. Elsevier-Pergamon, Oxford.
- Kleinmanns, I.C., Kramers, J.D., & Kamber, B.S. (2003) Importance of water for Archaean granitoid petrology: a comparative study of TTG and potassic granitoids from Barberton Mountain Land, South Africa. *Contributions to Mineralogy and Petrology*, **145**, 377–389.
- Knaack, C., Cornelius, S.B., & Hooper, P.R. (1994) Trace Element Analyses of Rocks and Minerals by ICP-MS. GeoAnalytical Lab, Washington State University, <http://www.sees.wsu.edu/Geolab/equipment/icpms.html>.
- Kogiso, T., Hirschmann, M.M., & Frost, D.J. (2003) High-pressure partial melting of garnet pyroxenite: possible mafic lithologies in the source of ocean island basalts. *Earth and Planetary Science Letters*, **216**, 603–617.
- Kreissig, K., Naegler, T.F., Kramers, J.D., van Reenen, D.D., & Smit, C.A. (2000) An isotopic and geochemical study of the northern Kaapvaal Craton and the Southern Marginal Zone of the Limpopo Belt: are they juxtaposed terranes? *Lithos*, **50**, 1–25.
- Kurhila, M.I., Luttinen, A.V., Foland, K.A., & Heinonen, J.S. (2008) $^{40}\text{Ar}/^{39}\text{Ar}$ ages of Karoo-related basaltic dikes from Vestfjella, Dronning Maud Land, Antarctica. The Gondwana 13 Conference, Program & Abstracts, Institute of Geology and Geophysics, Chinese Academy of Sciences, Beijing, China, p. 100.
- Larsen, L.M. & Pedersen, A.K. (2000) Processes in high-Mg, high-T magmas: evidence from olivine, chromite and glass in Palaeogene picrites from West Greenland. *Journal of Petrology*, **41**, 1071–1098.
- Le Bas, M.J. (2000) IUGS reclassification of the high-Mg and picritic volcanic rocks. *Journal of Petrology*, **41**, 1467–1470.
- Le Bas, M.J., Le Maitre, R.W., Streckeisen, A., & Zanettin, B.A. (1986) Chemical classification of volcanic rocks based on the total alkali-silica diagram. *Journal of Petrology*, **27**, 745–750.
- Le Roux, V., Lee, C.A., & Turner, S.J. (2010) Zn/Fe systematics in mafic and ultramafic systems: implications for detecting major element heterogeneities in the Earth's mantle. *Geochimica et Cosmochimica Acta*, **74**, 2779–2796.
- Leat, P.T., Luttinen, A.V., Storey, B.C., & Millar, I.L. (2006) Sills of the Theron Mountains, Antarctica: evidence for long distance transport of mafic magmas during Gondwana break-up. In *Dyke Swarms: Time Markers of Crustal Evolution* (eds E.J. Hanski, S. Mertanen, O.T. Rämö & J. Vuollo), pp. 183–199. Taylor & Francis, Abingdon.
- Lee, C.A., Luffi, P., Plank, T., Dalton, H., & Leeman, W.P. (2009) Constraints on the depths and temperatures of basaltic magma generation on Earth and other terrestrial planets using new thermobarometers for mafic magmas. *Earth and Planetary Science Letters*, **279**, 20–33.
- Li, C. & Ripley, E.M. (2010) The relative effects of composition and temperature on olivine-liquid Ni partitioning: Statistical deconvolution and implications for petrologic modeling. *Chemical Geology*, **275**, 99–104.
- Lightfoot, P.C., Naldrett, A.J., Gorbachev, N.S., Doherty, W., & Fedorenko, V.A. (1990) Geochemistry of the Siberian Trap of the Noril'sk area, USSR, with implications for the relative contributions of crust and mantle to flood basalt magmatism. *Contributions to Mineralogy and Petrology*, **104**, 631–644.
- Lightfoot, P.C., Hawkesworth, C.J., Hergt, J.M., Naldrett, A.J., Gorbachev, N.S., Fedorenko, V.A., & Doherty, W. (1993) Remobilisation of the continental lithosphere by a mantle plume: major-, trace-element, and Sr-, Nd-, and Pb-isotope evidence from picritic and tholeiitic lavas of the Noril'sk District, Siberian Trap, Russia. *Contributions to Mineralogy and Petrology*, **114**, 171–188.
- Luttinen, A.V. & Furnes, H. (2000) Flood basalts of Vestfjella: Jurassic magmatism across an Archaean-Proterozoic lithospheric boundary in Dronning Maud Land, Antarctica. *Journal of Petrology*, **41**, 1271–1305.
- Luttinen, A.V. & Huhma, H. (2005) Source characteristics of Jurassic ferropicrites from Dronning Maud Land, Antarctica. *Geochimica et Cosmochimica Acta Supplement*, **69**, Goldschmidt Conference Abstracts 2005, p. A106.
- Luttinen, A.V., Rämö, O.T., & Huhma, H. (1998) Neodymium and strontium isotopic and trace element composition of a Mesozoic CFB suite from Dronning Maud Land, Antarctica: Implications for lithosphere and asthenosphere contributions to Karoo magmatism. *Geochimica et Cosmochimica Acta*, **62**, 2701–2714.
- Luttinen, A.V., Zhang, X., & Foland, K.A. (2002) 159 Ma Kjaekbeinet lamproites (Dronning Maud Land, Antarctica) and their implications for Gondwana breakup processes. *Geological Magazine*, **139**, 525–539.
- MacDougall, J.D. (ed) (1988) *Continental Flood Basalts*. Kluwer Academic Publishers, Dordrecht, The Netherlands.
- McDonough, W.F. & Sun, S.S. (1995) The composition of the Earth. *Chemical Geology*, **120**, 223–253.
- McKenzie, D. (1985) The extraction of magma from the crust and mantle. *Earth and Planetary Science Letters*, **74**, 81–91.
- McKenzie, D. & Bickle, M.J. (1988) The volume and composition of melt generated by extension of the lithosphere. *Journal of Petrology*, **29**, 625–679.
- Meisel, T., Walker, R.J., Irving, A.J., & Lorand, J.P. (2001) Osmium isotopic compositions of mantle xenoliths: a global perspective. *Geochimica et*

- Cosmochimica Acta*, **65**, 1311–1323.
- Menzies, M.A. (1992) The lower lithosphere as a major source for continental flood basalts: a re-appraisal. In *Magmatism and the Causes of Continental Break-Up* (eds B.C. Storey, T. Alabaster & R.J. Pankhurst), pp. 31–39. Geological Society of London, Special Publication, **68**.
- Morgan, W.J. (1971) Convection plumes in the lower mantle. *Nature*, **230**, 42–43.
- Nishio, Y., Nakai, S., Ishii, T., & Sano, Y. (2007) Isotope systematics of Li, Sr, Nd, and volatiles in Indian Ocean MORBs of the Rodrigues triple junction: Constraints on the origin of the DUPAL anomaly. *Geochimica et Cosmochimica Acta*, **71**, 745–759.
- Niu, Y. (2009) Some basic concepts and problems on the petrogenesis of intra-plate ocean island basalts. *Chinese Science Bulletin*, **54**, 4148–4160.
- Niu, Y. & O'Hara, M.J. (2003) Origin of ocean island basalts: A new perspective from petrology, geochemistry, and mineral physics considerations. *Journal of Geophysical Research*, **108**, B4, doi:10.1029/2002JB002048.
- Pearce, J.A. (1996) A user's guide to basalt discrimination diagrams. In *Trace Element Geochemistry of Volcanic Rocks: Applications for Massive Sulphide Exploration* (ed D.A. Wyman), pp. 79–113. Geological Association of Canada, Short Course Notes, **12**.
- Peate, D.W., Baker, J.A., Blichert-Toft, J., Hilton, D.R., Storey, M., Kent, A.J.R., Brooks, C.K., Hansen, H., Pedersen, A.K., & Duncan, R.A. (2003) The Prins of Wales Bjerge Formation lavas, East Greenland: the transition from tholeiitic to alkalic magmatism during Palaeogene continental break-up. *Journal of Petrology*, **44**, 279–304.
- Peters, M. (1989) Die Vulkanite im westlichen und mittleren Neuschwabenland, Vestfjella und Ahlmannryggen, Antarktika; Petrographie, Geochemie, Geochronologie, Palaeomagnetismus, geotektonische Implikationen. *Berichte zur Polarforschung* **61**, Alfred Wegener-Institut für Polar- und Maareforschung, Bremerhaven. (In German)
- Pik, R., Deniel, C., Coulon, C., Yirgu, G., & Marty, B. (1999) Isotopic and trace element signatures of Ethiopian flood basalts: evidence for plume-lithosphere interactions. *Geochimica et Cosmochimica Acta*, **63**, 2263–2279.
- Putirka, K.D. (1999) Melting depths and mantle heterogeneity beneath Hawaii and the East Pacific Rise: constraints from Na/Ti and rare earth element ratios. *Journal of Geophysical Research*, **104**, B2, 2817–2829.
- Putirka, K.D., Perfit, M., Ryerson, F.J., & Jackson, M.G. (2007) Ambient and excess mantle temperatures, olivine thermometry, and active vs. passive upwelling. *Chemical Geology*, **241**, 177–206.
- Rajamani, V., Shivkumar, K., Hanson, G.N., & Shirey, S.B. (1985) Geochemistry and petrogenesis of amphibolites, Kolar schist belt, South India: evidence for komatiitic magma derived by low percentages of melting of the mantle. *Journal of Petrology*, **26**, 92–123.
- Reiners, P.W. & Nelson, B.K. (1998) Temporal-compositional-isotopic trends in rejuvenated-stage magmas of Kauai, Hawaii, and implications for mantle melting processes. *Geochimica et Cosmochimica Acta*, **62**, 2347–2368.
- Reisberg, L., Zindler, A., Marcantonio, F., White, W.M., Wyman, D., & Weaver, B.L. (1993) Os isotope systematics in ocean island basalts. *Earth and Planetary Science Letters*, **120**, 149–167.
- Richards, M.A., Duncan, R.A., & Courtillot, V.E. (1989) Flood basalts and hot-spot tracks: plume heads and tails. *Science*, **246**, 103–107.
- Riley, T.R., Leat, P.T., Curtis, M.L., Millar, I.L., Duncan, R.A., & Fazel, A. (2005) Early-Middle Jurassic dolerite dykes from Western Dronning Maud Land (Antarctica): Identifying mantle sources in the Karoo Large Igneous Province. *Journal of Petrology*, **46**, 1489–1524.
- Riley, T.R., Curtis, M.L., Leat, P.T., Watkeys, M.K., Duncan, R.A., Millar, I.L., & Owens, W.H. (2006) Overlap of Karoo and Ferrar magma types in KwaZulu-Natal, South Africa. *Journal of Petrology*, **47**, 541–566.
- Rudnick, R.L. & Gao, S. (2003) The Composition of the Continental Crust. In *The Crust* (ed R.L. Rudnick), Treatise on Geochemistry, **3**, pp. 1–64. Elsevier-Pergamon, Oxford.
- Ryabov, V.V., Bakumenko, I.T., & Fominykh, I.M. (1977) Dendritic megacrystals of clinopyroxene in trap rocks of the Norilsk region and some questions concerning their formation. *Akade. Nauk SSSR, Sibirskoe Otdelenie, Instituta Geologii i Geofiziki Trudy*, **349**, 47–74. (in Russian)
- Sano, T., Fujii, T., Deshmukh, S.S., Fukuoka, T., & Aramaki, S. (2001) Differentiation processes of Deccan Trap basalts: contribution from geochemistry and experimental petrology. *Journal of Petrology*, **42**, 2175–2195.
- Saunders, A.D. (2005) Large igneous provinces: origin and environmental consequences. *Elements*, **1**, 259–263.
- Saunders, A.D., Norry, M.J., & Tarney, J. (1988) Origin of MORB and chemically-depleted mantle reservoirs: trace element constraints. *Journal of Petrology*, Special Volume, **1**, 415–445.
- Segev, A. (2002) Flood basalts, continental breakup and the dispersal of Gondwana: evidence for periodic migration of upwelling mantle flows (plumes). *European Geosciences Union Stephan Mueller Special Publication Series*, **2**, 171–191.
- Shirey, S.B. & Walker, R.J. (1998) The Re-Os isotope system in cosmochemistry and high-temperature geochemistry. *Annual Review of Earth and*

- Planetary Sciences*, **26**, 423–500.
- Shirey, S.B., Krewin, K.W., Berg, J.H., & Carlson, R.W. (1994) Temporal changes in the sources of flood basalts: isotopic and trace element evidence from the 1100 Ma old Keweenaw Mamainse Point Formation, Ontario, Canada. *Geochimica et Cosmochimica Acta*, **58**, 4475–4490.
- Silver, P.G., Behn, M.D., Kelley, K.A., Schmitz, M., & Savage, B. (2006) Understanding cratonic flood basalts. *Earth and Planetary Science Letters*, **245**, 190–201.
- Sobolev, A.V., Hofmann, A.W., Sobolev, S.V., & Nikogosian, I.K. (2005) An olivine-free mantle source of Hawaiian shield basalts. *Nature*, **434**, 590–597.
- Sobolev, A.V., Hofmann, A.W., Kuzmin, D.V., Yaxley, G.M., Arndt, N.T., Chung, S., Danyushevsky, L.V., Elliott, T., Frey, F.A., Garcia, M.O., Gurenko, A.A., Kamenetsky, V.S., Kerr, A.C., Krivolutskaya, N.A., Matvienkov, V.V., Nikogosian, I.K., Rocholl, A., Sigurdsson, I.A., Sushchevskaya, N.M., & Teklay, M. (2007) The amount of recycled crust in sources of mantle-derived melts. *Science*, **316**, 412–417.
- Sobolev, A.V., Hofmann, A.W., Brüggmann, G., Batanova, V.G., & Kuzmin, D.V. (2008) A quantitative link between recycling and osmium isotopes. *Science*, **321**, 536.
- Song, X., Qi, H., Robinson, P.T., Zhou, M., Cao, Z., & Chen, L. (2008) Melting of the subcontinental lithospheric mantle by the Emeishan mantle plume: evidence from the basal alkaline basalts in Dongchuan, Yunnan, southwestern China. *Lithos*, **100**, 93–111.
- Spera, F.J. & Bohrsen, W.A. (2001) Energy-constrained open-system magmatic processes I: General model and energy-constrained assimilation and fractional crystallization (EC-AFC) formulation. *Journal of Petrology*, **42**, 999–1018.
- Srivastava, R.K., Chalapatthi Rao, N.V., & Sinha, A.K. (2009) Cretaceous potassic intrusives with affinities to aillikites from Jharia area: magmatic expression of metasomatically veined and thinned lithospheric mantle beneath Singhbhum Craton, eastern India. *Lithos*, **112**, 407–418.
- Stolper, E.M., Sherman, S., Garcia, M.O., Baker, M.B., & Seaman, C. (2004) Glass in the submarine section of the HSDP2 drill core, Hilo, Hawaii. *Geochemistry, Geophysics, Geosystems*, **5**, doi:10.1029/2003GC000553.
- Stone, W.E., Crocket, J.H., Dickin, A.P., & Fleet, M.E. (1995) Origin of Archean ferropicrites: geochemical constraints from the Boston Creek Flow, Abitibi greenstone belt, Ontario, Canada. *Chemical Geology*, **121**, 51–71.
- Stone, W.E., Deloule, E., Larson, M.S., & Leshar, C.M. (1997) Evidence for hydrous high-MgO melts in the Precambrian. *Geology (Boulder)*, **25**, 143–146.
- Storey, B.C., Alabaster, T., Hole, M.J., Pankhurst, R.J., & Wever, H.E. (1992) Role of subduction-plate boundary forces during the initial stages of Gondwana break-up: evidence from the proto-Pacific margin of Antarctica. In *Magmatism and the Causes of Continental Break-Up* (eds B.C. Storey, T. Alabaster & R.J. Pankhurst), pp. 149–163. Geological Society of London, Special Publication, **68**.
- Storey, M., Mahoney, J.J., & Saunders, A.D. (1997) Cretaceous basalts in Madagascar and the transition between plume and continental lithosphere mantle sources. In *Large Igneous Provinces: Continental, Oceanic, and Planetary Flood Volcanism* (eds J.J. Mahoney & M.F. Coffin), pp. 95–122. American Geophysical Union, *Geophysical Monograph*, **100**.
- Stracke, A., Bizimis, M., & Salters, V.J.M. (2003) Recycling oceanic crust: quantitative constraints. *Geochemistry, Geophysics, Geosystems*, **4**, doi:10.1029/2001GC000223.
- Sun, S.S. & McDonough, W.F. (1989) Chemical and isotopic systematics of oceanic basalts: Implications for mantle composition and processes. In *Magmatism in the Ocean Basins* (eds A.D. Saunders & M.J. Norry), pp. 313–345. Geological Society, Special Publications, **42**.
- Sweeney, R.J., Falloon, T.J., Green, D.H., & Tatsumi, Y. (1991) The mantle origins of Karoo picrites. *Earth and Planetary Science Letters*, **107**, 256–271.
- Sweeney, R.J., Duncan, A.R., & Erlank, A.J. (1994) Geochemistry and petrogenesis of central Lebombo basalts of the Karoo igneous province. *Journal of Petrology*, **35**, 95–125.
- Talarico, F., Borsi, L., & Lombardo, B. (1995) Relict granulites in the Ross Orogen of northern Victoria Land (Antarctica), II. Geochemistry and palaeotectonic implications. *Precambrian Research*, **75**, 157–174.
- Thompson, R.N. & Gibson, S.A. (2000) Transient high temperatures in mantle plume heads inferred from magnesian olivines in Phanerozoic picrites. *Nature*, **407**, 502–506.
- Tommasini, S., Manetti, P., Innocenti, F., Abebe, T., Sintoni, M.F., & Conicelli, S. (2005) The Ethiopian subcontinental mantle domains: geochemical evidence from Cenozoic mafic lavas. *Mineralogy and Petrology*, **84**, 259–281.
- Tuff, J., Takahashi, E., & Gibson, S.A. (2005) Experimental constraints on the role of garnet pyroxenite in the genesis of high-Fe mantle plume derived melts. *Journal of Petrology*, **46**, 2023–2058.
- Turner, S., Hawkesworth, C.J., Gallagher, K., Stewart, K., Peate, D., & Mantovani, M.S.M. (1996) Mantle plumes, flood basalts, and thermal models for melt generation beneath continents: assessment of a conductive heating model and application to the

- Parana. *Journal of Geophysical Research*, **101**, B5, 11,503–11,518.
- Walker, R.J., Morgan, J.W., Hanski, E.J., & Smolkin, V.F. (1997) Re-Os systematics of early Proterozoic ferropicrites, Pechenga Complex, northwestern Russia: evidence for ancient ^{187}Os -enriched plumes. *Geochimica et Cosmochimica Acta*, **61**, 3145–3160.
- Walter, M.J. (1998) Melting of garnet peridotite and the origin of komatiite and depleted lithosphere. *Journal of Petrology*, **39**, 29–60.
- Wasserburg, B.J., Jacobsen, S.B., DePaolo, D.J., McCulloch, M.T., & Wen, T. (1981) Precise determination of Sm/Nd ratios, Sm and Nd isotopic abundances in standard solutions. *Geochimica et Cosmochimica Acta*, **45**, 2311–2323.
- Watkeys, M.K. (2002) Development of the Lebombo rifted volcanic margin of Southeast Africa. In *Volcanic Rift Margins* (eds M.A. Menzies, S.L. Klemperer, C.J. Ebinger & J. Baker), pp. 27–46. Geological Society of America, Special Paper, **362**.
- White, R. & McKenzie, D. (1989) Magmatism at rift zones: the generation of volcanic continental margins and flood basalts. *Journal of Geophysical Research*, **94**, B6, 7685–7729.
- Wooden, J.L., Czamanske, G.K., Fedorenko, V.A., Arndt, N.T., Chauvel, C., Bouse, R.M., King, B.W., Knight, R.J., & Siems, D.F. (1993) Isotopic and trace-element constraints on mantle and crustal contributions to Siberian continental flood basalts, Noril'sk area, Siberia. *Geochimica et Cosmochimica Acta*, **57**, 3677–3704.
- Workman, R.K. & Hart, S.R. (2005) Major and trace element composition of the depleted MORB mantle (DMM). *Earth and Planetary Science Letters*, **231**, 53–72.
- Workman, R.K., Hart, S.R., Jackson, M.G., Regelous, M., Farley, K.A., Blusztajn, J.S., Kurz, M., & Staudigel, H. (2004) Recycled metasomatized lithosphere as the origin of the enriched mantle II (EM2) end-member: Evidence from the Samoan volcanic chain. *Geochemistry, Geophysics, Geosystems*, **5**, doi:10.1029/2003GC000623.
- Xue, X., Baadsgaard, H., Irving, A.J., Scarfe, C.M., & Brearley, M. (1990) Geochemical and isotopic characteristics of lithospheric mantle beneath West Kettle River, British Columbia: evidence from ultramafic xenoliths. *Journal of Geophysical Research*, **95**, B10, 15,879–15,891.
- Zhang, Z., Mahoney, J.J., Mao, J., & Wang, F. (2006) Geochemistry of picritic and associated basalt flows of the Western Emeishan flood basalt province, China. *Journal of Petrology*, **47**, 1997–2019.
- Zhang, X., Luttinen, A.V., Elliot, D.H., Larsson, K., & Foland, K.A. (2003) Early stages of Gondwana breakup: the $^{40}\text{Ar}/^{39}\text{Ar}$ geochronology of Jurassic basaltic rocks from western Dronning Maud Land, Antarctica, and implications for the timing of magmatic and hydrothermal events. *Journal of Geophysical Research*, **108**, B9, doi:10.1029/2001JB001070.
- Zolotukhin, V.V. & Al'mukhamedov, A.I. (1991) Basalts of the Siberian Platform: occurrence conditions, chemical composition, formation mechanism. *Akade. Nauk SSSR, Sibirskoe Otdelenie, Instituta Geologii i Geofiziki Trudy*, **803**, 7–39. (in Russian)
- Zolotukhin, V.V., Al'mukhamedov, A.I., & Tkachenko, N.A. (1991) Composition of main rock-forming minerals in Deccan and Siberian trap rocks: a comparison. *Akade. Nauk SSSR, Sibirskoe Otdelenie, Instituta Geologii i Geofiziki Trudy*, **803**, 140–177. (in Russian)

Appendix I. Electron microprobe analyses of minerals of the Vestfjella ferropicrites and related rocks (data that was not published in Papers I–III).

OLIVINE

CR	Sample	Analysis	SiO ₂	TiO ₂	Al ₂ O ₃	FeO	MnO	MgO	CaO	Cr ₂ O ₃	NiO	Total	Notes	Fo
1	117-KHG-91	117KHG/r2/19	38.53	0.04	0.02	21.37	0.26	40.00	0.41	0.02	0.24	100.88	c	0.77
2	117-KHG-91	117KHG/r4/27	38.79	0.02	0.04	19.07	0.26	41.34	0.28	0.01	0.21	100.03	c	0.79
2	117-KHG-91	117KHG/r4/28	39.00	0.01	0.05	15.06	0.22	43.73	0.23	0.04	0.41	98.76	c	0.84
2	117-KHG-91	117KHG/r4/29	36.66	0.17	0.01	29.47	0.49	33.25	0.37	0.03	0.21	100.66	r	0.67
3	117-KHG-91	117KHG/r4/31	38.26	0.04	0.05	19.58	0.25	40.84	0.36	0.04	0.29	99.70	c	0.79
4	117-KHG-91	117KHG/r4/32	38.52	0.03	0.05	16.95	0.28	41.94	0.36	0.02	0.30	98.45	c	0.82
5	117-KHG-91	117KHG/r4/33	38.34	0.04	0.07	17.65	0.25	42.70	0.31	0.05	0.31	99.71	c	0.81
6	117-KHG-91	117KHG/36	38.40	0.03	0.04	17.34	0.26	41.83	0.26	0.04	0.30	98.50	c	0.81
7	117-KHG-91	117KHG/38	38.91	0.00	0.05	18.88	0.29	41.46	0.23	0.02	0.28	100.13	c	0.80
8	117-KHG-91	117KHG/37	38.03	0.02	0.06	16.33	0.27	42.43	0.27	0.03	0.35	97.79	c	0.82
9	117-KHG-91	117KHG/39	39.18	0.05	0.08	16.19	0.20	43.55	0.25	0.03	0.39	99.94	c	0.83
1	ALWM1e-98	WM1e/r1/1	39.64	0.02	0.02	18.51	0.27	41.45	0.32	0.02	0.32	100.59	c	0.80
2	ALWM1e-98	WM1e/r1/2	40.76	0.06	0.11	13.77	0.18	44.92	0.47	0.10	0.39	100.75	c	0.85
3	ALWM1e-98	WM1e/r2/6	40.01	0.04	0.12	14.87	0.20	43.14	0.45	0.04	0.33	99.19	c	0.84
4	ALWM1e-98	WM1e/r2/9	39.93	0.02	0.05	14.64	0.22	44.50	0.41	0.07	0.37	100.21	c	0.84
5	ALWM1e-98	WM1e/r2/12	40.45	0.03	0.04	14.61	0.20	44.61	0.47	0.09	0.35	100.86	c	0.84
6	ALWM1e-98	WM1e/r2/13	39.95	0.00	0.07	15.27	0.22	43.89	0.41	0.10	0.38	100.30	mi1	0.84
6	ALWM1e-98	WM1e/r2/18	40.10	0.04	0.02	14.60	0.20	44.22	0.47	0.08	0.38	100.12	spl17	0.84
6	ALWM1e-98	WM1e/r2/20	40.07	0.01	0.04	14.65	0.21	44.61	0.50	0.02	0.34	100.44	mi2	0.84
7	ALWM1e-98	WM1e/r4/27	39.76	0.04	0.02	17.69	0.20	42.44	0.29	0.04	0.36	100.84	c	0.81
7	ALWM1e-98	WM1e/r4/28	40.78	0.01	0.04	13.86	0.19	44.87	0.34	0.04	0.38	100.50	r	0.85
8	ALWM1e-98	WM1e/r4/29	39.72	0.07	0.05	17.53	0.26	41.95	0.45	0.06	0.29	100.38	c	0.81
9	ALWM1e-98	WM1e/r4/30	39.23	0.03	0.01	19.25	0.31	41.26	0.29	0.04	0.30	100.71	c	0.79
9	ALWM1e-98	WM1e/r4/31	40.02	0.00	0.06	16.20	0.23	43.28	0.37	0.05	0.34	100.55	r	0.83
9	ALWM1e-98	WM1e/ol	39.44	0.04	0.05	17.62	0.27	42.64	0.37	0.00	0.30	100.73	c	0.81
10	ALWM1e-98	WM1e/ol2	39.34	0.04	0.03	17.85	0.16	42.31	0.40	0.02	0.32	100.46	c	0.81
11	ALWM1e-98	WM1e/r2/O1/r	39.33	0.02	0.02	17.00	0.23	42.77	0.36	0.02	0.31	100.07	mi	0.82
12	ALWM1e-98	WM1e/r2/O2/k	40.30	0.07	0.08	13.39	0.09	46.76	0.26	0.11	0.23	101.30	mi	0.86
13	ALWM1e-98	WM1e/r2/O2/i	39.03	0.00	0.03	18.48	0.20	42.02	0.39	0.05	0.33	100.53	miD	0.80
14	ALWM1e-98	WM1e/r2/O3/c	38.70	0.00	0.03	19.69	0.25	40.99	0.36	0.01	0.31	100.33	c	0.79
14	ALWM1e-98	WM1e/r2/O3/r	39.92	0.10	0.01	14.15	0.16	46.15	0.42	0.06	0.33	101.30	r	0.85
1	ALWM3a-03	WM3/r1/1	40.06	0.03	0.06	18.29	0.29	41.90	0.36	0.06	0.31	101.36	c	0.80
1	ALWM3a-03	WM3/r1/2	39.63	0.00	0.04	18.82	0.28	42.09	0.34	0.04	0.32	101.57	mi	0.80
2	ALWM3a-03	WM3/r3/27	39.42	0.05	0.03	19.58	0.27	41.48	0.45	0.08	0.36	101.72	spl26	0.79
2	ALWM3a-03	WM3/r3/28	39.94	0.00	0.05	19.20	0.25	41.34	0.44	0.04	0.29	101.57	c	0.79
2	ALWM3a-03	WM3/r3/29	40.29	0.04	0.06	17.36	0.26	42.46	0.46	0.14	0.30	101.37	spl30	0.81

Appendix I (continued)

CLINOPYROXENE

CR	Sample	Analysis	SiO ₂	TiO ₂	Al ₂ O ₃	FeO	MnO	MgO	CaO	Na ₂ O	Cr ₂ O ₃	V ₂ O ₃	Total	Notes
1	14-KHG-90	14-KHG/1	52.06	1.09	2.14	6.93	0.13	15.60	21.86	0.35	0.39	0.04	100.59	pcc
1	14-KHG-90	14-KHG/2	51.63	1.17	2.36	5.90	0.10	15.66	22.08	0.34	0.73	0.06	100.02	pcc
1	14-KHG-90	14-KHG/3	50.67	1.46	3.51	7.41	0.13	14.57	21.71	0.38	0.54	0.06	100.44	pcc
2	14-KHG-90	14-KHG/4	48.95	2.17	4.23	7.71	0.12	13.71	21.75	0.46	0.31	0.05	99.48	pcc
3	14-KHG-90	14-KHG/5	51.56	1.24	2.37	7.87	0.17	15.13	21.32	0.32	0.18	0.07	100.24	pcc
4	14-KHG-90	14-KHG/6	51.12	1.25	2.41	7.19	0.14	15.15	21.69	0.37	0.17	0.06	99.54	pcc
4	14-KHG-90	14-KHG/7	48.47	2.39	4.51	8.23	0.13	13.83	21.28	0.45	0.37	0.09	99.75	pccz1
4	14-KHG-90	14-KHG/8	52.10	1.05	1.87	6.15	0.10	15.93	22.37	0.27	0.37	0.06	100.27	pcc
5	14-KHG-90	14-KHG/9	51.74	1.21	2.55	6.34	0.10	15.80	22.07	0.30	0.57	0.04	100.72	pcc
5	14-KHG-90	14-KHG/10	51.17	1.36	2.87	6.53	0.12	15.22	22.00	0.36	0.58	0.07	100.27	pcc
5	14-KHG-90	14-KHG/11	50.14	1.61	3.49	7.60	0.12	14.62	21.78	0.41	0.39	0.04	100.20	pcc
6	14-KHG-90	14-KHG/12	52.00	1.11	2.03	7.08	0.11	15.66	21.47	0.32	0.30	0.05	100.13	pcc
7	14-KHG-90	14-KHG/13	52.45	0.94	1.83	6.99	0.14	16.08	20.92	0.30	0.49	0.04	100.18	pcc
7	14-KHG-90	14-KHG/14	50.45	1.56	3.29	7.34	0.11	14.39	21.96	0.36	0.33	0.05	99.82	pcc
7	14-KHG-90	14-KHG/15	50.68	1.46	3.28	7.37	0.09	14.77	21.75	0.37	0.61	0.07	100.46	pcc
8	14-KHG-90	14-KHG/16	49.60	1.91	4.28	7.84	0.10	14.10	21.44	0.46	0.39	0.08	100.20	pcc
8	14-KHG-90	14-KHG/17	52.17	1.28	2.37	7.98	0.11	15.19	21.62	0.31	0.13	0.07	101.22	pcc
9	14-KHG-90	14-KHG/18	51.86	1.12	1.97	6.48	0.12	15.82	21.56	0.30	0.41	0.04	99.67	pcc
1	JSH/B006	B006a/1	52.06	1.09	2.11	7.47	0.15	15.49	21.77	0.30	0.29	0.04	100.76	gm
2	JSH/B006	B006a/2	48.94	2.05	4.25	8.73	0.14	13.67	21.70	0.46	0.07	0.09	100.09	gm/amph3
3	JSH/B006	B006a/2/12	44.99	4.18	6.75	9.76	0.20	11.73	21.40	0.50	0.00	0.11	99.63	mi14r
3	JSH/B006	B006a/2/13	47.33	2.72	4.71	8.27	0.16	13.23	21.80	0.45	0.12	0.11	98.89	mi14c
4	JSH/B006	B006a/2/16	50.47	1.43	2.52	9.10	0.19	14.72	21.05	0.32	0.01	0.08	99.89	gmc/amph18
4	JSH/B006	B006a/2/17	46.91	2.78	5.18	8.98	0.14	12.63	21.48	0.47	0.01	0.08	98.67	gm/amph18
5	JSH/B006	B006a/2/20	50.41	1.41	2.47	9.06	0.19	14.66	21.41	0.33	0.00	0.07	99.79	gm/amph19
6	JSH/B006	B006b/4/10	47.09	3.18	7.07	12.33	0.24	10.12	21.22	0.56	0.01	0.10	102.10	mi-12
7	JSH/B006	B006b/4/16	53.45	0.94	1.65	6.90	0.11	16.93	20.83	0.38	0.53	0.04	101.75	gm
8	JSH/B006	B006b/4/17	50.26	1.43	3.24	7.58	0.12	14.77	22.15	0.43	0.42	0.04	100.44	gm
9	JSH/B006	B006b/5/19	46.43	3.37	6.64	10.29	0.19	11.66	21.31	0.54	0.01	0.14	100.58	mi20-21
10	JSH/B006	B006b/6/28	50.41	1.52	3.19	7.52	0.12	15.03	21.94	0.39	0.38	0.08	100.57	gmc
10	JSH/B006	B006b/6/29	47.54	2.48	4.97	8.84	0.16	12.69	22.21	0.44	0.00	0.11	99.43	gmr
11	JSH/B006	B006b/6/31	47.62	2.53	4.85	9.26	0.23	12.64	21.35	0.48	0.00	0.10	99.06	gm/amph32
12	JSH/B006	B006b/7/36	51.12	1.43	2.86	6.84	0.08	15.39	21.78	0.43	0.76	0.05	100.74	gm/amph37
13	JSH/B006	B006b/7/41	51.72	1.09	2.16	7.17	0.11	15.69	21.46	0.33	0.38	0.05	100.16	gm
1	AL/B7-98	B798/r1/4	51.24	1.00	1.93	11.47	0.28	15.60	18.83	0.22	0.00	0.04	100.61	
1	AL/B7-98	B798/r1/5	47.88	2.24	4.52	9.99	0.17	14.00	20.36	0.36	0.04	0.09	99.64	

Appendix I (continued)

CLINOPYROXENE

CR Sample	Analysis	SiO ₂	TiO ₂	Al ₂ O ₃	FeO	MnO	MgO	CaO	Na ₂ O	Cr ₂ O ₃	V ₂ O ₃	Total	Notes
2 AL/B7-98	B798/r1/7	48.08	1.35	2.95	8.32	0.14	15.80	19.91	0.30	0.46	0.04	97.36	
2 AL/B7-98	B798/r1/8	50.34	1.40	3.10	8.53	0.17	15.69	20.47	0.33	0.44	0.10	100.58	
3 AL/B7-98	B798/r1/9	49.85	1.69	3.59	9.39	0.18	14.86	20.00	0.33	0.10	0.08	100.07	
4 AL/B7-98	B798/r2/14	50.12	1.34	3.01	11.10	0.24	14.21	20.10	0.35	0.01	0.07	100.55	r
4 AL/B7-98	B798/r2/15	49.22	1.38	2.95	8.05	0.14	15.96	19.66	0.29	0.63	0.06	98.34	c
5 AL/B7-98	B798/r2/16	51.37	1.03	2.13	10.81	0.23	16.70	17.62	0.23	0.01	0.05	100.19	r
5 AL/B7-98	B798/r2/17	50.83	1.35	2.95	7.96	0.17	15.73	20.16	0.26	0.68	0.07	100.15	c
5 AL/B7-98	B798/r2/18	50.56	1.25	2.63	9.63	0.23	15.87	19.51	0.27	0.04	0.08	100.06	r
1 117-KHG-91	117KHG/r1/1	50.34	1.75	3.05	9.76	0.24	12.92	22.52	0.36	0.01	0.12	101.08	z1
1 117-KHG-91	117KHG/r1/2	44.62	3.93	8.00	9.03	0.13	11.28	22.32	0.44	0.02	0.18	99.95	z1
1 117-KHG-91	117KHG/r1/3	43.36	4.07	8.91	9.14	0.13	11.03	21.82	0.49	0.10	0.22	99.27	z2
1 117-KHG-91	117KHG/r1/4	48.93	2.07	4.41	8.21	0.14	13.42	22.31	0.30	0.03	0.15	99.98	z1
2 117-KHG-91	117KHG/r1/7	43.95	4.10	8.74	9.24	0.11	11.03	21.99	0.48	0.09	0.20	99.96	
2 117-KHG-91	117KHG/r1/8	43.62	4.20	9.01	8.91	0.13	11.24	22.36	0.36	0.17	0.20	100.21	
3 117-KHG-91	117KHG/r2/11	49.16	1.96	4.27	8.36	0.14	13.70	22.14	0.31	0.07	0.09	100.20	z1
3 117-KHG-91	117KHG/r2/12	44.73	3.85	8.30	9.00	0.16	11.43	22.10	0.43	0.07	0.22	100.29	z2
3 117-KHG-91	117KHG/r2/13	44.31	3.84	8.51	9.07	0.15	11.33	22.15	0.41	0.06	0.18	100.01	z2
3 117-KHG-91	117KHG/r2/14	48.94	1.87	3.96	7.63	0.12	13.34	22.42	0.38	0.08	0.11	98.84	z1
4 117-KHG-91	117KHG/r2/17	43.57	4.06	8.44	9.13	0.12	11.28	22.28	0.44	0.06	0.20	99.59	z2
4 117-KHG-91	117KHG/r2/18	48.00	2.02	4.07	7.91	0.16	13.43	22.59	0.34	0.03	0.16	98.72	z1
6 117-KHG-91	117KHG/r3/21	47.31	2.50	4.69	9.87	0.21	11.29	22.35	0.54	0.00	0.06	98.82	z2
6 117-KHG-91	117KHG/r3/22	48.29	2.01	3.68	7.99	0.17	13.30	22.20	0.34	0.01	0.14	98.15	z1
7 117-KHG-91	117KHG/r4/25	43.61	4.09	8.41	9.21	0.14	11.17	21.97	0.47	0.05	0.21	99.31	ac
8 117-KHG-91	117KHG/r4/34	43.23	3.75	7.48	8.07	0.13	11.74	22.40	0.44	0.08	0.17	97.50	z2
8 117-KHG-91	117KHG/r4/35	47.54	2.02	4.27	8.08	0.14	13.70	21.97	0.34	0.03	0.13	98.22	z1
1 ALWM1e-98	WM1e/r1/4	44.75	2.90	8.01	11.69	0.14	11.11	19.37	0.59	0.05	0.15	98.76	gm
2 ALWM1e-98	WM1e/r2/10	45.74	2.73	7.69	8.08	0.10	12.47	21.30	0.33	0.36	0.11	98.91	gm
3 ALWM1e-98	WM1e/r2/11	46.85	2.59	6.48	8.22	0.15	12.58	20.48	0.31	0.49	0.11	98.26	gm
4 ALWM1e-98	WM1e/r3/23	48.29	1.73	5.25	10.14	0.20	13.51	19.72	0.23	0.04	0.11	99.20	gm
5 ALWM1e-98	WM1e/r3/24	45.27	2.95	8.33	9.20	0.13	11.61	21.25	0.35	0.20	0.14	99.44	gm
6 ALWM1e-98	WM1e/r4/32	49.72	1.41	3.97	8.07	0.08	15.19	19.92	0.19	0.38	0.06	98.98	gm
7 ALWM1e-98	WM1e/r4/36	47.22	2.23	6.64	8.45	0.13	12.81	20.81	0.35	0.35	0.12	99.11	gm
8 ALWM1e-98	WM1e/r4/37	45.59	3.02	8.24	9.56	0.14	11.53	21.03	0.35	0.10	0.12	99.68	gm
9 ALWM1e-98	WM1e-98/r4/s1	44.03	3.35	8.85	11.69	0.14	9.00	20.90	0.42	0.01	0.00	98.39	mi
10 ALWM1e-98	WM1e-98/r4/1	43.76	3.85	8.88	12.01	0.22	8.69	20.95	0.41	0.00	0.00	98.78	mi
11 ALWM1e-98	WM1e-98-2	41.87	4.65	10.03	11.35	0.20	8.15	21.36	0.40	0.00	0.00	98.01	mi

Appendix I (continued)

CLINOPYROXENE

CR Sample	Analysis	SiO ₂	TiO ₂	Al ₂ O ₃	FeO	MnO	MgO	CaO	Na ₂ O	Cr ₂ O ₃	V ₂ O ₃	Total	Notes
11 ALWM1e-98	WM1e-98-2r	41.58	5.83	10.40	11.06	0.16	8.13	21.22	0.44	0.07	0.00	98.90	mi
12 ALWM1e-98	WM1e-98-1b	40.69	4.81	11.28	12.75	0.18	6.33	21.78	0.45	0.07	0.00	98.34	mi
13 ALWM1e-98	WM1e/r2/19	41.76	5.33	11.66	9.89	0.17	8.12	20.90	0.61	0.01	0.17	98.62	mi20
1 ALWM1b-98	WM1b/amfs1	41.57	4.44	10.27	11.60	0.22	9.16	20.90	0.47	0.06	0.00	98.68	mi
2 ALWM1b-98	WM1b/amfs2	44.56	3.10	8.58	14.11	0.31	8.31	20.21	0.48	0.00	0.00	99.66	mi
1 ALWM3a-03	WM3/r1/5	42.78	3.67	10.66	11.95	0.16	8.90	21.03	0.41	0.10	0.22	99.90	mi2
2 ALWM3a-03	WM3/r1/6	46.08	3.06	8.65	9.17	0.11	11.63	21.34	0.36	0.13	0.11	100.64	gm
3 ALWM3a-03	WM3/r1/7	45.09	3.24	8.31	9.70	0.14	11.82	21.34	0.37	0.20	0.16	100.37	gm
4 ALWM3a-03	WM3/r2/12	45.91	3.09	7.97	9.16	0.12	11.78	21.29	0.35	0.33	0.18	100.17	gm
5 ALWM3a-03	WM3/r2/13	46.10	2.86	7.92	8.90	0.10	11.92	21.84	0.34	0.25	0.13	100.36	gm
6 ALWM3a-03	WM3/r2/16	44.76	2.87	7.58	9.60	0.55	12.67	19.69	0.36	0.05	0.08	98.21	gm
7 ALWM3a-03	WM3/r3/21	44.29	3.60	9.18	10.49	0.16	10.61	21.33	0.41	0.07	0.18	100.33	gm
8 ALWM3a-03	WM3/r3/22	48.96	2.17	4.72	11.52	0.29	12.00	20.42	0.49	0.02	0.12	100.72	gm
9 ALWM3a-03	WM3/r3/23	44.83	3.15	8.95	10.10	0.16	10.88	21.49	0.41	0.06	0.17	100.20	gm
10 ALWM3a-03	WM3/r3/24	46.99	1.98	7.62	8.66	0.17	12.57	20.94	0.38	0.12	0.08	99.50	gm
1 ALWM3a-03	WM3/r1/3	41.59	3.20	11.25	12.64	0.24	8.01	19.51	0.76	0.02	0.15	97.38	mi2
5 AL/B5-03	B5/r3/20	51.68	0.82	3.09	5.81	0.09	16.43	21.17	0.24	0.92	0.10	100.35	pcc
5 AL/B5-03	B5/r3/21	52.30	0.73	3.01	5.92	0.12	16.45	21.54	0.21	0.45	0.06	100.79	pcc1
5 AL/B5-03	B5/r3/26	52.37	0.58	2.60	5.25	0.06	16.94	21.04	0.22	1.22	0.02	100.29	pcc2
5 AL/B5-03	B5/r3/23	51.50	1.03	2.95	8.40	0.20	16.22	19.57	0.23	0.06	0.09	100.24	pcr
1 128-KHG-91	128KHG/r1/8	47.56	1.86	5.33	10.72	0.19	13.08	21.24	0.41	0.06	0.10	100.57	c
2 128-KHG-91	128KHG/r1/9	49.05	1.86	3.96	11.34	0.30	13.15	20.61	0.47	0.00	0.09	100.83	plag6
3 128-KHG-91	128KHG/r1/10	49.15	1.47	4.01	10.56	0.20	13.77	20.74	0.37	0.00	0.10	100.38	c
4 128-KHG-91	128KHG/r2/15	47.75	1.90	5.56	10.60	0.18	13.03	21.53	0.38	0.06	0.09	101.08	c
5 128-KHG-91	128KHG/r2/16	47.27	2.14	5.85	10.36	0.16	13.05	21.12	0.39	0.20	0.08	100.62	c
6 128-KHG-91	128KHG/r2/17	50.36	1.03	3.01	10.23	0.22	14.61	20.80	0.28	0.00	0.08	100.62	c
7 128-KHG-91	128KHG/r3/22b	31.49	32.57	3.37	4.65	0.04	1.79	25.63	0.00	0.02	0.61	100.16	ox22
7 128-KHG-91	128KHG/r3/23	47.36	1.91	5.03	11.01	0.22	13.21	21.10	0.40	0.02	0.10	100.34	c
8 128-KHG-91	128KHG/r3/24	46.58	1.96	5.52	11.02	0.17	12.37	21.58	0.38	0.06	0.12	99.75	r
8 128-KHG-91	128KHG/r3/25	49.99	1.06	2.92	10.03	0.21	14.86	20.42	0.30	0.08	0.07	99.94	c
9 128-KHG-91	128KHG/r3/26	47.02	1.79	5.64	9.93	0.19	13.28	21.40	0.36	0.18	0.10	99.88	c
1 X2-KHG-90	X2/r1/1	51.61	1.37	1.81	12.04	0.33	13.70	20.38	0.26	0.05	0.12	101.67	
1 X2-KHG-90	X2/r1/2	51.26	1.28	1.93	11.71	0.27	14.03	19.83	0.29	0.00	0.14	100.76	
2 X2-KHG-90	X2/r1/3	49.38	1.98	3.03	12.54	0.25	12.36	20.88	0.38	0.00	0.11	100.91	
3 X2-KHG-90	X2/r1/4	48.10	2.50	4.57	11.48	0.22	12.89	20.12	0.36	0.07	0.22	100.52	
4 X2-KHG-90	X2/r1/5	51.36	1.26	1.86	11.99	0.31	13.87	19.59	0.28	0.06	0.11	100.70	

Appendix I (continued)

CLINOPYROXENE

CR Sample	Analysis	SiO ₂	TiO ₂	Al ₂ O ₃	FeO	MnO	MgO	CaO	Na ₂ O	Cr ₂ O ₃	V ₂ O ₃	Total	Notes
5 X2-KHG-90	X2/r2/12	48.81	1.96	3.41	12.29	0.32	12.93	20.52	0.37	0.01	0.11	100.72	c
5 X2-KHG-90	X2/r2/13	50.83	1.24	1.50	13.81	0.36	12.68	20.29	0.32	0.01	0.00	101.05	r
6 X2-KHG-90	X2/r2/14	50.76	1.17	1.41	14.36	0.43	12.68	20.11	0.27	0.00	0.06	101.25	c
6 X2-KHG-90	X2/r2/15	50.49	0.81	0.85	18.52	0.51	10.07	19.97	0.27	0.02	0.04	101.54	r
7 X2-KHG-90	X2/r2/16	48.65	2.05	3.58	11.40	0.26	13.23	20.94	0.38	0.03	0.12	100.64	
8 X2-KHG-90	X2/r2/20	47.86	1.93	3.79	12.82	0.23	12.95	19.25	0.37	0.00	0.14	99.33	

AMPHIBOLE

CR Sample	Analysis	SiO ₂	TiO ₂	Al ₂ O ₃	FeO	MnO	MgO	CaO	Na ₂ O	K ₂ O	P ₂ O ₅	Cr ₂ O ₃	V ₂ O ₃	Cl	F	Total	Notes
1 JSH/B006	B006a/3	39.28	5.46	13.16	16.74	0.23	9.60	10.94	2.47	0.76	0.15	0.00	0.04	0.03	0.48	99.34	cpx2
2 JSH/B006	B006a/r2/15	39.71	3.98	12.20	16.43	0.27	9.45	10.89	2.49	0.88	0.11	0.00	0.03	0.03	0.62	97.08	gm
3 JSH/B006	B006a/r2/18	39.42	3.60	13.08	16.80	0.25	9.66	11.01	2.48	0.88	0.40	0.01	0.04	0.02	0.61	98.26	cpx16-17
4 JSH/B006	B006a/r2/19	40.15	4.01	11.83	15.31	0.26	10.10	10.67	2.61	0.70	0.43	0.00	0.04	0.02	0.58	96.72	cpx20
5 JSH/B006	B006b/r4/8	41.32	5.32	10.22	13.06	0.16	10.52	14.74	1.94	0.69	0.01	0.02	0.17	0.02	0.36	98.54	mi14
6 JSH/B006	B006b/r6/30	39.20	5.47	13.03	15.84	0.24	9.80	10.99	2.47	0.69	0.23	0.00	0.05	0.01	0.46	98.48	gm
7 JSH/B006	B006b/r6/32	39.51	3.75	12.97	17.86	0.32	9.24	10.71	2.54	0.94	0.15	0.00	0.04	0.02	0.49	98.53	cpx31
8 JSH/B006	B006b/r6/33	39.56	5.23	12.49	15.26	0.26	9.94	10.82	2.60	0.70	0.19	0.00	0.05	0.01	0.50	97.62	gm
9 JSH/B006	B006b/r7/38	38.86	5.44	13	16.05	0.25	9.73	10.74	2.59	0.65	0.31	0.00	0.03	0.02	0.51	98.25	gm
1 AL/WM1b-98	WM1b/ami3	39.36	5.05	12.23	18.27	0.23	7.75	11.27	2.67	1.17	0.00	0.08	0.00	0.03	0.17	98.32	mi
1 AL/WM1b-98	WM1b/ami3-2	38.60	4.75	12.10	18.20	0.25	7.80	11.34	2.75	1.16	0.00	0.06	0.00	0.00	0.25	97.46	mi
1 AL/WM1b-98	WM1b/ami3-3	38.68	4.87	12.21	17.87	0.22	7.91	11.36	2.82	1.15	0.00	0.08	0.00	0.02	0.18	97.47	mi
1 AL/WM1e-98	WM1e/ami1	37.97	5.41	14.70	14.52	0.12	8.96	12.79	2.46	0.15	0.00	0.06	0.00	0.00	0.35	97.83	mi
1 AL/WM1e-98	WM1e/ami1-2	37.24	5.90	15.32	15.05	0.22	8.70	11.12	2.61	0.20	0.00	0.05	0.00	0.00	0.36	97.16	mi
2 AL/WM1e-98	WM1e/ami1r	38.64	5.62	14.90	13.60	0.20	10.00	10.98	2.70	0.20	0.00	0.03	0.00	0.01	0.40	97.58	mi
2 AL/WM1e-98	WM1e/ami1k	37.24	4.12	17.59	13.41	0.18	9.24	11.04	2.84	0.23	0.00	0.01	0.00	0.03	0.46	96.65	mi
3 AL/WM1e-98	WM1e/1a	37.66	5.79	14.52	14.59	0.15	8.78	12.67	2.41	0.18	0.00	0.05	0.00	0.01	0.42	97.57	mi-B
4 AL/WM1e-98	WM1e/1kev	37.36	4.63	17.40	13.87	0.29	9.03	11.03	2.80	0.23	0.00	0.05	0.00	0.00	0.44	97.38	mi
5 AL/WM1e-98	WM1e/r3/3-2	36.96	5.98	15.49	14.22	0.12	9.05	11.28	2.88	0.33	0.00	0.24	0.00	0.00	0.42	97.25	mi
6 AL/WM1e-98	WM1e/r4/2	38.53	5.62	14.54	13.73	0.19	10.03	11.22	2.76	0.21	0.00	0.00	0.00	0.00	0.40	97.55	mi

CR SPINEL

CR Sample	Analysis	SiO ₂	TiO ₂	Al ₂ O ₃	FeO	MgO	Cr ₂ O ₃	NiO	V ₂ O ₃	Total	Notes
1 JSH/B006	B006a/r2/10	0.02	7.80	6.60	45.25	8.14	26.97	0.28	0.38	95.45	ol9
2 JSH/B006	B006b/r6/27	0.00	6.61	6.86	46.73	7.53	29.08	0.23	0.39	97.43	ol-26
1 AL/WM1e-98	WM1e/r1/5	0.08	3.74	18.22	34.28	13.84	27.50	0.33	0.49	98.47	pc
2 AL/WM1e-98	WM1e/r2/15	0.53	2.97	18.66	32.22	11.52	30.48	0.31	0.37	97.05	mi13
3 AL/WM1e-98	WM1e/r2/16	2.35	3.14	19.47	30.58	12.07	27.87	0.31	0.37	96.15	ol18
4 AL/WM1e-98	WM1e/r2/17	0.17	3.21	20.02	31.62	12.52	28.74	0.28	0.42	96.98	ol18

Appendix I (continued)

CR SPINEL

CR Sample	Analysis	SiO ₂	TiO ₂	Al ₂ O ₃	FeO	MgO	Cr ₂ O ₃	NiO	V ₂ O ₃	Total	Notes
5 ALWM1e-98	WM1e/r3/22	0.21	2.44	15.30	34.54	11.10	32.83	0.23	0.27	96.92	pc
6 ALWM1e-98	WM1e/r4/38	0.15	4.51	19.12	34.91	12.10	26.04	0.33	0.60	97.77	pc
7 ALWM1e-98	WM1e/r4/39	0.11	3.02	18.93	31.04	13.08	30.51	0.33	0.42	97.44	pc
8 ALWM1e-98	WM1e/OI/k	0.06	3.59	15.09	40.22	8.63	27.21	0.28	0.45	95.53	oID
9 ALWM1e-98	WM1e-23	0.17	3.42	14.41	39.29	9.03	30.65	0.36	0.30	97.63	mi
1 ALWM3a-03	WM3/r1/9	0.08	4.13	14.43	43.62	9.40	25.43	0.28	0.56	97.93	ol-1
2 ALWM3a-03	WM3/r2/17	0.13	3.45	17.28	35.71	11.58	29.07	0.35	0.40	97.96	ol-15
3 ALWM3a-03	WM3/r2/18	0.13	4.02	18.03	36.47	12.95	26.79	0.34	0.48	99.20	ol-15
4 ALWM3a-03	WM3/r2/19	0.19	4.52	17.13	36.97	12.81	25.96	0.37	0.49	98.44	ol-15
5 ALWM3a-03	WM3/r3/25	0.07	4.71	16.91	37.83	12.07	25.54	0.35	0.49	97.97	gm
6 ALWM3a-03	WM3/r3/26	0.11	3.33	15.57	40.16	9.82	29.23	0.27	0.53	99.03	oI27
7 ALWM3a-03	WM3/r3/30	0.92	3.23	15.48	36.39	10.92	29.73	0.33	0.51	97.51	oI29

FE-Ti OXIDES

CR Sample	Analysis	SiO ₂	TiO ₂	Al ₂ O ₃	FeO	MgO	Cr ₂ O ₃	NiO	V ₂ O ₃	Total	Notes
1 JSH/B006	B006a/5	0.21	23.07	3.62	66.60	1.08	0.46	0.03	0.51	95.57	gm
2 JSH/B006	B006b/r4/11	0.03	24.31	3.14	62.42	1.44	0.22	1.28	0.94	93.78	mi-12
3 JSH/B006	B006b/r7/39	0.04	23.48	3.83	65.14	1.65	0.02	0.01	0.63	94.81	gm
4 JSH/B006	B006b/r7/40	0.13	24.31	4.36	64.40	0.40	0.02	0.02	0.73	94.37	gm
1 AL/B7-98	B798/r1/1	0.02	46.65	0.07	47.99	2.01	0.16	0.00	0.57	97.47	c
2 AL/B7-98	B798/r1/2	0.00	46.99	0.01	47.06	3.02	0.00	0.01	0.43	97.52	c
3 AL/B7-98	B798/r2/19	0.00	46.59	0.12	48.08	1.48	0.60	0.08	0.58	97.52	c
4 AL/B7-98	B798/r2/20	0.00	45.84	0.16	48.32	2.52	0.00	0.07	0.62	97.53	c
1 117-KHG-91	117KHG/r1/5	0.09	26.23	1.03	66.86	1.02	0.11	0.05	0.59	95.99	c
2 117-KHG-91	117KHG/r1/10	0.41	20.54	1.25	68.69	0.71	0.48	0.09	0.60	92.77	c
3 117-KHG-91	117KHG/r3/23	0.05	25.73	2.50	61.28	1.41	0.07	0.95	0.64	92.64	c
4 117-KHG-91	117KHG/r4/26	0.03	26.49	2.32	61.62	1.28	0.23	0.20	0.65	92.82	c
1 128-KHG-91	128KHG/r1/1	0.16	16.56	4.18	72.28	1.62	0.00	0.00	0.81	95.60	c
2 128-KHG-91	128KHG/r1/2	0.13	16.29	3.36	72.40	1.52	0.00	0.02	0.72	94.45	c
3 128-KHG-91	128KHG/r2/13	0.09	14.39	3.72	71.96	1.45	0.05	0.68	0.76	93.10	r
3 128-KHG-91	128KHG/r2/14	0.10	15.65	2.85	72.62	1.55	0.02	0.07	0.74	93.59	c
4 128-KHG-91	128KHG/r3/21	0.05	17.88	0.75	73.53	1.71	0.04	0.03	0.67	94.66	c
1 X2-KHG-90	X2/r1/10	0.82	23.99	0.52	69.66	1.00	0.40	0.02	0.47	96.89	c
2 X2-KHG-90	X2/r1/11	0.08	24.88	0.06	69.48	1.01	0.00	0.46	0.90	96.87	c
3 X2-KHG-90	X2/r2/21	0.08	25.40	1.88	67.39	0.98	0.00	0.06	0.98	96.76	c
3 X2-KHG-90	X2/r2/21	0.12	26.43	1.94	66.56	1.04	0.05	0.09	0.96	97.20	c

Appendix I (continued)

PLAGIOCLASE

CR	Sample	Analysis	SiO ₂	Al ₂ O ₃	FeO	MgO	CaO	Na ₂ O	K ₂ O	Total	Notes	An
1	JSH/B006	B006a/r/2/21	59.22	24.18	0.45	0.00	6.47	6.57	0.82	97.73	gm	0.35
2	JSH/B006	B006b/r/6/34	62.22	23.21	0.38	0.02	4.70	7.38	1.04	98.94	gm	0.26
3	JSH/B006	b006b/r/7/c10	62.27	23.93	0.32	0.01	5.25	7.39	0.93	100.09	gm	0.28
1	AL/B7-98	B798/r/1/3	55.22	26.39	0.62	0.05	10.07	5.34	0.31	98.00	c	0.51
2	AL/B7-98	B798/r/1/6	57.41	25.22	0.57	0.09	8.30	6.34	0.42	98.34	c	0.42
3	AL/B7-98	B798/r/2/10	54.36	27.16	0.71	0.07	10.91	4.97	0.31	98.49	c	0.55
4	AL/B7-98	B798/r/2/11	53.82	26.85	0.65	0.07	11.16	4.85	0.30	97.70	c	0.56
5	AL/B7-98	B798/r/2/12	54.32	27.15	0.79	0.10	10.94	4.98	0.30	98.58	c	0.55
6	AL/B7-98	B798/r/2/13	58.29	24.02	0.49	0.01	7.23	6.65	0.52	97.21	c	0.38
1	117-KHG-91	117KHG/r/1/6	54.10	28.13	0.42	0.05	11.45	4.46	0.40	99.01	c	0.59
2	117-KHG-91	117KHG/r/1/9	50.51	30.65	0.67	0.08	14.44	3.06	0.25	99.67	c	0.72
3	117-KHG-91	117KHG/r/2/15	51.54	30.07	0.61	0.07	13.45	3.38	0.21	99.33	c	0.69
4	117-KHG-91	117KHG/r/2/16	51.01	29.66	0.60	0.09	13.95	3.27	0.22	98.80	c	0.70
5	117-KHG-91	117KHG/r/4/30	50.42	29.20	0.57	0.08	13.41	3.56	0.26	97.50	c	0.68
1	AL/WM1e-98	WM1e/r/1/3	58.06	25.84	0.81	0.09	8.24	5.82	0.36	99.22	gm	0.44
2	AL/WM1e-98	WM1e/r/2/7	56.03	26.67	0.94	0.12	9.90	5.01	0.22	98.89	gm	0.52
3	AL/WM1e-98	WM1e/r/3/25	55.04	26.94	1.14	0.10	10.36	4.68	0.18	98.44	gm	0.55
4	AL/WM1e-98	WM1e/r/3/26	62.64	23.23	0.50	0.00	4.80	7.55	0.53	99.24	gm	0.26
5	AL/WM1e-98	WM1e/r/4/33	53.42	27.15	2.73	0.32	10.44	4.27	0.18	98.50	gm	0.57
6	AL/WM1e-98	WM1e/r/4/34	56.83	25.57	2.37	0.30	8.13	5.50	0.56	99.25	gm	0.45
7	AL/WM1e-98	WM1e/r/4/35	55.86	26.45	1.30	0.14	9.73	5.00	0.23	98.70	gm	0.52
1	AL/WM3a-03	WM3/r/1/8	56.78	26.56	0.97	0.42	9.61	5.13	0.20	99.68	gm	0.51
2	AL/WM3a-03	WM3/r/2/10	52.56	26.40	2.09	0.33	10.44	4.01	0.22	96.05	gm	0.59
3	AL/WM3a-03	WM3/r/2/14	55.43	27.23	0.96	0.11	10.69	4.57	0.20	99.18	gm	0.56
1	128-KHG-91	128KHG/r/1/3	51.45	29.75	0.84	0.18	13.85	3.43	0.13	99.62	c	0.69
2	128-KHG-91	128KHG/r/1/4	54.39	27.20	0.78	0.12	11.43	4.65	0.27	98.84	pcr	0.58
2	128-KHG-91	128KHG/r/1/5	54.68	27.27	0.77	0.11	11.25	4.91	0.27	99.25	pcc	0.56
2	128-KHG-91	128KHG/r/1/6	54.21	27.31	0.75	0.09	11.29	4.64	0.29	98.58	pcc	0.57
3	128-KHG-91	128KHG/r/1/7	53.09	28.62	0.97	0.14	12.94	4.07	0.16	99.99	c	0.64
4	128-KHG-91	128KHG/r/1/11	52.04	29.01	1.25	0.26	13.50	3.74	0.16	99.97	c	0.67
5	128-KHG-91	128KHG/r/1/12	51.00	29.37	0.90	0.16	13.86	3.44	0.11	98.85	c	0.69
6	128-KHG-91	128KHG/r/2/18	51.68	28.76	0.86	0.14	13.58	3.68	0.14	98.84	c	0.67
7	128-KHG-91	128KHG/r/2/19	56.96	26.52	0.76	0.08	9.73	5.67	0.28	100.00	c	0.49
8	128-KHG-91	128KHG/r/2/20	56.68	26.01	0.73	0.09	9.51	5.58	0.29	98.88	c	0.49
9	128-KHG-91	128KHG/r/3/27	50.73	28.34	1.02	0.12	13.69	3.64	0.13	97.66	c	0.68
10	128-KHG-91	128KHG/r/3/28	50.74	28.93	0.84	0.14	13.73	3.64	0.14	98.17	c	0.68

Appendix I (continued)

PLAGIOCLASE

CR	Sample	Analysis	SiO ₂	Al ₂ O ₃	FeO	MgO	CaO	Na ₂ O	K ₂ O	Total	Notes	An
11	128-KHG-91	128KHG/r3/29	50.66	28.65	0.91	0.15	13.85	3.45	0.11	97.77	c	0.69
12	128-KHG-91	128KHG/r3/30	51.89	28.50	0.99	0.12	13.16	3.96	0.14	98.74	c	0.65
1	X2-KHG-90	X2/r1/6	56.86	25.40	1.57	0.27	8.91	5.33	0.54	98.89	c	0.48
2	X2-KHG-90	X2/r1/7	54.11	27.25	0.81	0.15	11.23	4.27	0.33	98.16	c	0.59
3	X2-KHG-90	X2/r1/8	56.20	26.11	0.59	0.07	10.11	4.91	0.41	98.40	c	0.53
4	X2-KHG-90	X2/r1/9	59.72	24.39	0.42	0.08	7.42	6.20	0.73	98.97	c	0.40
5	X2-KHG-90	X2/r2/17	55.79	26.33	0.63	0.06	10.20	4.94	0.34	98.27	c	0.53
6	X2-KHG-90	X2/r2/18	56.60	25.69	0.61	0.10	9.71	5.22	0.42	98.34	c	0.51
7	X2-KHG-90	X2/r2/19	53.50	27.56	0.99	0.12	12.10	4.18	0.25	98.72	c	0.62

Mineral compositions determined at the Geological Survey of Finland with Cameca SX-100 electron microprobe. Analytical procedures used in the dataset: CR = crystal, c = core, r = rim, mi = melt inclusion, gm = groundmass, z = zone, pc = phenocryst, spl = close to spinel inclusion, amph = clinopyroxene with amphibole rim, ox = close to oxide grain, cpx = amphibole rim in clinopyroxene, ol = inclusion in olivine, Fo = forsterite content (Mg/(Mg+Fe²⁺)), An = anorthite content (Ca/(Ca+Na)).